The Design and Experimental Analysis of an Air Source Heat Pump for Extreme Cold Weather Operation

by

Tom Mackintosh, B.A.Sc., Mechanical Engineering

University of Ottawa

A thesis submitted to the Faculty of Graduate Studies and Postdoctoral Affairs in partial fulfillment of the requirements for the degree of

Master of Applied Science

in

Mechanical Engineering

Ottawa - Carleton Institute for Mechanical and Aerospace Engineering

Carleton University

Ottawa, Ontario

January, 2016

Abstract

Heat pumps offer the potential for significant energy savings in residential applications if they are implemented properly. Currently, air source heat pumps have limited performance at outdoor temperatures below -5°C and most are unable to operate at outdoor temperatures below -15°C. This means less efficient backup heating systems are necessary to meet heating requirements which has impeded widespread use of this technology in Canadian climates.

This research evaluates one method of increasing the performance of an air sourced heat pump to extend its operating range and eliminate the need for a backup heating system.

A study was conducted using the Engineering Equation Solver software package to identify the performance improvements that are attainable with variations of a two stage heat pump cycle. An experimental apparatus was constructed to compare the performance of the best performing variation - a two stage economized cycle - to that of a traditional single stage heat pump.

The two stage economized heat pump had a measured coefficient of performance of 1.45 when it was operated at an outdoor temperature of -31°C making it an energy efficient option for most Canadian climates. In addition, the heating capacity of the system was increased by a factor of 2.5 when compared to the single stage system.

Contents

List of Tables

List of Figures

Nomenclature

Acronyms

COP Coefficient of performance

cRIO Compact RIO

DAQ Data acquisition system

EES Engineering Equation Solver

FPGA Field programmable gate array

HP High pressure

HCFC Hydrochloroflourocarbon

HFC Hydroflourocarbon

IC Integrated circuit

LP Low pressure

NI National Instruments

PID Proportional-Integral-Derivative

PWM Pulse width modulation

RTD Resistance temperature detector

SPRT Secondary platinum resistance thermometer

SJ SJ series variable speed drive

SCPI Standard commands for programmable instruments

VFD Variable frequency drive

WJ WJ series variable speed drive

Symbols

$\bar{X}$ Arithmetic mean

B_i Bias error for a given component in the measurement system

B_j Bias error for the quantity produced by the measurement system

$\bar{V}$ Bulk fluid velocity

ρ Density

η	Efficiency
E	Energy within control volume
h	Enthalpy
S	Entropy
ϵ	Error
g	Force due to gravity
C_p	Heat capacity at constant pressure
$\dot{Q}$	Heat rate
$\dot{Q}_H$	Heating capacity
Z	Height
E_V	Induced voltage
B	Magnetic field flux density
$\dot{m}$	Mass flow rate
N	Number of instantaneous derived measurement quantities
pherr	Phase error
PF	Power factor
P	Power
$\bar{S}$	Precision error
P_r	Pressure ratio
P	Pressure
a, b, c	Regression coefficients
ω	Rotational speed
θ_j	Sensitivity factor used during uncertainty analysis
S	Standard deviation
t_s	Student T statistic
Σ	Summation
ΔT	Temperature differential

T Temperature

t Time

Tq Torque

B_T Total bias error for a derived quantity

$\bar{U}$ Total uncertainty margin for an average derived quantity

$\vec{V}$ Velocity

V Volume

$\dot{W}$ Work rate

Unit Prefix

c Centi

k Kilo

m Milli

Subscripts

acc Accuracy

$C.V.$ Control volume

$elec$ Electrical

i Entering $C.V.$

ϵ_T Error of temperature measurement

e Exiting $C.V.$

eS Exiting state assuming isentropic process

rms Root mean square

$suction$ State at compressor inlet

$discharge$ State at compressor outlet

$1, 2, 3, ...$ State point location reference

T Temperature

Units

A Amps

°C	Degrees Celsius
Ω	Electrical resistance
Hz	Frequency (Hertz)
g	Grams
J	Joules
L	Litres
m	Metres
min	Minutes
rpm	Revolutions per minute
rev	Revolutions
s	Seconds
Vac	Voltage - alternating current
Vdc	Voltage - direct current
V	Voltage
W	Watts

Chapter 1

Introduction

1.1 Motivation

The Canadian heating season is an extreme case of climate variability. Southern Canada experiences heat and humidity during the summer while being subject to moderately cold average temperatures with occasional periods of extremely cold temperatures in the winter. The northern regions of Canada experience low to moderate temperatures in summer and extremely cold temperatures in the winter. Although the required heating capacity varies throughout the year in each of these climates, building codes require the heating system to be sized to provide adequate heat during the lowest temperatures experienced in their respective regions [1].

Heating systems can be categorized into two groups. The first group includes systems whose performance is reasonably independent of outdoor temperature, and can be scaled to handle the worst case loading expected for the house. This category includes gas furnaces, boilers, and systems which operate within the home, and therefore their operation is only dependent on the internal temperature of the home.

The second group includes systems whose performance and heating capacity are negatively affected by the ambient temperature outside the home, including air source heat pumps. For this type of system there is a more complicated solution to assure that adequate heating capacity is available during the extreme low temperatures. Historically, heat pump systems have been sized to accommodate the load at a specific outdoor temperature, below which a backup system is used. To meet the requirements of the building code, the backup system is sized for the worst case loading and the

heat pump is used when the ambient temperature permits. Backup systems are usually resistive heating elements because houses that use heat pumps typically do not have primary energy sources other than electricity. Resistive elements are a low cost addition to the original heat pump system, however they are expensive to operate.

To understand the issue of using a resistive heating element as a main heating source, the coefficient of performance (COP) for a heating system is calculated using its general definition in Equation 1.1.

$$COP_{Heating} = \frac{HeatingCapacity}{EnergyInput} \tag{1.1}$$

The COP gives a metric for comparing heating systems. In the most basic study, the COP of a heat pump system is a function of the temperatures of the heat source and the heat sink that it operates between. In home heating systems, the source is the ambient air and the sink is the house. Because the house temperature is relatively stable, the COP is directly proportional to the temperature of the ambient air and can range from less than 1 to greater than 5. A resistive heating element has a COP of 1 as it is 100% efficient at converting electrical energy into thermal energy. This is the foundation of the argument that there is no benefit to using a heat pump when its COP is below 1, as a resistive heating element would have better performance. Most heat pumps available today automatically switch over to their backup system at a preset temperature. This may be an attempt to conserve energy or a result of mechanical limitations. Unfortunately, in many cases, backup systems take over well before the heat pump COP drops below 1.

The lower operating range for a heat pump greatly depends on its design and varies from one manufacturer to another. A typical lower operating point for current state-of-the-art systems is in the range of -5°C to -15°C. Below this temperature, the system cannot or does not operate and the backup system is used. This presents the

question: What percentage of the time are temperatures lower than this encountered in Canadian cities?

In order to quantify this, Environment Canada climate data [2] from four Canadian cities were evaluated for the years 2007 to 2011. The study included two reasonably populated non-maritime cities - Ottawa and Edmonton - and two extreme northern cities - Cambridge Bay and Resolute.

For this study, an hour that required heating was defined as an hour during the heating season when the outdoor ambient temperature was below 15°C. This was done to neglect hours when the outdoor temperature was above 15°C as these were assumed to not require heating. For each city, the heating season was defined as the months of the year when the average daily temperature was less than 15°C. This means that hourly outdoor temperatures below 15°C that occurred outside of the heating season were neglected. For example, cool summer nights do not require heating. Table 1.1 states the months that were considered to be the heating seasons for each city.

Table 1.1: Months Included in Heating Season Data

City	Heating Season
Ottawa	September to May
Edmonton	September to June
Cambridge Bay	Full Year
Resolute	Full Year

Figures 1.1, 1.2, 1.3 and 1.4 plot temperature against the percentage of hours when the outdoor temperature was at or below that temperature. For example, in Figure 1.1, which displays Ottawa temperature data, the outdoor temperature was at or below 12°C for 90% of the hours that required heating.

Figures 1.1, 1.2, 1.3 and 1.4 indicate that in each of the cities studied, assuming heat pump shutoff temperatures of -5°C or -15°C, there would have been a substantial amount of time when a backup heating system was required if a typical heat pump

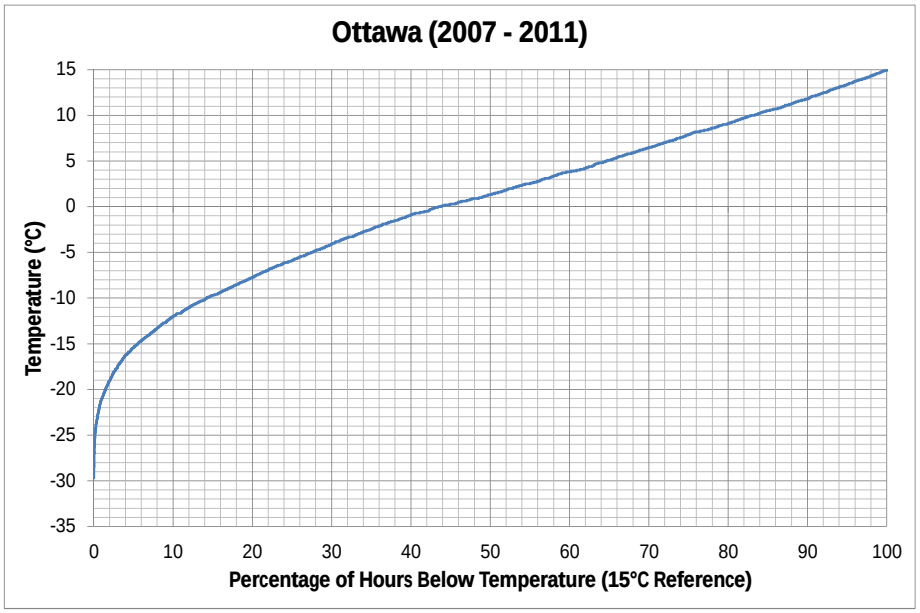

Figure 1.1: Ottawa Heating Season Climate Data (September - May)

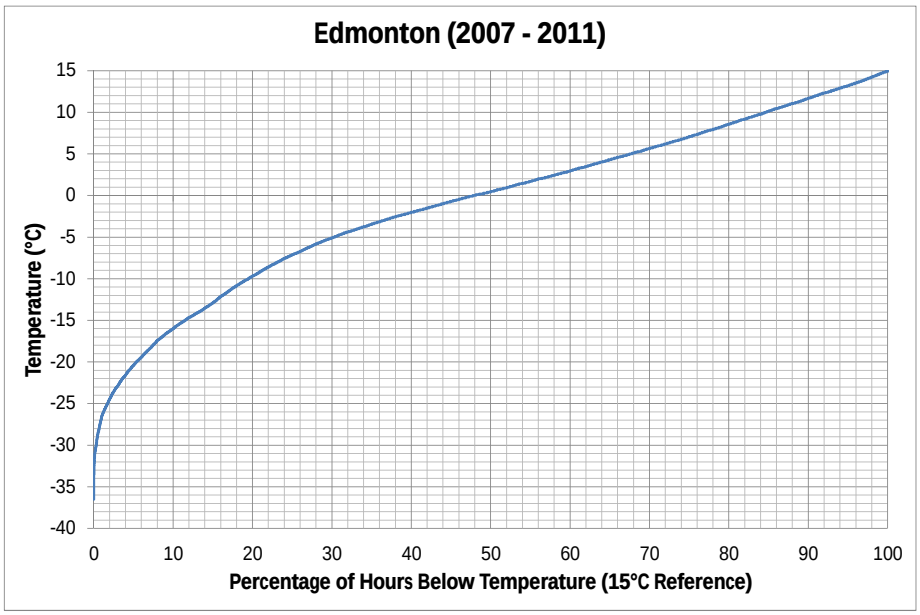

Figure 1.2: Edmonton Heating Season Climate Data (September - June)

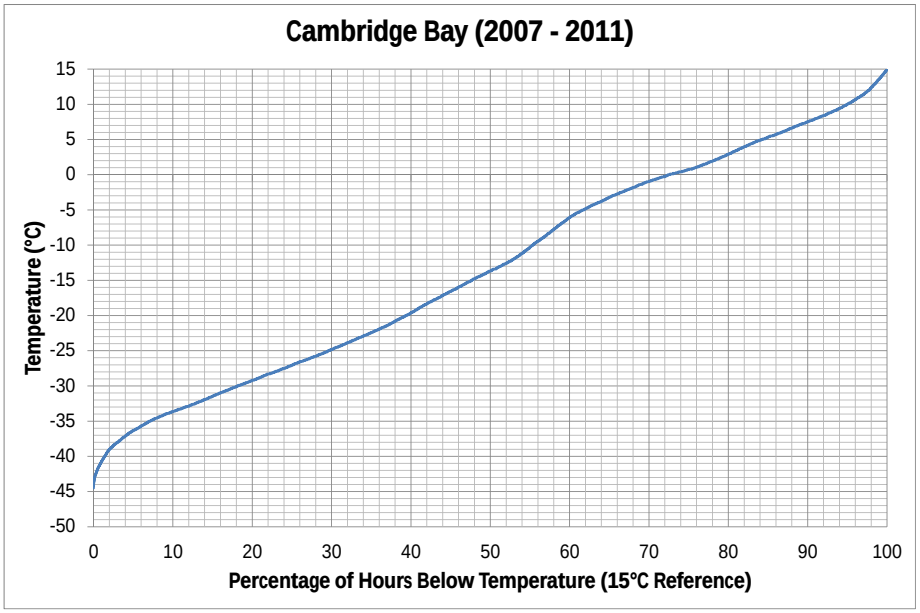

Figure 1.3: Cambridge Bay Heating Season Climate Data (Full Year)

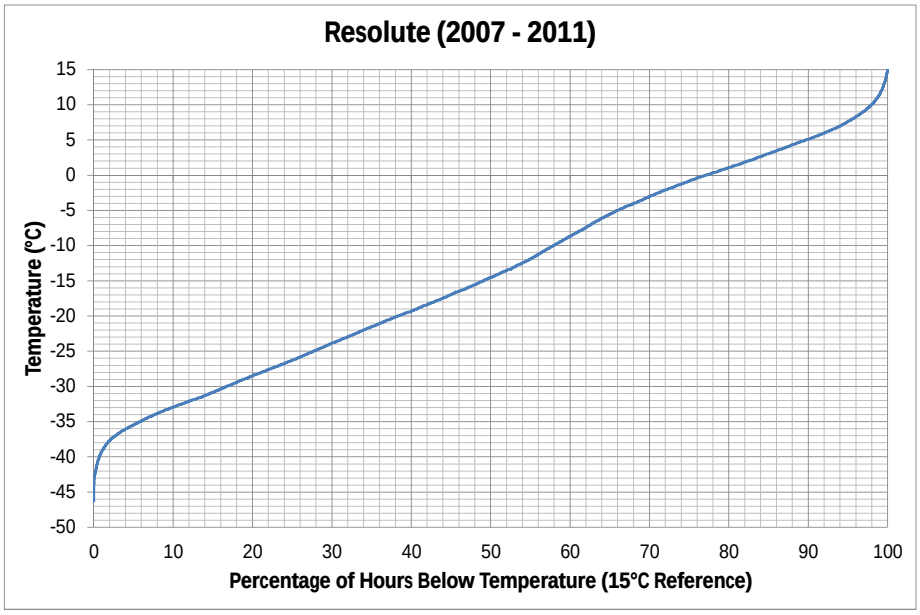

Figure 1.4: Resolute Heating Season Climate Data (Full Year)

was used to heat a home. Table 1.2 shows the amount of time during the heating season when the backup system would have been required to operate in each city. This data is presented as the percentage of hours that required heating during the heating season when the ambient temperature was at or below the heat pump shutoff temperature and also as the number of hours during the heating season when the ambient temperature was at or below the heat pump shutoff temperature.

Table 1.2: Backup Heating System Operating Time

	Operating Limitation of Heat Pump			
	-5°C		-15°C	
Climate	% Below	Hours	% Below	Hours
Ottawa	27%	1763	6%	391
Edmonton	30%	2182	12%	873
Cambridge Bay	60%	5256	47%	4117
Resolute	65%	5694	49%	4292

These results indicate that there would have been significant benefit from using an air source heat pump that is capable of operating at reduced temperatures while maintaining both a reasonable COP and sufficient capacity to heat the home. To determine the current state of research in this area, a literature review was conducted.

1.2 Literature Review

In the past decade, there has been an effort to increase the performance of heat pump cycles. This was motivated by regulations which restrict the use of certain refrigerants and the public interest in reducing energy consumption.

1.2.1 Environmental Regulations

The regulations under the Montreal Protocol and the amendments from the United Nations Environmental Programme currently dictate the phasing out of hydrochlorofluorocarbons (HCFCs) by 2030 [3]. This has driven a wave of innovation in creating new refrigerants and developing new cycles that better suit these refrigerants. Hydrofluorocarbon (HFC) refrigerants are one option, although there are indications that these refrigerants will also be phased out in the future [4]. As a result of these phase outs, it is important to be reasonably confident that refrigerants being studied will be available in the future.

In addition, there have been studies focused on increasing the performance and operating range of heat pump cycles in general.

1.2.2 Cascade Cycle

The simplest approach to improving heat pump cycles focuses on extending the operating range using a cascade cycle. This arrangement uses two or more single stage vapour compression cycles in series[1], which allows the low temperature cycle to use a refrigerant which is better suited to lower temperatures, while also splitting the work between multiple compression processes which allows a higher total pressure ratio to be achieved than is possible with a single compressor.

Parekh et al. [5] studied a cascade cycle which used R-507a and R-23 refrigerants. The study included steady state modelling with the intention of extending the range of the system to operate at lower temperatures. The study showed that the system was capable of operating at ambient temperatures below -50°C, although the COP at these temperatures was expected to be on the order of 0.8. The authors assumed compressor isentropic efficiencies of 80%.

[1]The Single Stage Cycle and Cascade Cycle schematics are included in Chapter 2.

Bhattacharyya et al. [6] performed a similar study on a two stage cascade heat pump using N_2O and CO_2 as refrigerants. The cycle they studied used additional internal heat exchangers that super-heated the refrigerant at the compressor inlets by drawing heat from the liquid refrigerant after it was condensed. The researchers performed optimization on parameters which included: intermediate heat exchanger overlap temperature, intermediate temperature and heat exchanger effectiveness. The authors' report predicted COPs of 2.5 at an ambient temperature of -35°C and 2 at an ambient temperature of -65°C. They did not discuss operation at temperatures above this range.

1.2.3 Multi-stage Cycles

Another approach to increasing heat pump performance is to use multiple compression stages with a single refrigerant. This may include the use of additional performance improving features related to cycle arrangement.

Bertsch et al. performed an extensive study of two stage air source heat pumps. Their initial investigation focused on determining which cycle would be best suited to residential applications where the supplied heating temperature was 50°C and the ambient temperature was as low as -30°C [7]. This study compared the relative performance of a two stage inter-cooled cycle, a two stage economized cycle[2], and a cascade cycle to a standard single stage cycle. The two stage inter-cooled cycle functioned by removing heat from the refrigerant after the first compression stage via an additional heat exchanger. Depending on its temperature, the heat was either used for heating or dumped as waste heat. A schematic of the two stage inter-cooled cycle is shown in Figure 1.5.

[2]The two stage economized cycle schematic is included in Chapter 2.

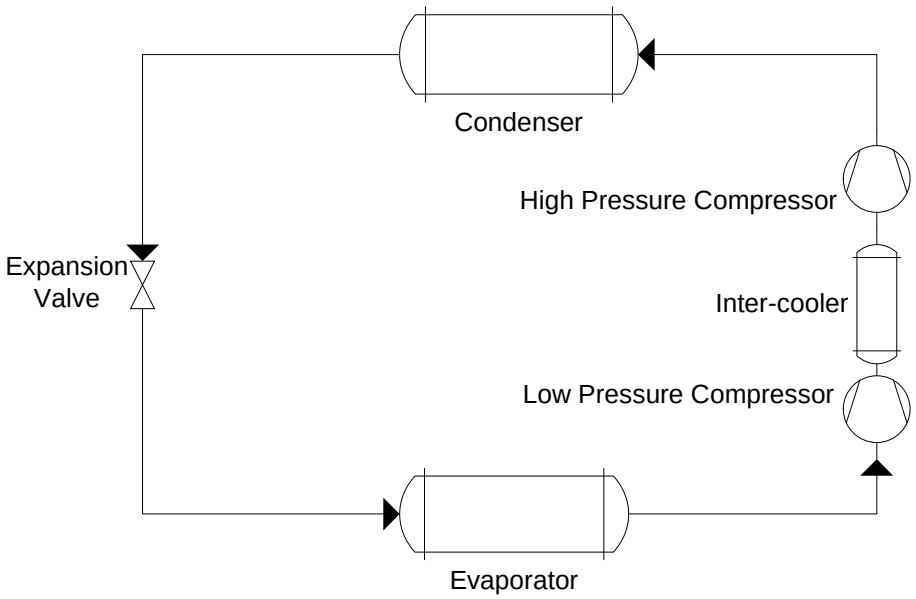

Figure 1.5: Two Stage Inter-cooled Cycle Diagram

They concluded that each of the studied cycles had their own strengths and weaknesses and the best cycle would depend on the operating environment of the end user.

A second study conducted by Bertsch et al. included building an experimental system based on their previous work [8]. The two stage economized cycle was chosen as the base for this study. Their experimental apparatus was designed to operate in both a two stage and a traditional single stage configuration to allow for comparison. This study showed that their two stage cycle was able to achieve a COP of 2.1 at an ambient temperature of -30°C. The authors also observed an increase in the amount of deliverable heat by a factor of roughly 2 when compared to single stage operation. When the authors compared the experimental results with their original modelling study, they found the modelled performance was approximately 20% higher than the measured performance. They concluded this was reasonable based on the simplicity of the model. The authors also concluded that oil management is very important in multiple stage cycles that are operated at low temperatures. Their system used

a manual approach to maintain the oil distribution between the compressors before each test run.

The work of Bertsch et al. was continued by Caskey [9] and Menzi [10] who each performed a study using an improved version of the cycle that Bertsch et al. worked with. This version of the cycle included a low pressure compressor bypass system which allowed the system to operate as a single stage cycle at warmer ambient temperatures.

Caskey's work focused on a TRNSYS study which compared the performance of the two stage economized air source heat pump to a gas furnace in a military barracks in Indiana using an updated version of the original model. The study showed that a yearly COP of 3.67 for the system could be expected with an operating cost savings of 25% and a reduction in CO_2 emissions of 30%.

Menzi's study included a larger set of cases within a TRNSYS simulation of the military barracks in Indiana. This study compared the performance of three different systems: a standard gas furnace, a single stage air source heat pump, and the two stage economized air source heat pump. The single stage system used an electrical backup heater to help with cold weather operation and was used for comparison in two studies. The first study used the original buildings, and the second study used the buildings with upgraded insulation and air tightness. The two stage system also used these two scenarios, as well as a case where the upgraded building also used ambient heating or cooling when it was available. This allowed the outdoor ambient air to heat or cool the interior directly if the outdoor temperature allowed. There were additional cases added for the two stage system which included a latent heat storage system that was regenerated daily with outdoor air, a night time setback program in the thermostat, and a case where the thermostat could switch between heating and cooling based on outdoor temperature. Altogether, eight cases were used and the results presented for each were primary energy consumption, heating/cooling

delivered, CO_2 emissions, cost, and relative energy usage compared to a gas furnace. Menzi concluded that for this installation, both the single stage and the two stage system operated similarly, as the cold weather operation was mainly above -20°C in this region. It was his recommendation that the time below -15°C be studied to determine whether or not the two stage system was beneficial.

Wang et al studied the benefits of using a single compressor with an intermediate injection port [11]. An intermediate injection port allows refrigerant to be injected into the compressor part way through the compression process. This essentially splits the compression process into two stages within a single machine. This study included an experimental investigation of both the economized and the flash tank method for vapour injection[3]. These cycles were similar to those studied by Bertsch et al., except for the use of a single compressor with a vapour injection port. The study used R-410a as the refrigerant and the vapour injected mass was varied from 0 kg/s to the maximum amount possible for each cycle. It was shown that the capacity of the system could be increased during both heating and cooling, while the COP showed appreciable gains during the heating season only. Wang also concluded that both approaches had different advantages. He states that the flash tank was slightly more efficient, although it required a more advanced control strategy.

1.2.4 Auto-cascade Cycle

There has also been work done with the auto-cascade cycle. This cycle uses a single compressor with a mixture of refrigerants. The operating principle separates refrigerants by taking advantage of their different saturation temperatures for a given pressure. The mixture of vapour refrigerants is compressed, after which they are separated one by one in different condensing steps. After a fluid condenses, it is expanded and used as a heat sink to condense the next fluid. Any number of fluids can be

[3]The flash tank cycle schematic is included in Chapter 2.

used to obtain the required temperature reduction. A schematic of a two-refrigerant auto-cascade cycle is shown in Figure 1.6.

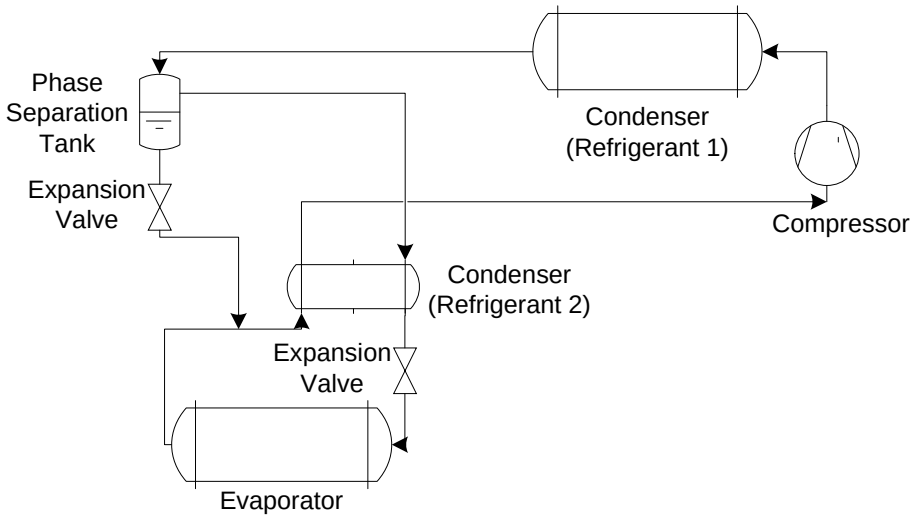

Figure 1.6: Two Stage Auto-cascade Cycle Diagram

Du et al. [12] studied the auto-cascade cycle as a means for ultra-low temperature refrigeration in the range of -60°C. The authors conducted an experimental study which used a mixture of R-134a and R-23. They successfully operated their system with an evaporator temperature of -60°C. They concluded that this cycle could perform with a good COP. However, the additional heat exchangers and phase separators required would all need to be optimized as they increase energy losses when compared to a more standard cycle.

1.2.5 Carbon Dioxide Cycle

Carbon dioxide (CO_2) is being used more often in small scale systems. Carbon dioxide is an interesting fluid in that it has a global warming potential of 1 as it is the reference gas for this parameter. It also has a critical point of 31.1°C which allows it to be used in a trans-critical cycle within air source heat pumps. Trans-critical cycles

replace the condenser with a gas cooler, which reduces entropy generation during the heat transfer process.

Austin performed an extensive review of trans-critical carbon dioxide heat pumps in 2011 [13], which highlights the benefits of such systems. Austin notes that the main disadvantage of using carbon dioxide as a refrigerant is its extremely high pressure requirements ($\geq$11 MPa) which present challenges in system design, but he also states that carbon dioxide systems are smaller than comparable systems due to the high volumetric heating capacity of CO_2. Austin states that in earlier studies there were many conflicting results which showed poor performance. This conflict has been attributed to the vastly varying properties of CO_2 near its critical temperature. The author states that if the changes in viscosity and heat capacity are modelled accurately, there is a substantial improvement in the predicted performance. Austin also presents market data showing that trans-critical CO_2 heat pumps are available in Japan from various manufacturers sold under the name Eco-Cute. As of 2009, there have been 2 million of these units sold. Austin also notes that Coca Cola has stated that its vending machines will be replaced with trans-critical CO_2 units by 2015.

1.2.6 Hydrocarbon Refrigerants

Recent studies have also investigated using hydrocarbons as refrigerants. Westphalen converted a military environmental control unit to operate on propylene rather than R-407c and studied the resulting change in performance [14]. The system previously had a heating capacity of 15.9 kW. The author determined that a 12% increase in output and a 10% increase in the COP were attainable by simply switching refrigerants. The author also determined that this translates to a reduction in the required heat exchanger surface area of 8.5% if the original heating requirement was retained. Lastly, the author investigated the potential explosion and fire hazards that could result from a leak of refrigerant. It was determined that due to the small mass of

refrigerant, there would only be a flammable mixture present for a short period of time. However, in the design used, no ignition sources were present within the system and it was not considered a safety hazard.

1.2.7 Compressor Technology

Residential heat pump compressors are typically positive displacement machines. This has been driven by air conditioning expertise which has a much greater market share than residential heat pumps in North America. These compressors are typically either piston-based or scroll-based, with the current trend favouring scroll compressors for their simplicity, relative performance, and low-noise operation. Larger commercial scale heat pumps also use screw and centrifugal compressors although this technology is starting to emerge in studies at smaller scales as well. Typical isentropic efficiencies of residential-sized positive displacement compressors are in the range of 40% to 70% [15].

There have been recent studies on the possibility of using turbo-machinery derived compressors for residential heat pumps. Schiffman et al. [16][17] conducted a study on the feasibility of using a small centrifugal compressor in a residential-sized heat pump. Their main goal was to exploit the wide operating range of centrifugal machines in terms of mass flow rates and pressure ratios as a way to increase the heat pump efficiency. They also note the benefits of oil-free operation, reduced compressor size, and a potential increase in isentropic efficiency associated with centrifugal machines. The study included a modelling investigation of the compressor, using the assumption of one-dimensional internal flow, followed by the design of a prototype and an experimental investigation. The system was intended to produce hot water at a rate of 12 kW at a temperature of 60°C and operated with an evaporator temperature of -12°C. The study showed that the predicted results were lower than what was measured during the experiment by approximately 5%, the compressor was able

to operate over a wide flow rate range of 27 g/s to 55 g/s, the isentropic efficiency was above 70% for most of the operating range, and the compressor could reach a maximum isentropic efficiency of 80%. This was all achieved using a compressor with an exducer diameter of 20 mm which presents an incredibly small footprint when compared to a similar capacity scroll compressor.

1.3 Research Objectives

The previous section outlines the work which has been conducted related to residential air source heat pumps. With the exception of the work done by Bertsch et al. [7][8], and Du et al. [12], this work has been limited to either modelling or experimentation at ambient temperatures above -15°C. This demonstrates a need to extend the operating performance of air source heat pumps to temperatures below -30°C through experimentation. This thesis will outline the work that was done in this area through the following research objectives:

1. Conduct an investigation of different heat pump cycles using Engineering Equation Solver (EES) to determine the best heat pump candidate for the Canadian climate. The cycles that will be considered are:
    - Single stage
    - Two stage cascade
    - Two stage economized
    - Two stage flash separation
2. Design and build an experimental prototype of the best performing cycle as determined by Objective 1.
3. Characterize the cold climate performance of the prototype through experimental investigation.

At the time of this research, a modern air source cold climate heat pump was made available which allowed the experimental prototype to be constructed by modifying a market ready system. The system was designed to operate on R-410a and as such, the modelling study was limited to this refrigerant.

1.4 Thesis Outline

With the research objectives defined, the remainder of this thesis is organized as follows:

- Chapter 2 will describe the modelling study that was conducted to determine which cycle should be constructed for the experimental work.
- Chapter 3 will describe the construction of the experimental prototype and the instrumentation that was used to characterize its performance.
- Chapter 4 will outline the work done to characterize the uncertainty of the measured results.
- Chapter 5 will outline the test plan that was followed to characterize the performance of the system. The operation of the prototype heat pump will also be described here.
- Chapter 6 will outline the results of the experimental investigation and discuss their implications.
- Chapter 7 will present a conclusion of the work that is discussed in this thesis.

Chapter 2

Modelling

This chapter outlines the work that was done during the modelling study. The study was intended to show the performance of the two stage cycles relative to a single stage cycle and also identify which cycle should be studied further during the experimental phase of this work. A simple thermodynamic model for each cycle was developed using the software package Engineering Equation Solver (EES) which is developed by F-Chart. EES is designed to solve coupled algebraic and differential equations. It also includes built-in thermodynamic state equations for many fluids. This software is extremely powerful for these types of studies as it reduces the time required to formulate the problem and eliminates the need to manually input fluid property information. The cycle models that are outlined in this chapter have been included in Appendix A.

2.1 Refrigerant

As outlined in Section 1.3, the modelling study was limited to the refrigerant R-410a which is a 50/50 mass percentage blend of R-32 and R-125. EES calculates the fluid properties for R-410a using the pseudo-pure fluid equations of state that were developed by Lemmon [18]. These equations are able to predict the properties of R-410a with an accuracy of 0.1% when compared to experimental data.

2.2 Model Components

The models for each cycle were constructed using component models which created links between the state points of the cycles. The component models are described in the following sections.

2.2.1 Compressors

Each compression process was modelled using the approach that is outlined in this section. Figure 2.1 shows the control volume that was used to model a compressor.

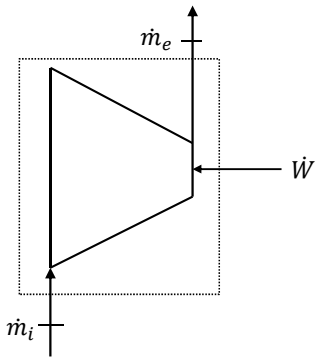

Figure 2.1: Compressor Control Volume

The compression process was modelled by simplifying the First Law of Thermodynamics for a control volume which is shown in Equation 2.1.

$$\frac{dE_{C.V.}}{dt} = \dot{Q}_{C.V.} - \dot{W}_{C.V.} + \Sigma\dot{m}_i\left(h_i + \frac{1}{2}\vec{V_i}^2 + gZ_i\right) - \Sigma\dot{m}_e\left(h_e + \frac{1}{2}\vec{V_e}^2 + gZ_e\right) \quad (2.1)$$

where $\frac{dE_{C.V.}}{dt}$ is the rate of change in energy within the control volume, $\dot{Q}_{C.V.}$ is the rate at which heat is added to the control volume, $-\dot{W}_{C.V.}$ is the rate at which work is extracted from the control volume, $\Sigma\dot{m}_i$ and $\Sigma\dot{m}_e$ are the sum of the mass flows that enter and exit the control volume respectively, h is the enthalpy of a flow as it

crosses the boundary of the control volume, $\frac{1}{2}\vec{V}^2$ is the kinetic energy of a flow as it crosses the boundary of the control volume, and gZ is the potential energy of a flow as it crosses the boundary of the control volume.

Equation 2.1 was simplified using the following assumptions:

1. The process is steady state.
2. There is no heat loss from the system.
3. The change in kinetic energy is negligible.
4. The change in potential energy is negligible.
5. There is a single inlet and outlet in the control volume.

Equation 2.1 is shown below in its full form with the cancelled terms crossed out.

$$\cancel{\frac{dE_{C.V.}}{dt}}^{1} = \cancel{\dot{Q}_{C.V.}}^{2} - \dot{W}_{C.V.} + \cancel{\Sigma}^{5} \dot{m}_i \left(h_i + \frac{1}{2}\cancel{\vec{V}_i^2}^{3} + \cancel{gZ_i}^{4} \right) - \cancel{\Sigma}^{5} \dot{m}_e \left(h_e + \frac{1}{2}\cancel{\vec{V}_e^2}^{3} + \cancel{gZ_e}^{4} \right)$$

Lastly, conservation of mass for a system operating at steady state dictates that $\dot{m}_i = \dot{m}_e = \dot{m}$. The simplified form of Equation 2.1 is shown in Equation 2.2.

$$\dot{W}_{C.V.} = \dot{m}(h_i - h_e) \tag{2.2}$$

Equation 2.2 shows that the work consumed by the compressor is directly related the mass flow of refrigerant flowing through it and the difference in the enthalpies of the refrigerant between its inlet and outlet. For this work the inlet pressure and temperature were known while only the outlet pressure was known. To determine the outlet state, the isentropic efficiency was used as defined in Equation 2.3

$$\eta_{Isentropic} = \frac{\dot{W}_{IsentropicCompression}}{\dot{W}_{RealCompression}} \tag{2.3}$$

where, $\dot{W}_{IsentropicCompression}$ is the work required for an isentropic compression process and $\dot{W}_{RealCompression}$ is the work required for a real compression process that includes the mechanical and electrical losses. This relation allows the outlet state of the compression process to be estimated using isentropic efficiencies which are representative of a real machine. For a given mass flow rate and by substitution of Equation 2.2, Equation 2.3 becomes:

$$\eta_{Isentropic} = \frac{h_i - h_{eS}}{h_i - h_e} \tag{2.4}$$

where h_{eS} is the outlet enthalpy for the isentropic process and h_e is the outlet enthalpy for the real process. Equation 2.4 was rearranged to allow the outlet state to be solved directly. The final form of the compressor model is shown in Equation 2.5.

$$h_e = h_i + \frac{h_{eS} - h_i}{\eta_{Isentropic}} \tag{2.5}$$

This approach requires the isentropic efficiency to be defined in order to solve the outlet conditions. For this work, the isentropic efficiency was determined by fitting a second order polynomial to the manufacturer's performance data of a Copeland ZP36K5E-PFJ R-410a scroll compressor. Copeland publishes performance data for all of their compressors online [15]. The ZPE36K5E-PFJ was chosen as it is representative of a high performance modern scroll compressor that was designed for operation with R-410a. The equation that was fitted to the data is shown in Equation 2.6.

$$\eta_{Isentropic} = a + b * P_r + c * P_r^2 \tag{2.6}$$

where P_r is the pressure ratio across the compressor. The coefficients were regressed using condenser data for 51°C as this was representative of expected testing conditions. The coefficients are shown in table 2.1.

Figure 2.2 plots the range of isentropic efficiencies that result from Equation 2.6.

Table 2.1: Compressor Isentropic Efficiency Coefficients for Equation 2.6

Coefficients	Regressed values
a	93.8
b	-8.14
c	0.156

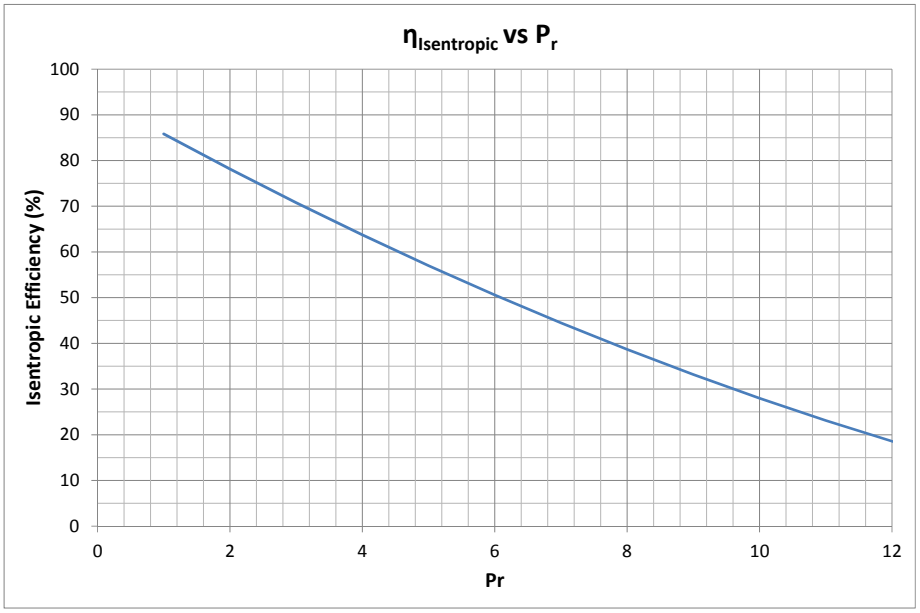

Figure 2.2: Range of Isentropic Efficiencies Calculated using Equation 2.6

The compressor data was only applicable for P_r greater than 2.6, for lower pressure ratios, a constant isentropic efficiency of 70% was used. This was done to limit the isentropic efficiency to a maximum that is representative of the compressor data.

In reality, the compressor efficiency is also a function of suction density, and this correlation may not be considered representative of what could be expected from the low pressure (LP) stage if this compressor was used for this purpose. However, it was assumed that a compressor could be selected that would give similar results at lower densities. Therefore this correlation was used for both the high pressure (HP) and LP stages.

2.2.2 Heat Exchangers

The heat exchangers were not modelled based on actual components. Instead, it was assumed that a heat exchanger with similar performance could be designed for each cycle. To account for the heat exchange process, the temperature of the ambient air and the indoor air were assumed to be constant throughout the heat exchanger. This was considered to be a reasonable assumption because these heat exchangers are typically the tube and fin type where the air stream flows perpendicular to the refrigerant. To ensure the heat transfer process was possible, the temperature difference between the refrigerant and the heat source or the heat sink at the pinch point was assumed to be 3°C. This value was used as it agrees with the experimental results that were published by Bertsch et al. [8].

2.2.2.1 Condenser

The condensing process was assumed to provide a fixed amount of 8.3°C of sub-cooling at the refrigerant outlet. This means that the refrigerant exited the condenser at 8.3°C below its saturation temperature. This value was chosen because it corresponds to the value used by Copeland during their compressor performance testing. Defining the amount of sub-cooling at the outlet of the condenser, dictated the saturation temperature, and therefore the pressure of the condenser. Figure 2.3 shows the temperature of the refrigerant as it passes through the condenser.

To model this process, the saturation temperature was fixed using Equation 2.7.

$$T_{sat_{Cond}} = T_{supply} + T_{pinch} + T_{sub-cool} \tag{2.7}$$

where $T_{sat_{Cond}}$ is the saturation temperature of the refrigerant in the condenser, T_{supply} is the temperature of the air supplied to the house, T_{pinch} is the temperature differential required to drive the heat transfer process, and $T_{sub-cool}$ is the desired amount

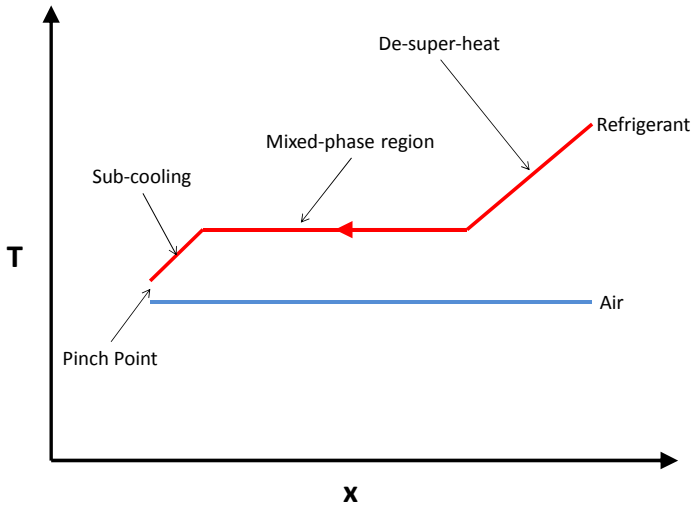

Figure 2.3: Condenser Heat Transfer Diagram

.

of sub-cooling at the condenser outlet. For this work, a value of 50°C was used for T_{supply}. This value was chosen as it was the value used by Bertsch et al.[7] during their work. This temperature is representative of what is required for a forced air heating system.

2.2.2.2 Evaporator

The evaporation process was assumed to provide a fixed amount of 11.1°C of super-heat at the refrigerant outlet. This means that the refrigerant exited the evaporator at 11.1°C above its saturation temperature. This value corresponds to the amount of super-heat that was used by Copeland during their compressor performance testing. Defining the amount of super-heat at the outlet of the evaporator, dictated the saturation temperature, and therefore the pressure of the evaporator. Figure 2.4 shows the temperature of the refrigerant as it passed through the evaporator.

To model this process, the saturation temperature was fixed using Equation 2.8.

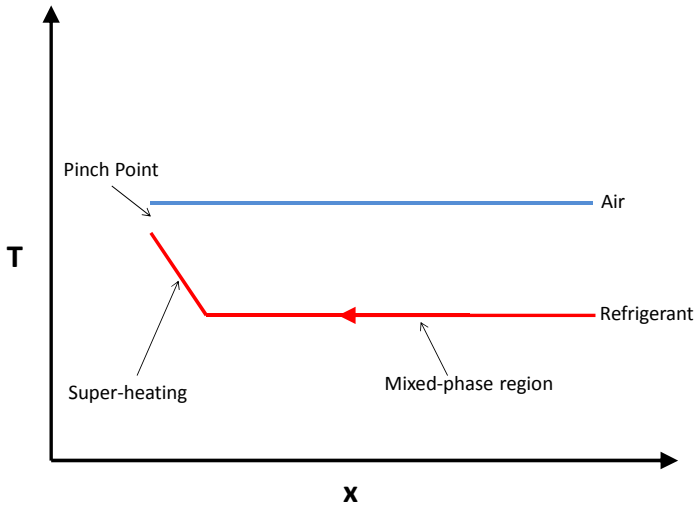

Figure 2.4: Evaporator Heat Transfer Diagram

.

$$T_{sat_{Evap}} = T_{ambient} - T_{pinch} - T_{super-heat} \tag{2.8}$$

where, $T_{sat_{Evap}}$ is the saturation temperature of the evaporator, $T_{ambient}$ is the temperature of the ambient air, and $T_{super-heat}$ is the desired amount of super-heat at the evaporator outlet.

2.2.3 Expansion Valves

The expansion valves were modelled using the same assumptions outlined in Section 2.2.1, with the additional assumption that no work is done on the system during the expansion process. This further reduced Equation 2.2 to give Equation 2.9, which was used to determine the outlet state of the expansion valve.

$$\cancelto{0}{\dot{W}_{C.V.}} = \dot{m}(h_i - h_e)$$

$$h_e = h_i \tag{2.9}$$

2.3 Single Stage Cycle

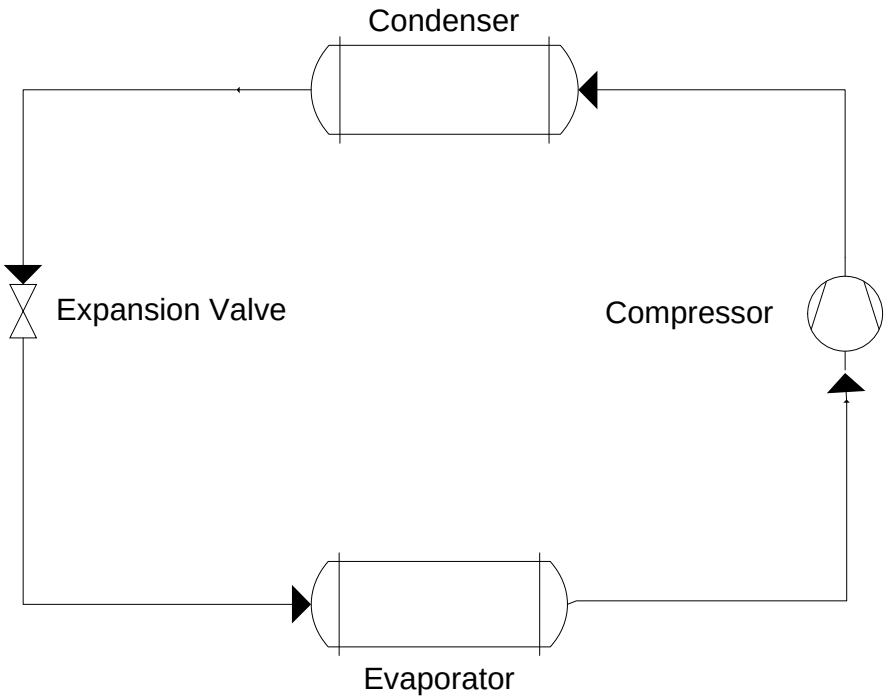

Figure 2.5: Single Stage Cycle Diagram

The single stage cycle diagram, shown in Figure 2.5, was modelled by linking the previously mentioned component models. The supply temperature was set to 50°C and the ambient temperature was set for the desired case. The model was then solved on a per-unit mass basis for the COP and the process was repeated to populate the ambient temperature range of -20°C to 20°C in 10°C increments. This range was chosen because it spans the operating range of currently available cold climate heat pumps. Figure 2.6 shows the Temperature-Entropy diagram for the single stage cycle when operated at an ambient temperature of 0°C.

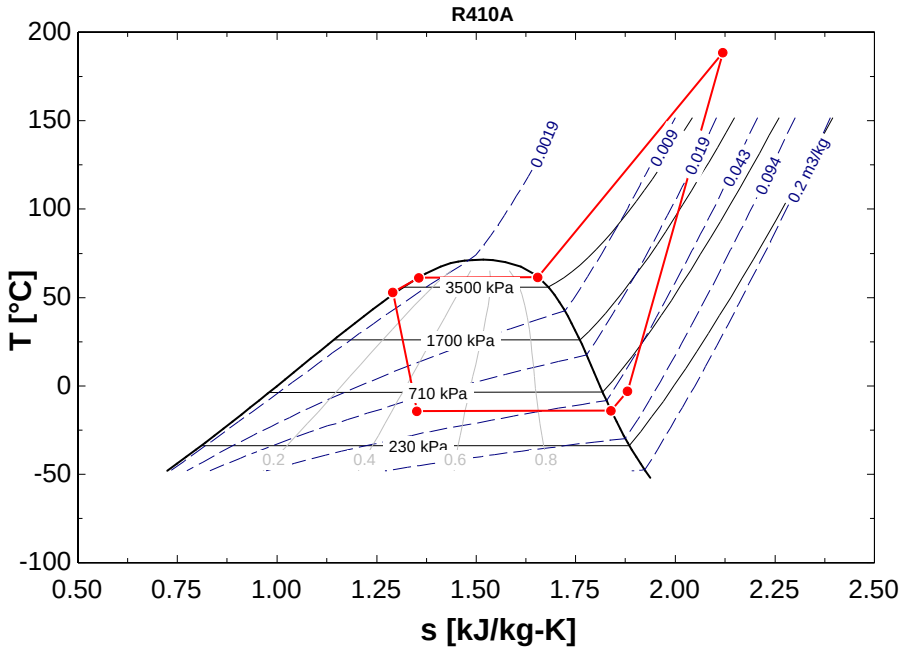

Figure 2.6: Single Stage TS Diagram ($T_{ambient}$ = 0°C, T_{supply} = 50°C)

2.4 Two Stage Cascade Cycle

The two stage cascade cycle diagram, shown in Figure 2.7, operated using two separate single stage cycles that were connected via an intermediate heat exchanger which acted both as the LP stage's condenser and the HP stage's evaporator.

This new heat exchanger was also modelled by assuming a 3°C temperature difference at its pinch point. This heat exchanger was assumed to be a counterflow type. Figure 2.8 shows the temperature of the refrigerant flows as they pass through the intermediate heat exchanger.

To model this process, the HP stage's evaporator saturation temperature was set to the intermediate saturation temperature and the LP stage's condenser saturation temperature was calculated using Equation 2.10.

$$T_{Sat_{LPCond}} = T_{intermediate} + T_{pinch} + T_{sub-cool} \tag{2.10}$$

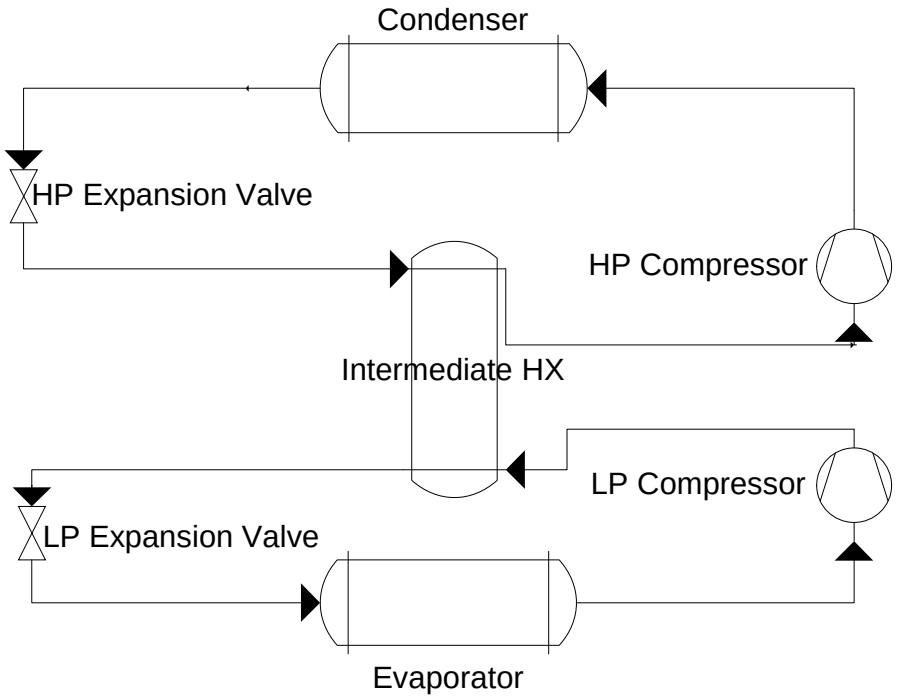

Figure 2.7: Two Stage Cascade Cycle Diagram

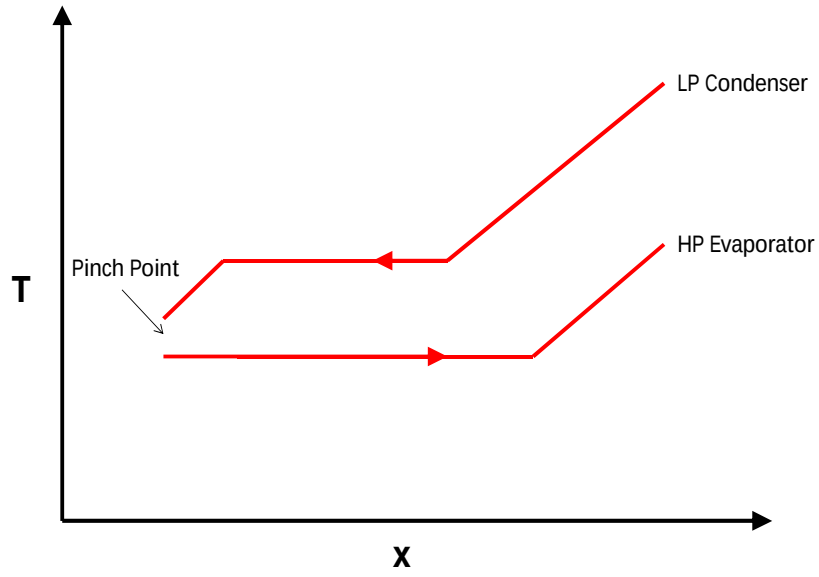

Figure 2.8: Intermediate Heat Exchanger Heat Transfer Diagram

where, $T_{Sat_{LPCond}}$ is the saturation temperature of the LP stage's condenser, and $T_{intermediate}$ is the intermediate saturation temperature.

The two stage cascade cycle was solved by setting the supply temperature to 50°C and setting the ambient temperature for the desired case. The intermediate saturation temperature was than varied in 1°C increments from $T_{ambient}$ to T_{supply} to locate the operating point that resulted in the highest COP. The process was repeated to populate the ambient temperature range of -40°C to 0°C in 10°C increments.

2.5 Two Stage Flash Separation Cycle

The two stage flash separation cycle diagram, shown in Figure 2.9, uses two expansion valves which split the expansion process. After the first expansion, the flash separation tank separates the two phase fluid into its liquid and gaseous states. The liquid is further expanded by the second expansion valve while the vapour phase is injected between the two compression processes.

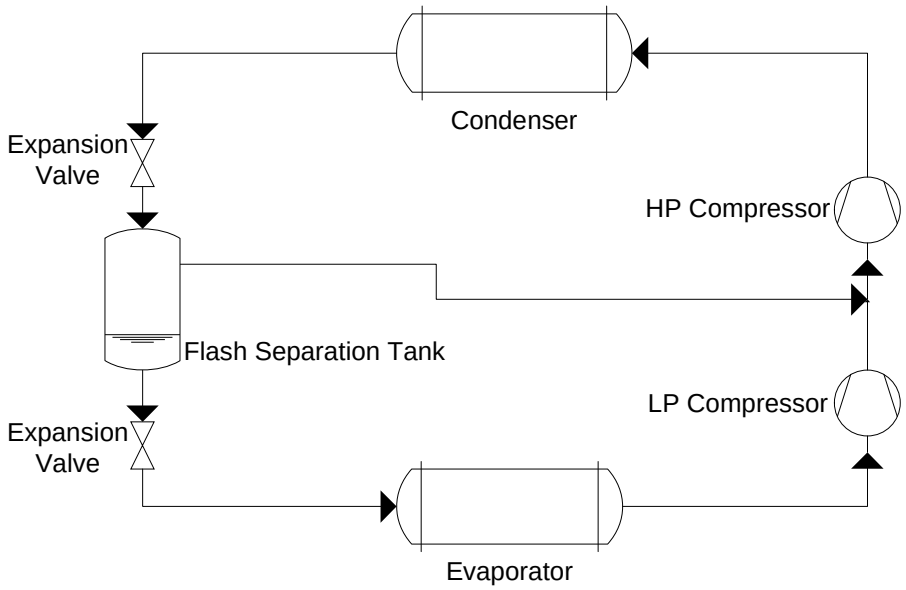

Figure 2.9: Two Stage Flash Separation Cycle Diagram

To model this cycle, the flash tank and mixing process were modelled using the following approaches.

2.5.1 Flash Separation Tank

The flash separation tank was modelled using the assumptions that (a) during steady state operation the liquid level in the tank is constant, and (b) the liquid and vapour exiting flows are single phase flows. Therefore, the quality of the two phase fluid entering the tank determines the division of vapour and liquid mass flows that must exit the tank to maintain the liquid level. The pressure of the flash separation tank was assumed to be the saturation pressure that corresponded to the intermediate temperature used for the given case.

2.5.2 Interstage Mixing

The interstage mixing process was modelled using the control volume shown in Figure 2.10.

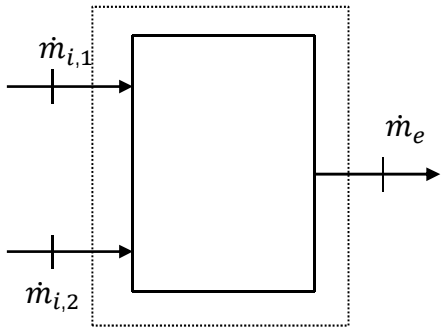

Figure 2.10: Interstage Mixing Control Volume

Equation 2.1 was reduced using the following assumptions:

1. The process is steady state.

2. There is no heat loss from the system.

3. The change in kinetic energy is negligible.

4. The change in potential energy is negligible.

5. There is no work done on the system.

Equation 2.1 is shown below in its full form with the cancelled terms crossed out.

$$\cancel{\frac{dE_{C.V.}}{dt}}^{1} = \cancel{\dot{Q}_{C.V.}}^{2} - \cancel{\dot{W}_{C.V.}}^{5} + \Sigma\dot{m}_i\left(h_i + \frac{1}{2}\cancel{\vec{V}_i^2}^{3} + \cancel{gZ_i}^{4}\right) - \Sigma\dot{m}_e\left(h_e + \frac{1}{2}\cancel{\vec{V}_e^2}^{3} + \cancel{gZ_e}^{4}\right)$$

Lastly, conservation of mass for a system operating at steady state dictates that $\Sigma\dot{m}_i = \Sigma\dot{m}_e$, or specific to this case $\dot{m}_{i,1} + \dot{m}_{i,2} = \dot{m}_e$. The resulting form of Equation 2.1 was rearranged to allow the outlet state to be solved directly. The final form of the interstage mixing model is shown in Equation 2.11.

$$h_e = \frac{\dot{m}_{i,1} * h_{e,1} + \dot{m}_{i,2} * h_{i,2}}{\dot{m}_{i,1} + \dot{m}_{i,2}} \tag{2.11}$$

2.5.3 Two Stage Flash Separation Model Solution

The two stage flash separation model was solved by setting the supply temperature to 50°C and setting the ambient temperature for the desired case. The intermediate saturation temperature was than varied in 1°C increments from $T_{ambient}$ to T_{supply} to locate the operating point that resulted in the highest COP.

2.6 Two Stage Economized Cycle

The two stage economized cycle diagram, shown in Figure 2.11, used two expansion valves. The second expansion valve was used to directly control the interstage injection mass flow rate. An additional heat exchanger, or economizer, was used to

increase the sub-cooling of the main refrigerant flow, as well as increase the vapour mass fraction of the injection stream.

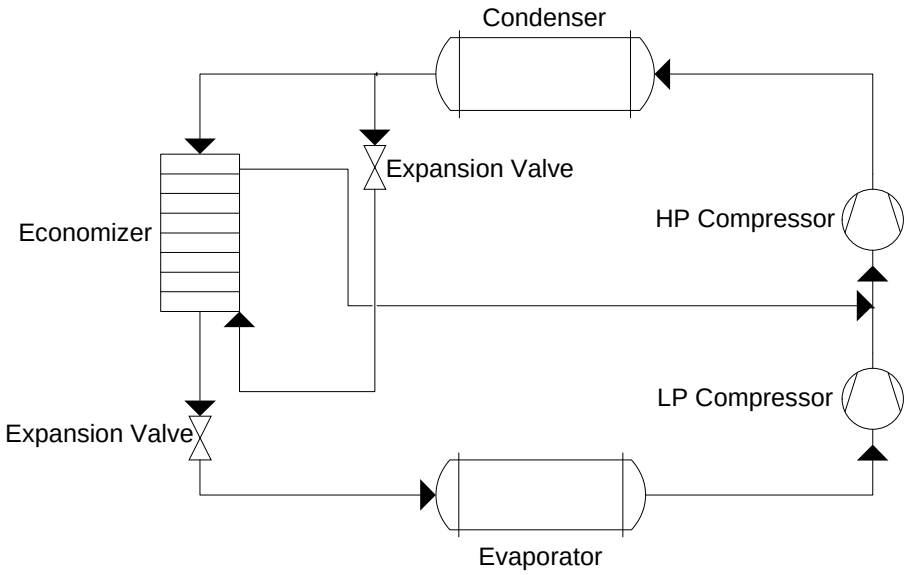

Figure 2.11: Two Stage Flash Separation Cycle Diagram

The method described in Section 2.5.2 was used to solve the interstage mixing process.

2.6.1 Economizer

The economizer was modelled as an ideal heat transfer process. The outlet states were calculated by solving the energy balance that is shown in Equation 2.12.

$$\dot{m}_1 * (h_1 - h_2) = \dot{m}_2 * (h_4 - h_3) \tag{2.12}$$

Where, $\dot{m}_1$ is the mass flow of the main refrigerant stream with states 1 and 2 referring to the inlet and outlet respectively, and $\dot{m}_2$ is the mass flow of the injected stream with states 3 and 4 referring to the inlet and outlet conditions respectively.

2.6.2 Two Stage Economized Model Solution

The two stage economized model was solved by setting the supply temperature to 50°C and setting the ambient temperature for the desired case. At each ambient temperature, the model was solved for all possible intermediate saturation temperatures between the ambient and supply temperatures. The mass flow rate of injection was than varied at each intermediate temperature by varying the injection ratio from 0 to 0.8, as defined in Equation 2.13.

$$X_{injection} = \frac{\dot{m}_{injection}}{\dot{m}_{condenser}} \tag{2.13}$$

where, $\dot{m}_{injection}$ is the mass flow of the injection stream and $\dot{m}_{condenser}$ is the mass flow through the condenser. The optimal COP was then chosen for each ambient temperature.

2.7 Modelling Results

The resulting COPs for each cycle were plotted for comparison across the operating range. These results are shown in Figure 2.12.

The results indicate that a substantial improvement in the COP of a heat pump can be achieved when two compressors are used. This is evident at all ambient temperatures that were studied. There is also a strong indication that the operating range of a heat pump can be extended to lower ambient temperatures than are currently being achieved by residential systems. Lastly, a COP of greater than 1.5 can be maintained at temperatures below -40°C which could eliminate the need for a backup heating system and reduce the energy consumption of these systems. Each of the two stage cycles shows similar performance with the cascade cycle being slightly lower performing than the flash separation and economized cycles. This is a result

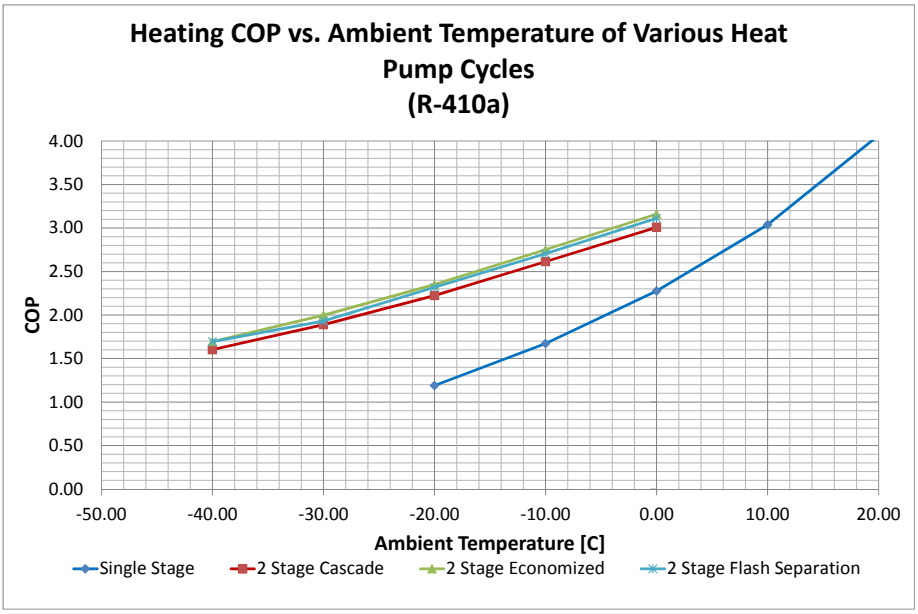

Figure 2.12: Modelling Results

of the additional work that is required to provide the temperature difference in the intermediate heat exchanger.

2.7.1 Effect of Intermediate Pressure on Performance

The optimal intermediate pressures for the two stage cycles were determined through trial and error. To illustrate the effect this parameter has on the performance of the cycles, the two stage economized model was used to plot the COP of the cycle against intermediate saturation pressure shown in Figure 2.13.

This indicates that there is an optimal intermediate pressure that corresponds to the maximum COP of the heat pump for each ambient temperature. The results show three regimes of performance. Below 350 kPa, the isentropic efficiency of the LP compressor is fixed at 70%, as the pressure ratio of this compressor is less than 2.6. Between 350 kPa and 950 kPa, both compressors are operating with pressure ratios greater than 2.6 and the isentropic efficiency is calculated using Equation 2.6. Above 950 kPa, the isentropic efficiency of the HP compressor is fixed at 70%, as the

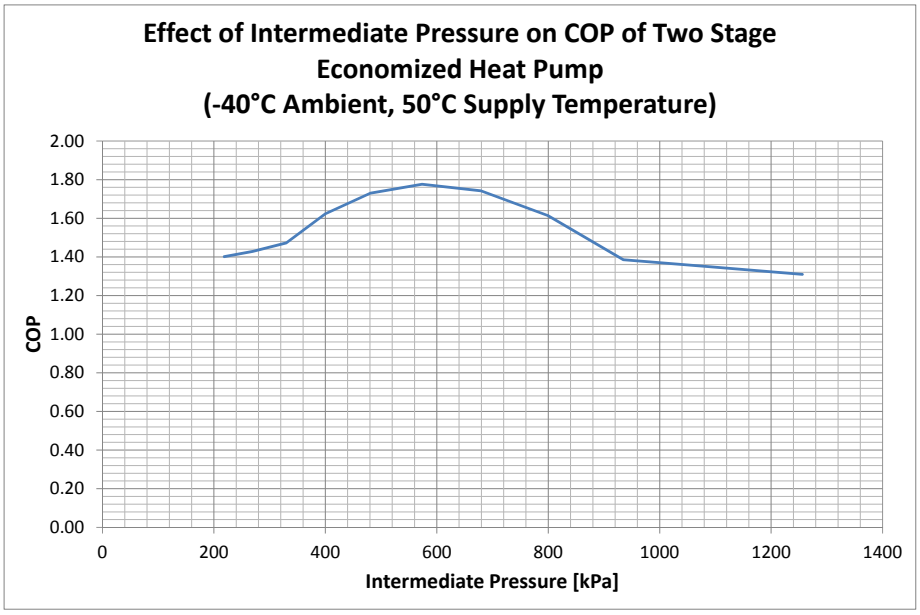

Figure 2.13: Effect of Intermediate Pressure on Two Stage Economized Heat Pump COP.

pressure ratio of this compressor is less than 2.6. In this example, a peak COP of 1.7 was reached at a saturation pressure of 570 kPa.

2.8 Closing Remarks

Because the two stage economized cycle shows the best performance across the operating range, it was considered to be the best candidate to use for the experimental stage. The remainder of this thesis will focus on the work that was done to build and test an experimental two stage economized heat pump.

Chapter 3

Experiment Design and Construction

This chapter outlines the work that was done to construct, instrument, and control the experimental two stage economized heat pump that was used for testing. This work was intended to allow the performance of the experimental system to be measured when it was operated in ambient temperatures that are comparable to Canadian climates.

3.1 Apparatus

Previously, work had been conducted at CanmetENERGY with a Mitsubishi Zuba cold climate heat pump. The Zuba is a single stage cold climate heat pump which incorporates a modulating compressor and an economized vapour injection system. This heat pump was modified to create a two stage economized cycle in a cost effective manner.

The Zuba heat pump is a two piece system consisting of an indoor and an outdoor unit. The indoor unit is a refrigerant-to-air heat exchanger that would be installed in an air handler within the home. The outdoor unit contains the outdoor refrigerant-to-air heat exchanger, the compressor, the four-way valve, the expansion valves, the economizer, the drier, the power receiver, and all of the electronics that are required to operate the heat pump. The system uses a variable speed scroll compressor and

operates using R-410a refrigerant as a working fluid. Figure 3.1 shows the refrigeration cycle for the Mitsubishi Zuba when operated in heating mode.

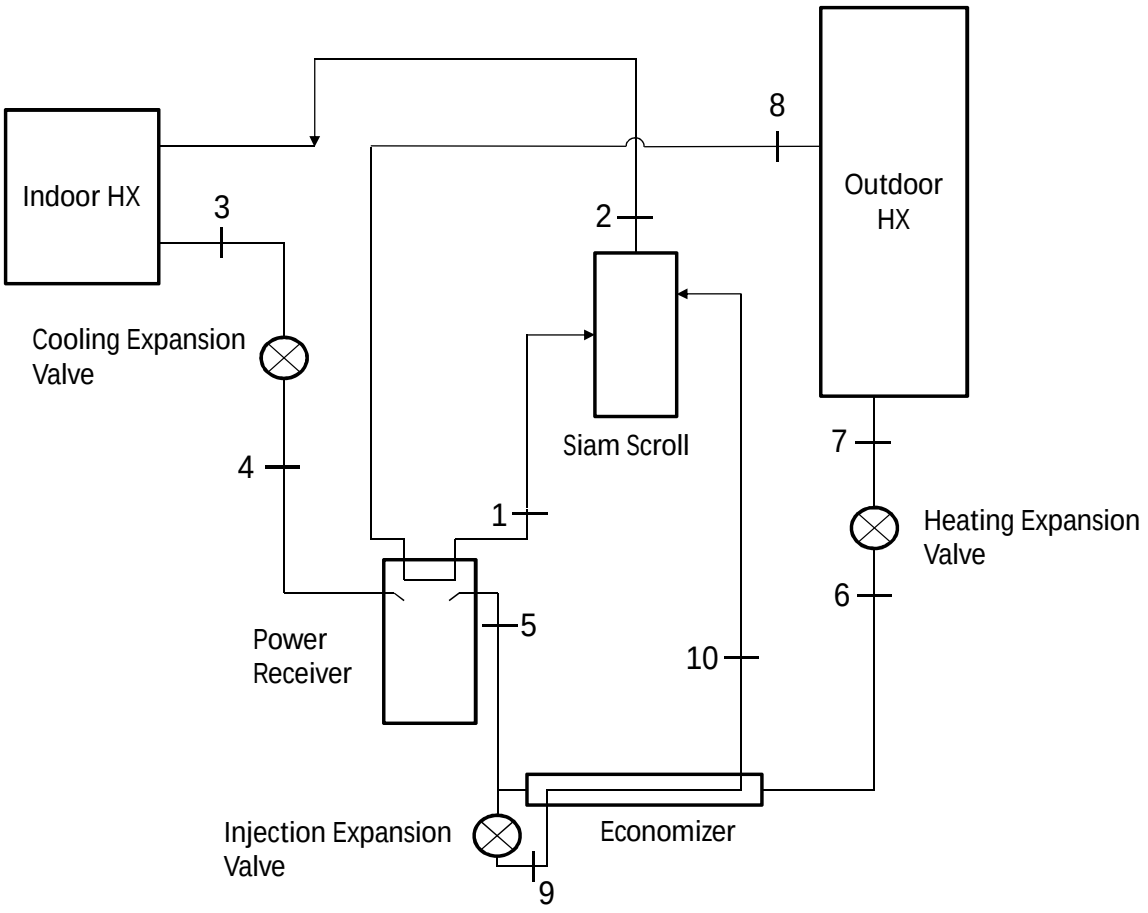

Figure 3.1: Mitsubishi Zuba Heat Pump Cycle (Heating Mode)

3.1.1 Refrigerant Path

Starting from the outlet of the compressor, labeled as point (2) on Figure 3.1, super-heated refrigerant flows to the indoor heat exchanger. The refrigerant condenses to a sub-cooled liquid as it exits at point (3) by transferring heat to the house. The liquid refrigerant then flows through the cooling expansion valve to the power receiver. The cooling expansion valve is always fully opened when the system is operated in heating mode. The power receiver serves two purposes in the cycle. First it ensures that a

supply of liquid is available to the expansion valves, and second, it provides additional super-heat to the suction gas for compressor protection. From the receiver, the liquid refrigerant at point (5) is split into two streams. The injection stream is expanded through the injection expansion valve to point (9) where it is then evaporated to a high vapour mass fraction state at point (10) which is injected into the compressor. The main stream at point (5) is further sub-cooled as it flows through the economizer to point (6) where it is expanded to point (7) through the heating expansion valve. It then travels through the outdoor heat exchanger where it is evaporated to a super-heated vapour at point (8) by absorbing heat from the ambient air. The main stream then flows through the power receiver to point (1), which increases the amount of super-heat of the vapour, before it enters the suction port of the compressor.

As this investigation was focused on the system operating in heating mode, the outdoor unit will be referred to as the evaporator and the indoor unit will be referred to as the condenser for the remainder of this document.

3.2 Cycle Modifications

In order to increase the accuracy of the heat transfer measurements, the condenser was replaced with a refrigerant-to-water heat exchanger. The heat produced by the heat pump was measured and dumped via a hydronic system at CanmetENERGY.

3.2.1 Low Pressure Compressor

A Denso ES-18c variable speed scroll compressor was sourced from a local auto wreckers for the second compressor. The ES-18c is a permanent magnet-based scroll compressor which uses an external inverter drive and was designed for operation with R-134a refrigerant in the second generation Toyota Prius. The choice to use this compressor was based solely on the price of acquisition and it should be noted that

this is not considered to be the optimal choice for a two stage system. Ideally, residential compressors would have been considered.

Three main concerns were raised about operating this compressor on R-410a refrigerant. First, the lubrication would need to be compatible with the new refrigerant and the old lubricant would need to be flushed from the compressor. Second, the compressor would need to structurally withstand the higher working pressures of R-410a. Third, the motor current would need to be the same or less than that of the designed motor current to avoid damaging the windings.

Lubrication compatibility was ensured by disassembling the compressor and flushing the parts using a Polyolester-based oil that is R-410a compatible. After reassembly, a small amount of the new oil was added to ensure lubrication during operation.

Structural soundness was ensured by imposing operating parameters. The compressor casing had pressure ratings of 1.67 MPa and 3.53 MPa for the suction and discharge ports respectively. A pressure of 1.67 MPa corresponds to a saturation temperature of 25°C for R-410a. Therefore, in order to ensure safe operation, the inlet saturation temperature was maintained below 25°C at all times.

To investigate the change in motor current that was expected when the compressor was operated with R-410a, a study of the motor torque was conducted in EES. This study compared the operating conditions of R-410a and R-134a that would be present at the compressor when delivering 1 kW of heat with a condenser saturation temperature of 40°C and an evaporator saturation temperature of 10°C. The relevant inlet and outlet conditions are shown in Table 3.1.

This indicates that for the given case study, when using R-410a, the Denso compressor would be subjected to a roughly doubled inlet pressure, and a pressure ratio of roughly one and one half times greater then when operated on R-134a. The compressor has a volumetric displacement of 18 cm^3/rev which was used to determine the rotational speed required to deliver the mass flow rate for each case. The torque

Table 3.1: Motor Torque Compatibility Study

Refrigerant	R-134a	R-410a
$P_{suction}$ [kPa]	414.9	1087
$P_{discharge}$ [kPa]	1017	2422
$\rho_{suction}$ [kg/m^3]	19.1	38.7
$\dot{W}_{compressor}$ [kW]	0.1039	0.1108
$\dot{m}$ [kg/s]	0.0052	0.0047
ω [rad/s]	95.9	43
Tq [Nm]	1.08x10^{-3}	2.58x10^{-3}

was calculated from the calculated work and the rotational speed. The torque is an important parameter because it is directly related to the electrical current that would be present in the motor. As this study used an arbitrary heating load, the additional torque doesn't directly imply that the motor would be overloaded when operated on R-410a. However, it does indicate that care must be taken to ensure that this is not the case. To minimize the risks associated with switching refrigerants, the Denso was installed as the LP stage in the cycle which ensured that the pressures were kept as low as possible. Also, since the density of R-410a at -20°C is close to that of R-134a at 10°C, the compressor was operating with suction densities similar to those it was designed for.

3.2.2 System Piping and Auxiliary Components

As the Zuba heat pump already incorporated an economizer, only slight modifications to the piping were required in order to change the location of the injection from within the original compressor to the new location between the LP and HP stages. Valving was also added to the cycle to allow the system to operate as either the original cycle, or the modified two stage economized cycle. Figure 3.2 shows the modified heat pump cycle that was operated in heating mode for testing. To operate the system in the original configuration, Vav-1 and Sol-2 were opened while Sol-1 was closed. To

operate the system in two stage mode, Vav-1 and Sol-2 were closed while Sol-1 was opened.

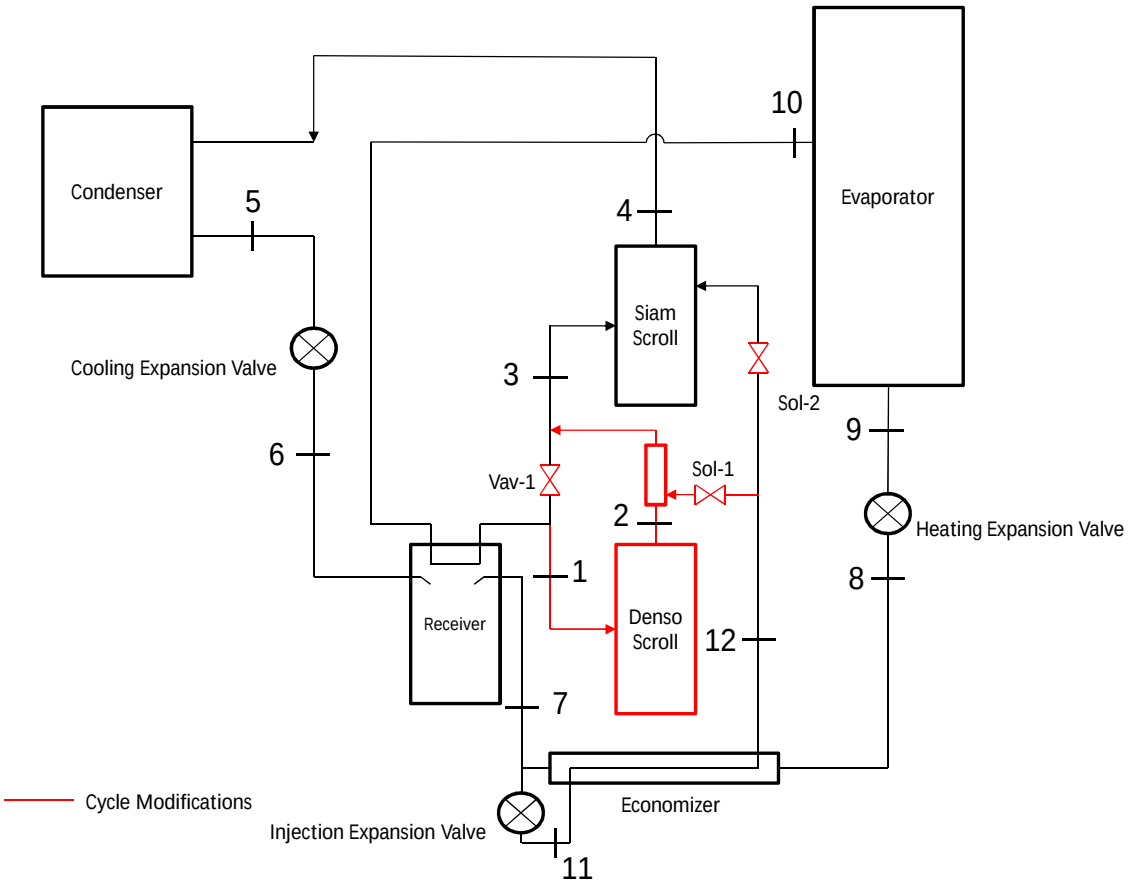

Figure 3.2: Two Stage Economized Heat Pump Cycle (Heating Mode)

3.2.3 Modified Refrigerant Path

To illustrate the operation of the heat pump in two stage economized mode, a detailed explanation of the refrigerant path is discussed here. Starting from the outlet of the compressor, labeled as point (4) on Figure 3.2, super-heated refrigerant flows to the indoor heat exchanger. The refrigerant condenses to a sub-cooled liquid as it exits at point (5) by transferring heat to the house. The liquid refrigerant then flows through

the cooling expansion valve to the power receiver. The cooling expansion valve is always fully opened when the system is operated in heating mode. The power receiver serves two purposes in the cycle. First it ensures that a supply of liquid is available to the expansion valves, and second, it provides additional super-heat to the suction gas for compressor protection. From the receiver, the liquid refrigerant at point (7) is split into two streams. The injection stream is expanded through the injection expansion valve to point (11) where it is then evaporated to a high vapour mass fraction state at point (12) which is injected between the two compressors through Sol-1. The main stream at point (7) is further sub-cooled as it flows through the economizer to point (8) where it is expanded to point (9) through the heating expansion valve. It then travels through the outdoor heat exchanger where it is evaporated to a super-heated vapour at point (10) by absorbing heat from the ambient air. The main stream then flows through the power receiver to point (1), which increases the amount of super-heat of the vapour, before it enters the suction port of the LP compressor. The refrigerant exits the LP compressor at point (2) where it is mixed with the injection stream from Sol-1, which reduces its temperature as it passes through point (3) before it enters the HP compressor. A picture of the modified heat pump is shown in Figure 3.3.

3.3 Control

In order to have direct control of the operating conditions in the heat pump, a new control system and auxiliary equipment were developed to replace the existing controls which offered limited user inputs. Table 3.2 outlines the individual components that were controlled.

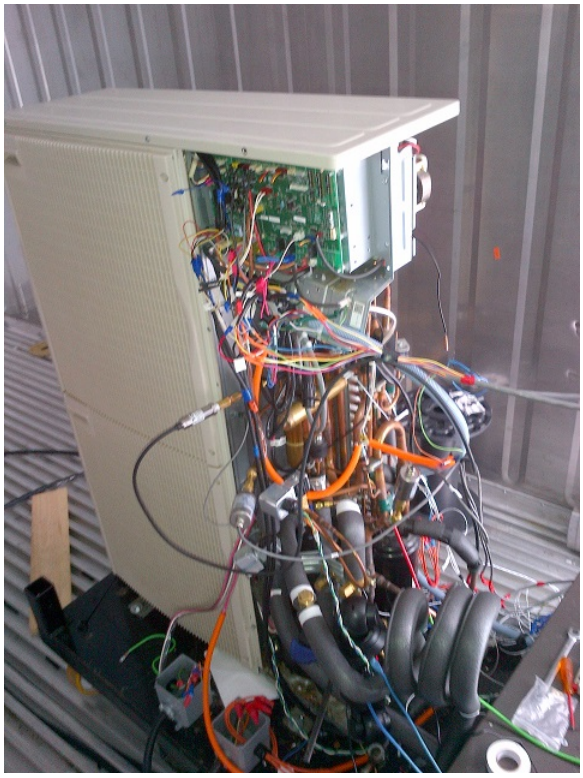

Figure 3.3: Modified Heat Pump

3.3.1 System Controller

The controller used was a National Instruments (NI) Compact RIO (cRIO) 9074. The NI cRIO-9074 is an embedded controller that runs the LabVIEW real-time operating system. It includes a 400 MHz processor, 128 MB of ram, 512 MB of storage and contains a Field Programmable Gate Array (FPGA). The operation of an FPGA is outlined in Appendix B. This controller uses the NI C-series modules for inputs and outputs which can be interchanged depending on the needs of the user. The modules used for this work are outlined in Table 3.3.

3.3.2 LP Compressor

The LP compressor was operated using a Hitachi WJ-200-022LF variable frequency drive (VFD). This VFD was chosen as it is designed to drive permanent magnet motors. The compressor speed was controlled using a 0 - 10 Vdc signal from the NI

Table 3.2: Controlled Components

Component	# to control	Component Input
LP Compressor	1	Three Phase Power, Variable Frequency/Voltage/Amperage
HP Compressor	1	Three Phase Power, Variable Frequency/Voltage/Amperage
Expansion Valve	3	Four Phase Stepper Motor Coil
Solenoid	2	120 Vac Power
4 Way Valve	1	240 Vac Power
Outdoor Fans	2	300 Vdc Power, 12 Vdc, and 0 - 6 Vdc Speed Control

Table 3.3: NI cRIO-9074 Modules

Module #	Type	# of Channels	Function
1	9217	4	100 Ω RTD
2	9217	4	100 Ω RTD
3	9217	4	100 Ω RTD
4	9217	4	100 Ω RTD
5	9219	4	Universal Analog Input
6	9263	4	0 - 10 V Analog Output
7	9401	8	High Speed Digital Input/Output
8	9401	8	High Speed Digital Input/Output

cRIO-9074 controller. Table 3.4 contains the parameters that were used to program the VFD.

3.3.3 HP Compressor

The HP compressor was operated using two different VFDs during the experiment. Initially a Hitachi SJ700-075LFUF2 was used. However, once it was installed it became apparent that the HP compressor was constructed using a permanent magnet motor and the SJ700 (SJ) series of VFDs is not designed to control these types of motors. Due to budgetary restrictions, initial testing was conducted using this VFD. The compressor was able to be operated for a small speed range using the simple

Table 3.4: Denso Motor Parameters

Parameter	Value
Motor Capacity	2.2 kW
Motor Poles	6
Motor Voltage	208 Vac
Motor Amperage	8 Arms
Motor Speed	340 Hz

voltage/frequency mode of this drive. This mode operates the motor by controlling the voltage applied to the windings for a given frequency based on table data that is entered by the user. After a portion of the testing was completed, a more suitable Hitachi WJ200-075LF (WJ) VFD became available and was installed. The performance of the system with the new VFD was compared to the data collected with the old VFD and the difference was found to be negligible. The only benefit was an increase in the controllability of the compressor which was not exploited for this work.

Table 3.5 outlines the parameters that were used to program the WJ VFD. The compressor speed was controlled using a 0 - 10 Vdc signal from the NI cRIO-9074 controller.

Table 3.5: Mitsubishi Motor Parameters

Parameter	Value
Motor Capacity	7.4 kW
Motor Poles	6
Motor Voltage	200 Vac
Motor Amperage	37 Arms
Motor Speed	360 Hz

3.3.4 Expansion Valves

The expansion valves were linear type valves which use a stepper motor to control their position. They are constructed with four electrical coils that were energized in a specific order to control the rotation. A FPGA code and an external current amplification circuit were used to control these valves during testing. A detailed explanation of the expansion valve control system can be found in Appendix C.

3.3.5 Solenoids and 4-Way Valve

The 4-way valve was used to switch the location of the evaporator and the condenser within the cycle. This allowed the system to provide either heating or cooling depending on the position of the valve. The solenoids were used to change the location of the economized vapour injection. This allowed for the vapour to be injected either at the original mid-compressor location, or at a new location between the LP and HP compressors. The solenoids and 4-way valve were operated by energizing electrical coils. A set of relays were used to control the solenoids and the 4-way valve from within the control software.

3.3.6 Fans

The fans in the outdoor unit were capable of variable speed operation. They required a 300 Vdc main power supply, a 15 Vdc power supply and a 0 - 6.5 Vdc signal to operate. A 300 Vdc power supply was constructed that rectified a 208 Vac power source. A two channel Sorensen bench top power supply was used to provide the 15 Vdc power supply and the 0 - 6.5 Vdc control signal. The fans were run at their maximum speed during testing to simplify the control of the system. A detailed explanation of the fan control circuits can be found in Appendix D.

3.3.7 Auxiliary Systems

The auxiliary systems included the remaining components that were required to test the heat pump system. These components controlled the evaporator and condenser temperatures.

As mentioned in Section 3.2, the condenser used during testing was a refrigerant-to-water type. The auxiliary system for the condenser side of the heat pump included a hydronic system that monitored the thermal energy produced by the heat pump and supplied the condenser with a controlled fluid temperature. This system was constructed using two separately controlled loops which were connected by a central buffer tank, as shown in Figure 3.4.

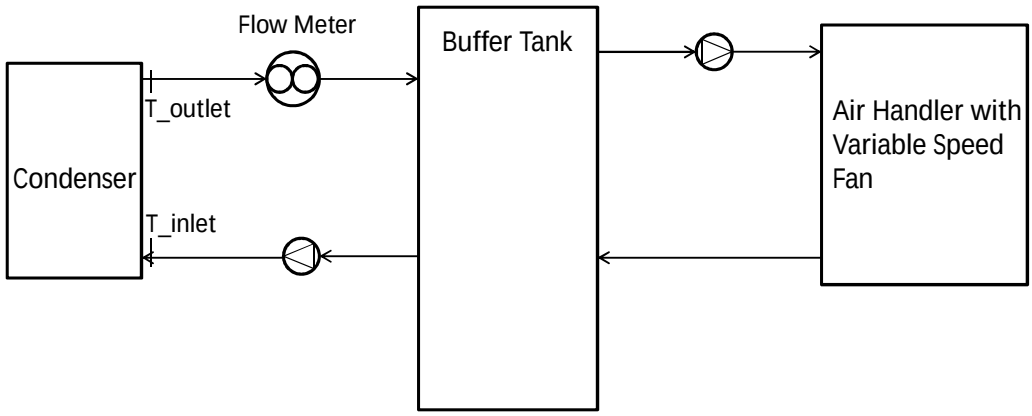

Figure 3.4: Hydronic System Schematic

The loop that connected to the heat pump included a pump, a flow meter and temperature sensors. The second loop included a pump and an air handler with a variable speed fan. The purpose of this loop was to remove heat from the system at a rate that provided a controlled supply temperature to the condenser inlet. The variable speed fan was controlled via a 0 - 10 Vdc signal from the NI cRIO-9074 controller. A picture of the hydronic system is shown in Figure 3.5.

Figure 3.5: Hydronic System

The evaporator temperature was controlled by placing the outdoor unit inside a refrigerated container. The original intent was to test the system at outdoor temperatures of -40°C and also have control over the ambient conditions. However, during commissioning it was discovered that the lower limit of the container's refrigeration cycle was -30°C and that only slightly colder temperatures could be achieved when the heat pump was operating. A picture of the refrigerated container is shown in Figure 3.6.

3.3.8 Programming

The programming was conducted using NI LabVIEW and it was implemented through four separate applications that were distributed across three pieces of hardware.

The NI cRIO-9074, outlined in Section 3.3.1, was used to control everything within the heat pump and also acted as the main data logger for the system.

Figure 3.6: Refrigerated Container

A second NI cRIO-9074 was used to run the hydronics lab. This controller was programmed to maintain the liquid supply temperature to the heat pump during testing.

Lastly, a desktop PC was used to control and provide feedback for the system via a user interface. A detailed explanation of the software can be found in Appendix E.

3.3.9 Instrumentation

The system instrumentation was split into two categories: critical and support. The instrumentation used to measure the performance of the system was considered critical and all efforts were made to minimize the inherent errors associated with their measurements. The additional instrumentation used for control and system operation was considered as support.

3.3.9.1 Critical Measurements

Critical measurements included all parameters that were required to determine the heating capacity ($\dot{Q}_H$) and coefficient of performance (COP) of the heat pump. The heating capacity was calculated using Equation 3.1.

$$\dot{Q}_H = \dot{V}\rho C_p \Delta T \tag{3.1}$$

where $\dot{V}$ is the volumetric flow rate of the fluid, ρ is the density of the fluid, C_p is the heat capacity of the fluid, and ΔT is the temperature differential of the fluid across the condenser.

The COP was calculated using Equation 3.2.

$$COP = \frac{\dot{Q}_H}{P_{elec}} \tag{3.2}$$

where $\dot{Q}_H$ is the heating capacity as defined in Equation 3.1 and P_{elec} is the electrical power required to operate the system.

The volumetric flow rate was measured using a Sparling Economag FM-618-0D1-000-01 flow meter. This meter operates using Faraday's Law of Magnetic Induction which is defined in Equation 3.3.

$$E_V = BL\bar{V} \tag{3.3}$$

where E is the induced voltage, B is the flux density of the magnetic field, L is the distance between the electrodes, and $\bar{V}$ is the bulk flow velocity of the liquid. The meter imposes a magnetic field across the pipe and uses electrodes to measure the induced voltage which is then converted to a volumetric flow rate inside the meter based on the cross sectional area of the pipe.

The temperature differential was measured using two Omega P-M-1/10-1/8-6-0-T-3 platinum resistance temperature detectors (RTD). RTDs operate based on the principle that the resistance of a conductor is a function of its temperature. The sensors selected were 100 Ω, 1/10 DIN accuracy 4 wire probes that were placed in thermowells located as close to the condenser as was possible. The thermowells were filled with a thermally conductive grease, and the piping and wiring were insulated as much as possible.

The fluid properties were assumed to be constant throughout testing and the values used in calculations were based on an operating temperature of 45°C. A detailed study of the implications of this assumption are included in Section 4.4.

The electrical power, P_{elec}, included the power required to drive both compressors, the outdoor unit fans, the indoor unit fans, and the internal electronics. Due to the nature of the experiment, the indoor unit fan power could not be included because this unit is internal to the hydronic system. The internal electronics were also replaced with NI equipment which was not representative of what would be used to operate a system like this in real-world applications. For these reasons, only the outdoor unit fan power and the power supplied to the compressors were included in the COP measurement. This may have caused the COP to show the system as over performing. However, modern air handlers with electronically commutated motors typically have very low power consumption compared to the total consumption of the heating system. Also, the consumption of the electronic controller was assumed to be negligible, as they typically consume less than 20 W. Lastly, the outdoor fan unit was determined to have a variable consumption of between 50 W to 300 W and during testing the fan was operated at full speed. In a market ready system, the fan speed would be reduced to match the capacity of the system to save power. Together, these factors resulted in more power consumption than was necessary, and any over statement of the COP was considered to be minimal.

All electrical measurements were made using two Tektronix PA-4000 power analyzers. These power analyzers are extremely flexible and are necessary to measure the advanced waveforms that are present in VFD systems. Each power analyzer includes four independent channels for the measurement of voltage and current. Both of the compressors were three phase machines and required three channels each. Each PA-4000 was programmed to measure three phase power and was set to pulse width modulation (PWM) mode. This mode allows for the high order harmonics, which are present when using VFDs, to be included in the measurement which was necessary to accurately measure the compressor power consumption. To ensure safe connections could be made during the measurements, electrical patch boxes, shown in Figure 3.7, were constructed to allow for the connection of insulated banana connectors between the power circuit and the PA-4000 analyzer. Five patch boxes were constructed and installed before and after each VFD and also at the fan circuit.

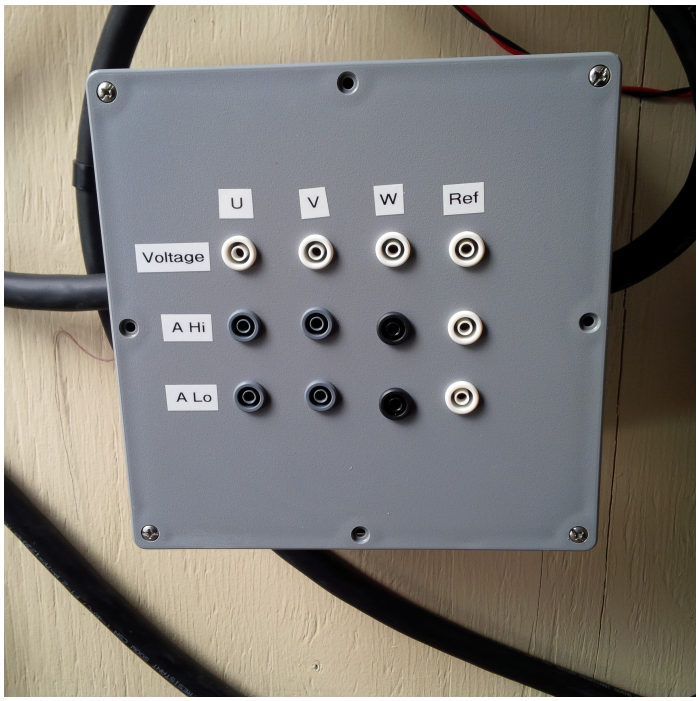

Figure 3.7: Power Measurement Patch Box

All of the measurements performed by the power analyzers were recorded on the desktop computer via a connection across the local network using LabVIEW and the standard commands for programmable instruments (SCPI) protocol. SCPI is a standardized text-based communication syntax which is widely used by laboratory instruments and makes these connections trivial.

3.3.9.2 Support Instrumentation

The support instrumentation provided the measurements that were used to control and monitor the refrigeration cycle. Pressure measurements were taken for the condenser, the evaporator and the intermediate pressures. These measurements were used to calculate the saturation temperatures of the refrigerant for control purposes. The evaporator and intermediate pressures were measured using Omega PX-303-300A5V pressure transducers and the condenser pressure was measured using an Omega PX409-500AI transducer. Theses sensors operate by measuring the strain present in a stainless steel diaphragm. The measured fluid is in contact with one side of the diaphragm while the other side is exposed to either ambient air or a vacuum depending on whether the sensor measures gauge or absolute pressure. The PX-303 transducers measured gauge pressure while the PX409 transducer measured absolute pressure.

Twelve temperatures were measured at locations throughout the refrigerant cycle using platinum RTDs. For these temperature measurements Omega PR-20-2-100-1/8-2-E-T sensors were used. These are class A RTDs which are less expensive than the 1/10 DIN RTDs used for the critical measurements. The sensors were installed by surface mounting the probes on the copper pipes and insulating them as much as possible. Figure 3.8 illustrates the installation of these probes.

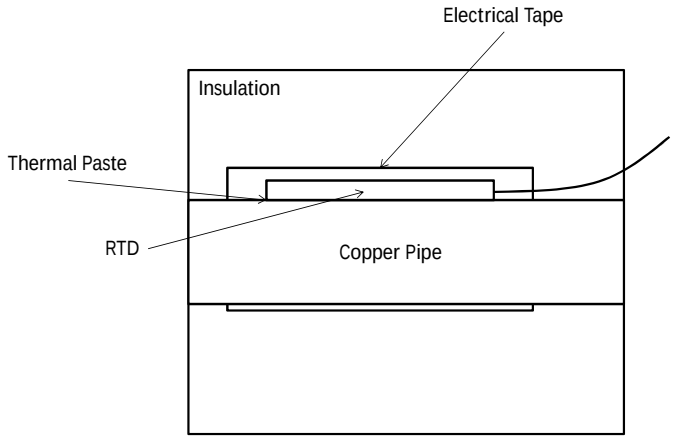

Figure 3.8: Surface Mounted RTD Section View

Figure 3.9 shows the location of the pressure sensors and the eleven temperature sensors that were installed on the heat pump. The remaining temperature sensor was used to measure the temperature of the air that was supplied to the evaporator.

3.4 Closing Remarks

An experimental apparatus was constructed and instrumented to allow the performance of a two stage economized heap pump to be characterized during cold weather operation. The following chapter outlines the work that was done to determine the uncertainty associated with the instrumentation.

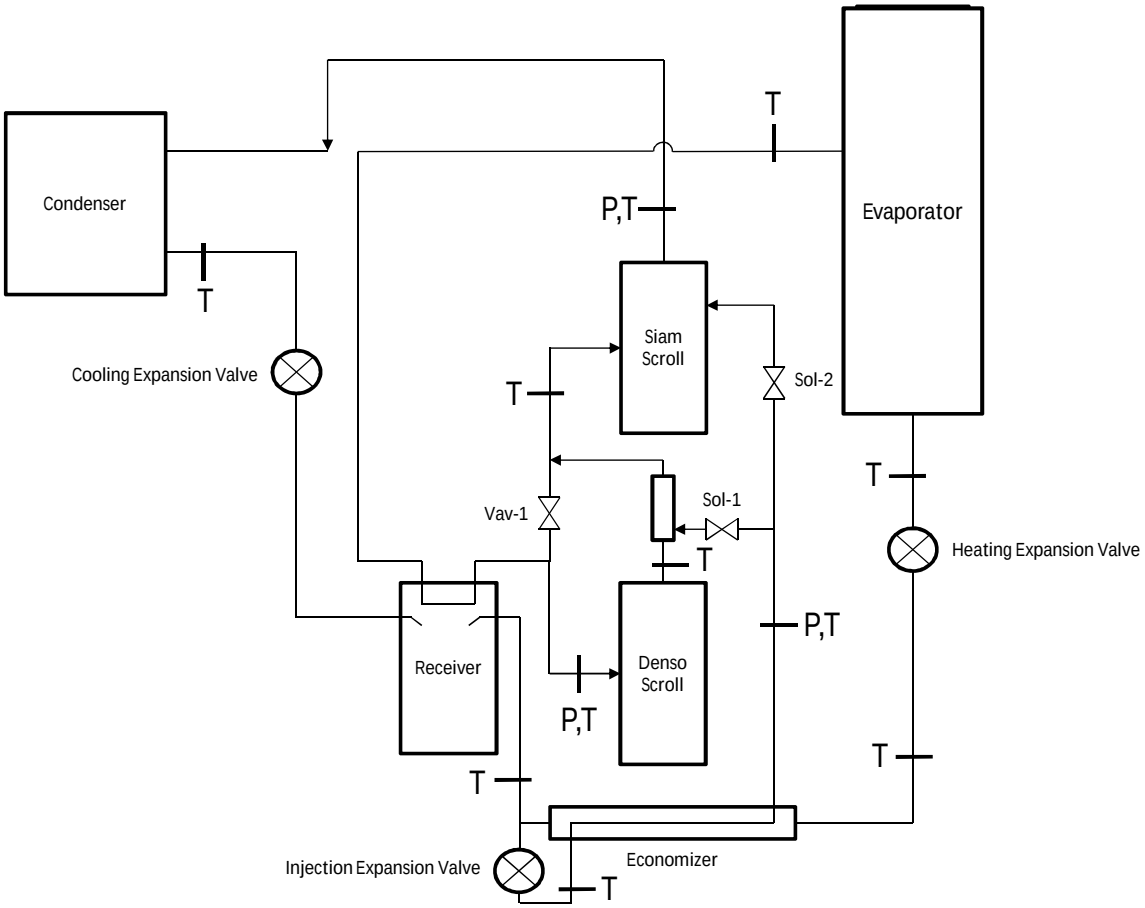

Figure 3.9: Installation Location of Support Instrumentation

Chapter 4

Uncertainty

To ensure the accuracy of the critical measurements outlined in Section 3.3.9.1, an uncertainty analysis was conducted using the procedure outlined by Moffat [19]. For each measured parameter, the associated error can be quantified by its precision error and its bias error. The precision error is used to describe the random error that occurs during an experiment while the bias error is used to describe the repeatable error margin for a single measured value.

4.1 Bias Error

Each measured value has multiple sources of bias associated with it that correspond to the individual components which make up the measurement system. These vary depending on the type of measurement being performed. The bias for the measured quantity can be determined by combining the bias associated with each component in the measurement system using Equation 4.1.

$$B_j = \sqrt{B_i^2} \tag{4.1}$$

where B_i is the bias for a given component in the measurement system and B_j the bias for the quantity produced by the measurement system.

The total bias error for a derived quantity can be computed by combining the individual bias error associated with each contributing measured value with a sensitivity factor, θ_j, using Equation 4.2.

$$B_T = \sqrt{\sum_j (\theta_j B_j)^2} \tag{4.2}$$

where B_T is the total bias error for the derived quantity, and θ_j is the sensitivity coefficient as described my Moffat [19], such that:

$$\text{For: } r = f(P_1, P_2, ...P_i)$$

where the derived quantity, r, is a function of the measured quantities, P_i. The sensitivity coefficient is defined using Equation 4.3.

$$\theta_j = \frac{\partial r}{\partial P_j} \tag{4.3}$$

4.2 Precision Error

The precision error for the average derived quantities, $\bar{S}$, can be calculated using the standard deviation, S, and the number of instantaneous derived measurement quantities, N, recorded over the sampling period, as shown in Equation 4.4.

$$\bar{S} = \frac{S}{\sqrt{N}} \tag{4.4}$$

4.3 Overall Uncertainty

The overall uncertainty margin, $\bar{U}$, for the average derived quantity can be determined by combining the total bias error and the precision error weighted by a student T statistic, t_s, as shown in Equation 4.5.

$$\bar{U} = \sqrt{B_T^2 + t_s \bar{S}} \tag{4.5}$$

where the student T statistic is chosen based on the number of samples and the desired confidence interval. For the testing conducted, the average derived values were based on a sample size of 300. When the number of samples is greater than 120, the standard deviation is considered to be an accurate representation of the population. Therefore, the student T statistic was replaced with a value of 2 to give a confidence interval of 95.4%.

4.4 Heating Capacity Uncertainty

The uncertainty of the heating capacity measurement was calculated using the approach outlined above. A sample calculation has been included in this section for clarity. The heating capacity was calculated using Equation 3.1. The example given here corresponds to a flow rate of 0.35 L/s and a temperature differential of 2.5°C with a mean fluid temperature of 45°C which is representative of what was observed during testing.

The volumetric flow rate was measured using the Sparling flow meter as outlined in Section 3.3.9. The meter was scaled to a maximum flow of 30.28 L/min and outputted a 4 - 20 mA signal that is linearly proportional to the flow rate. The signal was measured using a NI-9219 universal 24 bit input module that was configured to measure 0 - 25 mA. The software calculated the flow rate using Equation 4.6 which converts the mA signal from the meter to a flow rate in L/s.

$$\dot{V} = (A - 0.004) * 31.545 \tag{4.6}$$

where $\dot{V}$ is the volumetric flow rate of the fluid and A is the measured signal in amps. Table 4.1 shows the rated component level accuracies and the corresponding bias error associated with the flow rate measurement.

Table 4.1: Heating Capacity Component Bias Errors for Example Case

Sparling Meter Rating [Flow = 0.35 L/s]	
Rated bias	0.75 % Rate
Sparling Meter B_i Components	
$B_{Sparling}$	± 0.00263 L/s
NI 9219 Rating[Signal = 0.0151 A]	
Gain Error	± 0.1 % Reading
Offset Error	± 30 ppm Range
NI 9219 B_i Components	
$B_{NI_{Gain}}$	± 3.5x10^{-4} L/s
$B_{NI_{Offset}}$	± 2.37x10^{-5} L/s
Volumetric Flow Rate Bias Error	
B_j	± 2.65x10^{-3} L/s

The heat transfer fluid used was Diversitech ProTek-PLUS which is a 95% pure propylene glycol fluid with corrosion inhibitors making up the balance. The fluid was diluted during commissioning and the mixture was determined by measuring the fluid's refractive index using an ATAGO PAL-RI meter. Diversitech does not publish the heat capacity of its fluids so the refractive index was used to look up the corresponding values in the Dow document, A Guide to Glycols [20] which contains information about aqueous solutions of propylene glycol and is available on their website.

As testing was conducted with the heat transfer fluid operating in the temperature range of 40°C to 50°C, the values for both the density and the heat capacity were taken at 45°C, and these values were assumed constant throughout testing. To account for the variation in the fluid properties caused by changes in fluid temperature, the bias of the fluid properties were based on the variation of the fluid properties across the temperature range of 40°C to 50°C. These fluid properties and their associated bias errors are shown in Table 4.2.

Table 4.2: Heat Transfer Fluid Properties and Associated Bias Errors for Example Case

Aqueous Propylene Glycol Solution	
Refractive Index [n]	1.3604
Glycol % by Volume	23.4
Glycol % by Weight	24
Density	
$\rho_{45°C}$	1.007 kg/L
B_ρ	± 0.003 kg/L
Heat Capacity	
$Cp_{45°C}$	4.0386 kJ/kg C
B_{Cp}	± 0.00586 kJ/kg C

The temperature difference was measured using two platinum RTDs that were connect via four wire circuits to a NI 9217 24 bit RTD input module. The resistance was measured and converted to temperature in software using a calibrated polynomial fit whose associated bias error was orders of magnitude smaller than the other relevant sources of error and was therefore neglected. Information regarding the polynomial fitting is outlined in Section 4.6.1. Table 4.3 outlines the sources of error that were considered for the temperature measurement.

Table 4.3: Temperature Differential Bias Error

1/10 DIN Platinum RTD	
B_{RTD}	± 0.08°C
NI 9217 RTD Module	
B_{daq}	± 0.15°C
Temperature Bias Error	
$B_{Temperature}$	± 0.17°C
Differential Bias	
$B_{\Delta T}$	± 0.24°C

The total bias error for the derived quantity $\dot{Q}_H$ was calculated using Equation 4.2. The sensitivity factors, total bias errors, and contributing bias terms are shown

Table 4.4: Heating Capacity Sensitivity Factors and Total Bias Error

Heating Capacity Sensitivity Factors for Example Case		
Factor	Equation	Example Value
$\theta_{\dot{V}} = \frac{\partial \dot{Q}}{\partial \dot{V}}$	$\theta_{\dot{V}} = \rho Cp \Delta T$	10.167 $\frac{kJ}{m^3}$
$\theta_{\rho} = \frac{\partial \dot{Q}}{\partial \rho}$	$\theta_{\rho} = \dot{V} Cp \Delta T$	3.534 $\frac{kJ*m^3}{kg*s}$
$\theta_{Cp} = \frac{\partial \dot{Q}}{\partial Cp}$	$\theta_{Cp} = \dot{V} \rho \Delta T$	0.881 $\frac{kg*^\circ C}{s}$
$\theta_{\Delta T} = \frac{\partial \dot{Q}}{\partial \Delta T}$	$\theta_{\Delta T} = \dot{V} \rho Cp$	1.423 $\frac{kJ}{s*^\circ C}$
Contribution to Derived Quantity Bias Error for Example Case		
Term	Total Bias Error [kW]	
$\theta_{\dot{V}} B_{\dot{V}}$	0.027	
$\theta_{\rho} B_{\rho}$	0.011	
$\theta_{C_p} B_{C_p}$	0.005	
$\theta_{\Delta T} B_{\Delta T}$	0.341	
Heating Capacity Total Bias Error [B_T]		
$B_{\dot{Q}}$	$\pm$ 0.343 kW	

in Table 4.4. As expected, the bias errors associated with the temperature difference are the dominating contributers to the total bias error of the derived heating capacity.

The precision error was combined with the total bias error using Equations 4.4 and 4.5. For this example, the standard deviation used was based on typical values observed during testing. Table 4.5 shows the relevant parameters used to calculated the total uncertainty of the measured heating capacity of the system.

Table 4.5: Heating Capacity Total Uncertainty for Example Case

Precision Error Calculation [2 Standard Deviations]		
Parameter	Definition	Example Value
S	Standard Deviation of Average Derived Quantity	0.015
N	Number of Samples Measured	300
$\bar{S}$	8.66x10^{-4}	
Heating Capacity Total Uncertainty [$\bar{U}$]		
$\bar{U}$	$\pm$ 0.346 kW	

For this example, the thermal output was 3.56 kW which represents an error of 9.7% for the derived quantity.

4.5 COP Uncertainty

The same process was used to calculate the uncertainty of the COP measurement. The example used in Section 4.4 will be reused in this section, assuming an input work of 1.5 kW.

The COP was calculated using Equation 3.2. The power was measured using the PA-4000 power analyzer which measured three phase voltage and current and calculated the power internally. According to the manual, the power measurement accuracy of the analyzer is defined using Equation 4.7.

$$\begin{aligned} P_{acc} = (V_{rms_{acc}} A_{rms} PF) \\ \pm(A_{rms_{acc}} V_{rms} PF) \\ \pm(V_{rms} A_{rms}(\cos\theta - \cos(\theta \pm (Vh1_{pherr} \pm Ah1_{pherr}))) \end{aligned} \tag{4.7}$$

where V_{rms} is the measured root mean square (RMS) Voltage, A_{rms} is the measured RMS Amperage, PF is the measured power factor, θ is the measured phase angle, $V_{rms_{acc}}$ is the accuracy of the voltage reading, $A_{rms_{acc}}$ is the accuracy of the amperage measurement, $Vh1_{pherr}$ is the accuracy of the phase of the first voltage harmonic, and $Ah1_{pherr}$ is the accuracy of the phase of the first amperage harmonic.

Each of the accuracy terms listed have different values that depend on the voltage, current and frequency ranges the power analyzer was configured for during measurement. As this calculation is quite complex and lengthy, the details of this process are not included in this thesis. However, the parameters listed in Equation 4.7 that

were used during the uncertainty analysis are included in Appendix F, along with the calculated bias errors associated with the power measurements.

The largest bias error for the three phase power measurement that was calculated during testing was 0.0043 kW. This value is used for the following example.

The bias errors that were calculated are shown in Table 4.6 along with the sensitivity factors and the total bias error for the COP measurement.

Table 4.6: COP Bias Error Calculation for Example Case

Bias Components		
$B_{\dot{Q}}$	± 0.343 kW	
B_{elec}	± 0.0043 kW	
Sensitivity Factors		
Factor	Equation	Example Value
$\theta_{P_{elec}}$	$\theta_{P_{elec}} = \frac{\partial COP}{\partial P_{elec}} = -\frac{\dot{Q}}{P_{elec}^2}$	1.582 $\frac{1}{kW}$
$\theta_{\dot{Q}}$	$\theta_{\dot{Q}} = \frac{\partial COP}{\partial \dot{Q}} = \frac{1}{P_{elec}}$	0.667 $\frac{1}{kW}$
COP Total Bias Error		
B_{COP}	± 0.229	

The standard deviation for this example was taken as a typical value observed during testing where S was in the range of 0.015. Table 4.7 shows the precision error and the total uncertainty calculation for the COP.

Table 4.7: COP Precision Error and Total Uncertainty for Example Case

Precision Error	
S	0.015
N	300
$\bar{S}$	± 8.66x10^{-4}
Total Uncertainty	
$\bar{U}$	± 0.233

For this example, the COP was 2.37 and the corresponding error would be 9.8%.

4.6 Calibration and Uncertainty Reduction

As the dominant source of uncertainty in the derived quantities is associated with the temperature differential measurement, additional effort was made to improve the bias associated with these measurements.

The procedure used here is based on the steps outlined in Sections 4.1, 4.2, and 4.3 with an alternate approach used to quantify the bias error associated with the temperature measurements. The first approach assumed that the bias errors in the system were independent from one another and took the worst case approach when combining them, where each bias increases the total bias of the measurement system. This approach can be said to be valid for interchangeability. This means the calculated uncertainty is valid for any physical hardware that shares the same rated bias and is combined in the same configuration.

The modification used here considers the measurement system as a whole, and results in the direct measurement of the total bias error for the derived quantity $B_{Temperature}$. It is based on two assumptions. First, the rated bias of a component includes a level of quality control during manufacturing and an individual component could have a bias that is lower than its rating. Second, it is conceivable that when real devices are combined to create a measurement system, some of the bias errors may combine to reduce the total bias of the measured quantity.

Using these assumptions, this procedure presents a systematic approach to quantifying and monitoring the bias of a measurement system using a calibrated reference system. It requires the use of additional specialized equipment and it is not valid for interchangeability. This means the bias is specific to the hardware as it is installed, and any changes made to the components or system would require the procedure to be repeated. The procedure is split into three steps: calibration, quantification and verification which are described in the following sections.

4.6.1 Calibration

The calibration procedure requires the use of a calibrated reference thermometer and an environment that is stable enough to allow comparison between the reference thermometer and the temperature measurement system. A Fluke 5616-12 Secondary Platinum Resistance Thermometer (SPRT) and a Fluke 1502A SPRT digital readout were used as the calibrated reference thermometer. A calibrated Fluke 7340 liquid bath that was filled with Dow Corning silicone oil 200.10 was used as the stable environment.

As the calibration was conducted by considering the measurement system as whole, the procedure was conducted after the RTDs were installed in the experimental apparatus and connected to the data acquisition system (DAQ). The cabling allowed the RTDs to be placed in the bath without requiring any electrical disconnections and the resistance readings were recorded by the DAQ. The SPRT was also placed into the bath and the readout was recorded via a serial connection with a desktop computer. Both data sources were recorded at ten second intervals. The bath was programmed to span the temperature range of 40°C to 61°C in 3°C steps where it would hold the temperature at each step for 20 minutes once the bath reached stability. The dataset was reduced by averaging the last 5 minutes of data for each temperature point.

Lastly, the resistance measurements of the RTDs were regressed to the temperature measurements of the SPRT using a second order polynomial. The polynomials were added to the DAQ software to allow for direct temperature readings with units of degrees Celsius. This step produced a calibrated temperature measurement system for each RTD channel that was used for the remainder of the procedure. This step was also conducted for the support RTDs with the bath spanning the range of -30°C to 110°C in 10°C increments.

4.6.2 Bias Quantification

The approach used to quantify the bias of the calibrated temperature measurement system was based on a statistical analysis of the calculated error between the calibrated temperature measurements and the measurements of the SPRT. This required a dataset that captured the long term drift and instabilities that were present in the system. As the amount of data required to accomplish this was unknown, an assumption was made based on the nature of the measurement, and the verification stage was used to confirm an appropriate sample was acquired.

The bath was set to 50°C and data were collected for multiple days. Ideally, this procedure would have been repeated for a variety of temperatures spanning the operating range of the system, but due to time restrictions, only one temperature was used for the quantification stage.

Figure 4.1 plots the raw temperature readings directly against the readings from the SPRT. It shows a normal distribution in the measured error relative to the SPRT.

The error for each sample was calculated using Equation 4.8

$$\epsilon_T = T_{Calibrated} - T_{Reference} \tag{4.8}$$

where ϵ_T is the measured error associated with a sample in the data.

Figure 4.2 plots the time series of the calculated error in the readings from the RTDs relative to the SPRT. It shows that each channel contains some noise, as well as a diurnal fluctuation, with $T_{waterout}$ fluctuating greater and in opposition to $T_{waterin}$. The difference in rising edge to trailing edge slope in the $T_{waterout}$ measurement is thought to be caused by the morning sun warming a portion of the measurement system. However, it is not the intention of this thesis to determine the cause of the errors, but simply to quantify them.

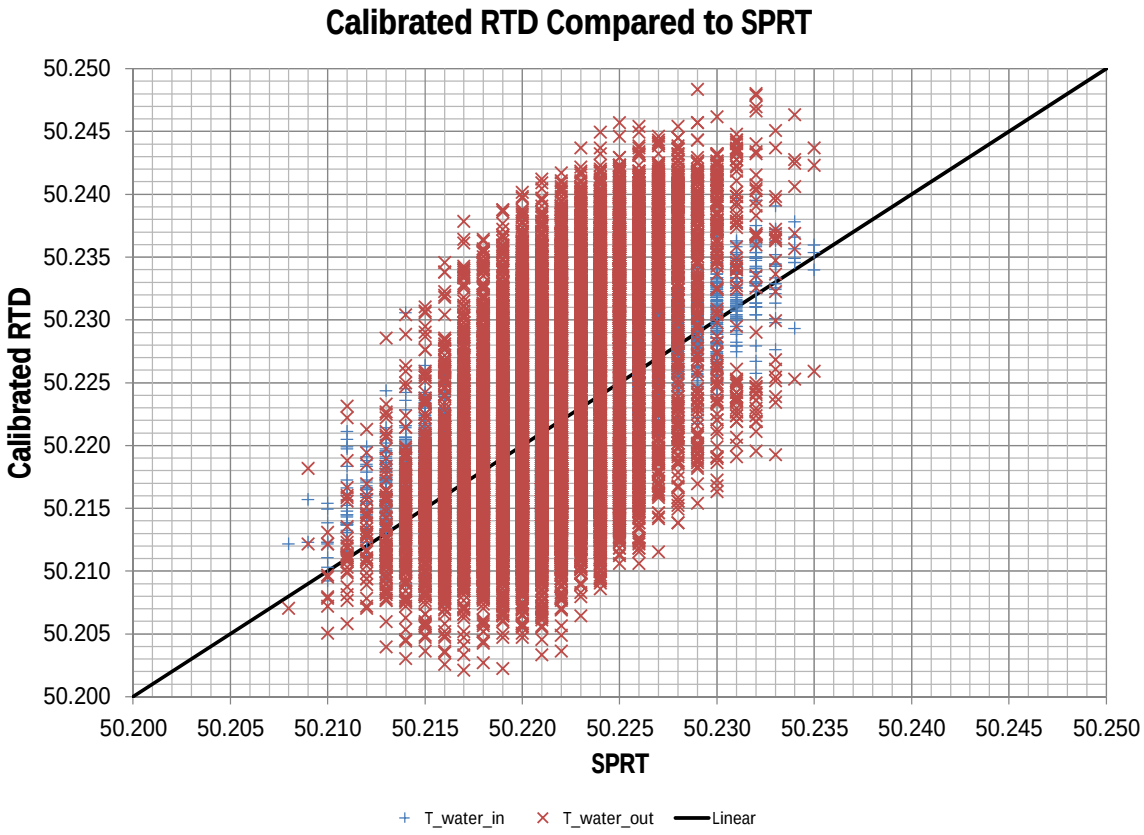

Figure 4.1: Measured Temperature vs. SPRT Reading

Figures 4.1 and 4.2 each give a representation of how well the calibrated temperature measurements agree with that of the reference SPRT. If this comparison was continued during the experimental work, then the calculated bias of the data would be an exact measurement of the bias of the temperature system with respect to the SPRT. Unfortunately this is not realistic, as the sensors cannot be in the bath during experimentation. Therefore, this measured approach was used to estimate the bias in the temperature measurement system.

The bias errors associated with the temperature measurements were calculated by combining the absolute value of the mean of the errors with three standard deviations using Equation 4.9.

$$B_{TemperatureMeasurement} = |\bar{X}_{\epsilon_T}| + 3 * S_{\epsilon_T} \tag{4.9}$$

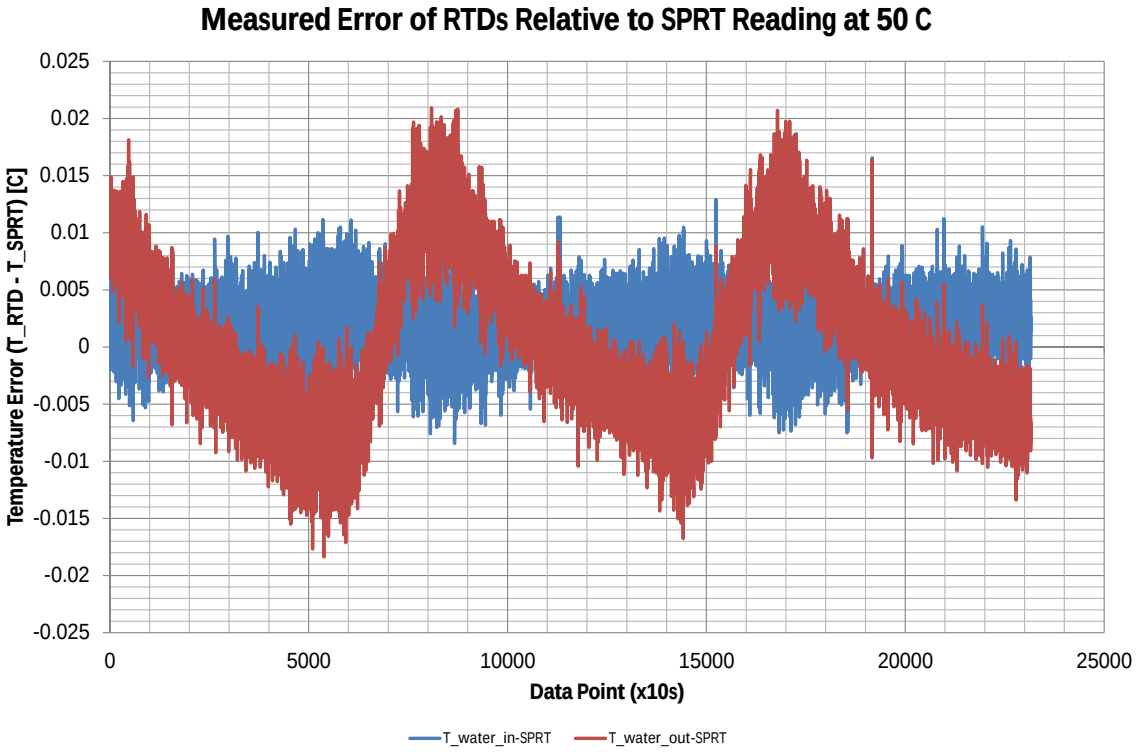

Figure 4.2: Time Series of Long Term Temperature Difference Data

where $\bar{X}_{\epsilon_T}$ and S_{ϵ_T} are the mean and standard deviation of the errors respectively. The calculated bias for $T_{WaterOut}$ was used for both the inlet and outlet water temperature measurements in order to slightly overestimate the bias of the temperature differential and to add additional confidence to the data that were collected. Since the SPRT and readout were used as the reference for comparison and they each contain bias error terms, their bias errors were combined with the calculated bias of the data using Equation 4.1. The bias errors for the temperature measurements and the calculated temperature differential that resulted from this approach are shown in Table 4.8.

This approach shows a significant improvement over the bias error that was calculated in Table 4.3. If the example from Sections 4.4 and 4.5 is repeated using the measured bias error, the uncertainty of the measured heating capacity is reduced from $\pm$ 0.346 kW to $\pm$ 0.072 kW and the error is reduced from 9.7% to 2%. The uncertainty and error of the COP measurement is improved by similar amounts.

Table 4.8: Measured Temperature Differential Bias Error [$B_{\Delta T}$]

Measured Error Absolute Mean	
$\bar{X}_{\epsilon_{T_{WaterIn}}}$	0.0020°C
$\bar{X}_{\epsilon_{T_{WaterOut}}}$	0.0004°C
Measured Error Standard Deviation	
$\sigma_{T_{WaterIn}}$	0.0023°C
$\sigma_{T_{WaterOut}}$	0.0067°C
Calculated Bias Relative to SPRT	
$B_{T_{WaterIn}}$	0.0088°C
$B_{T_{WaterOut}}$	0.021°C
SPRT Bias Error	
B_{SPRT}	± 0.011°C
$B_{Readout}$	± 0.009°C
Combined Bias Error	
$B_{TemperatureMeasurement}$	± 0.0254°C
$B_{\Delta T}$	± 0.036°C

4.6.3 Verification

The verification step is intended to show that the measured bias error is repeatable and give confidence that the original dataset was large enough to accurately quantify the bias error.

Verification is the process of occasionally checking the calibrated temperature measurement system against the reference system. This is done by comparing the measured relative bias between the measured temperatures and the reference probe with the relative bias that was calculated in Section 4.6.2. The frequency of verification should be representative of the criticality of the measurements in order to give confidence in the measurement accuracy. For the experimental work presented here, verification was done once testing was completed. The original calibration and quantification procedures were conducted on September 25 and 26, 2014 respectively and the verification was conducted on February 2, 2015. This was considered to be reasonable as it would have captured any long term drift in the electronics that occur due to either time or seasonal changes in temperature and humidity.

During verification, the temperature probes were returned to the temperature bath with the SPRT, and data were collected at 30°C and 50°C with each temperature checked twice to increase the sample size of the data. Data were recorded for five minutes at each temperature at a rate of one sample per second. This produced four sets of data consisting of 300 samples for each of the temperature channels, as shown in Figures 4.3 and 4.4.

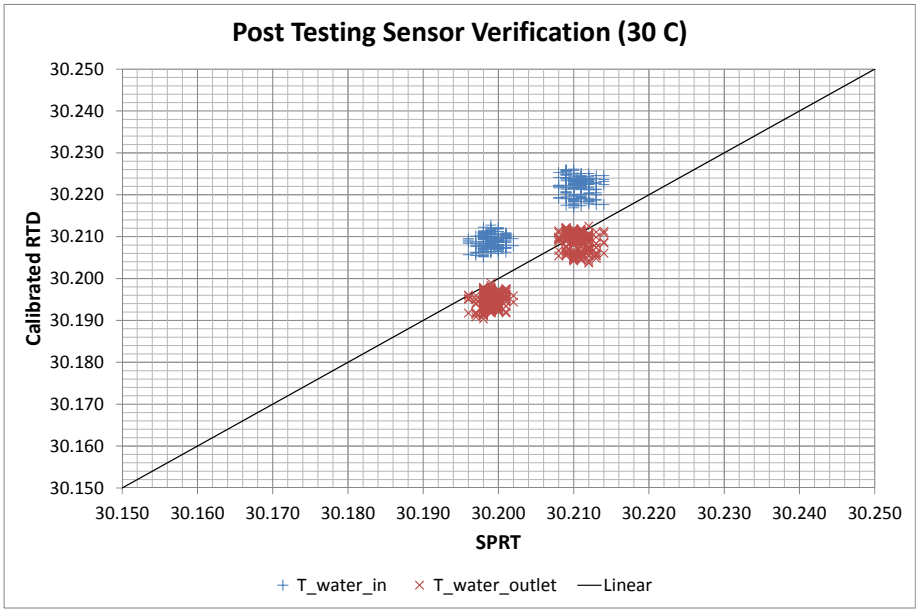

Figure 4.3: Verification Data 30°C

The measured bias error was calculated for each dataset using the method outlined in Section 4.6.2. The results shown in Table 4.9 verify the quality of the data that were used during quantification. The highest relative bias error calculated during verification was 0.022°C which is 0.001°C greater than the relative bias that was calculated in Section 4.6.2. This increase indicates a negligible difference between the calculated uncertainties of the results, therefore, the procedure outlined here was considered to be a valid method of reducing the uncertainty of the measurement system.

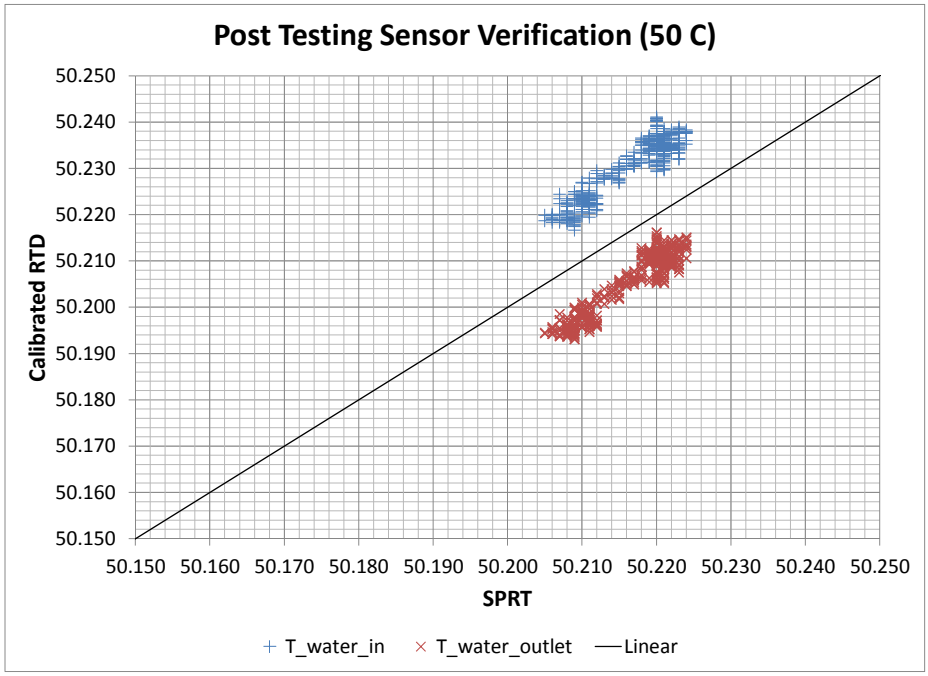

Figure 4.4: Verification Data 50°C

Table 4.9: Measured Temperature Bias Error During Verification

	$T_{WaterInlet}$			$T_{WaterOutlet}$		
T_{Bath}	$\lvert\bar{X}_{\epsilon_T}\rvert$	σ_{ϵ_T}	$B_{T_{Relative}}$	$\lvert\bar{X}_{\epsilon_T}\rvert$	σ_{ϵ_T}	$B_{T_{Relative}}$
30°C	0.012°C	0.003°C	0.019°C	0.002°C	0.002°C	0.010°C
50°C	0.014°C	0.002°C	0.020°C	0.010°C	0.002°C	0.017°C
50°C	0.014°C	0.003°C	0.022°C	0.012°C	0.002°C	0.019°C
30°C	0.010°C	0.002°C	0.015°C	0.004°C	0.002°C	0.010°C

Chapter 5

Test Plan and System Operation

The experimental work was intended to quantify the steady state performance of the system when operated at ambient temperatures that are present in Canadian climates. Table 5.1 outlines the test matrix that was used during the planning stages of the experiment.

Table 5.1: Test Matrix 50°C Supply Temperature

	Ambient Temperature [°C]				
System Mode	0°C	-10°C	-20°C	-30°C	-40°C
Single Stage					
Single Stage Economized					
Two Stage Economized					

During commissioning, it was discovered that the lowest temperature achievable in the cold chamber was -31°C. Also, the HP compressor outlet temperature was above the rated maximum when the supply temperature was 50°C. The test plan was modified by removing the -40°C test point and lowering the supply temperature to 40°C to reflect these limitations. During single stage and single stage economized operation, the HP compressor outlet temperature continued to be above the rated maximum when the ambient temperature was below -23°C. The test plan was further modified to avoid single stage operation below this temperature. Table 5.2 shows the modified version of the test matrix that was used during testing.

The system operating modes are defined as follows:

Table 5.2: Modified Test Matrix 40°C Supply Temperature

	Ambient Temperature [°C]			
System Mode	0°C	-10°C	-20°C	-30°C
Single Stage				NA
Single Stage Economized				NA
Two Stage Economized				

- Single Stage - The original cycle configuration without economized vapour injection.
- Single Stage Economized - The original cycle configuration with economized vapour injection.
- Two Stage Economized - The modified cycle with interstage economized vapour injection.

The cycle schematics for each of these operating modes are shown in Figure 5.1.

For all of these configurations, the HP compressor was initially operated at a fixed speed of 90 Hz. This speed resulted in stable operation of the motor when the SJ series VFD was used. Also, this speed kept the mass flow rates of each stage within a range that would allow for operation in the two stage economized configuration. The HP compressor was able to operate at much higher speeds; however, doing so would increase the mass flow in the system beyond the operating range of the smaller LP compressor. To investigate the effect the HP compressor speed had on the operating performance, the tests were repeated with the HP compressor operating at 80 Hz once the WJ series VFD was installed.

5.1 System Operation

The strategy used to test the system was developed during commissioning and allowed for good stability with minimal downtime between test points.

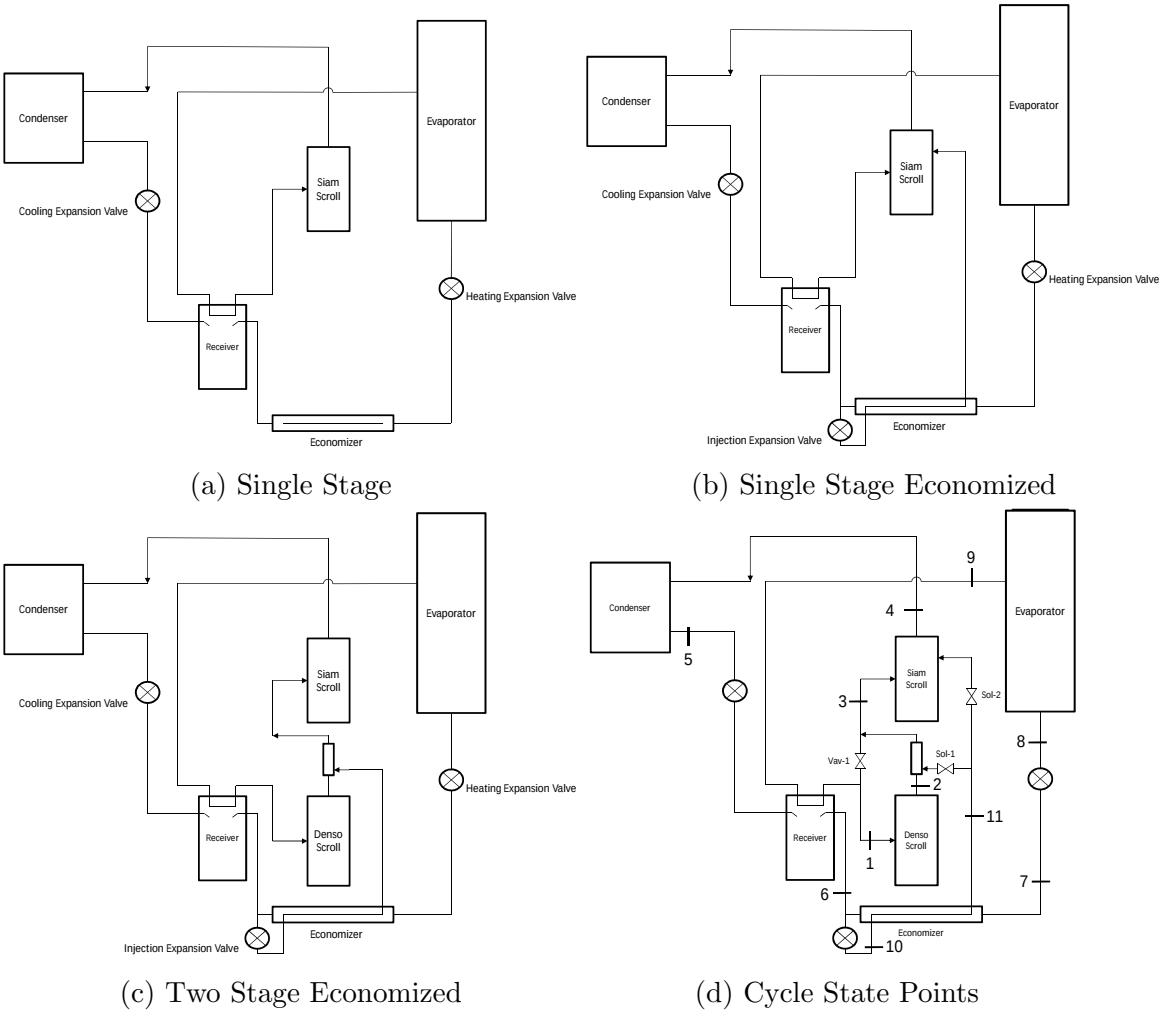

(a) Single Stage

(b) Single Stage Economized

(c) Two Stage Economized

(d) Cycle State Points

Figure 5.1: System Operating Schematics

5.1.1 System Preheating

Each day the hydronic system, shown in Figure 3.4, needed to be preheated to the testing temperature of 40°C. As this system was recently commissioned, the only source of fluid heating was the heat pump itself. Preheating was achieved by operating the heat pump in single stage mode with the cold chamber set to 0°C. This allowed the buffer tank and hydronic system to be preheated within two hours. Once the system was preheated, the heat pump was shut down and configured for the cycle to be tested.

5.1.2 Startup Procedure

The heat pump was started each day using manual controls. The required support equipment was powered and software was used to confirm communication with all devices. The expansion valves were calibrated and manually set to either their fully-opened or fully-closed position. Since the system was operating in heating mode, the cooling expansion valve was opened and the heating and injection valves were fully closed.

The pumps and fans were enabled, and the compressors were brought to their minimum speeds. To avoid a slug of liquid entering the compressor at startup, the heating expansion valve remained closed so the compressor suction would decrease the mass of refrigerant that had accumulated in the evaporator during system shutdown. Once the liquid was removed, the suction pressure would drop and the automatic super-heat control algorithm was enabled to control the heating expansion valve.

5.1.2.1 Super-heat Control Algorithm

The super-heat control algorithm was used to control the amount of super-heat that was present at the evaporator outlet. The saturation temperature of the evaporator was determined by measuring its pressure, as outlined in Section 3.3.9.2, and looking up the corresponding saturation properties in a table which was embedded in software. The desired super-heat was calculated using Equation 5.1.

$$T_{super-heat} = T_{evap_{outlet}} - T_{evap_{saturation}} \tag{5.1}$$

where, $T_{super-heat}$ is the amount of super-heat that is present in the refrigerant at the outlet of the evaporator, $T_{evap_{outlet}}$ is the refrigerant temperature at state point 9, as shown in Figure 5.1d, and $T_{evap_{saturation}}$ is the refrigerant saturation temperature that corresponds to the evaporator pressure.

During testing the super-heat was controlled at 8°C using a Proportional-Integral-Derivative (PID) feedback algorithm that was programmed into the main controller. The algorithm functioned by reducing the error between the set point of 8°C and the super-heat calculated with Equation 5.1 by controlling the position of the heating expansion valve. The details of the super-heat control algorithm are included in Appendix G.

5.1.3 Economized Operation

During single stage economized operation, the injection expansion valve was opened in small increments and the system was monitored to determine if further adjustments were needed. In this mode of operation, there was no way to determine the amount of refrigerant mass that was being injected into the compressor. Also, since the system was not operated using the Mitsubishi controller, there was no way to confirm what a normal injection rate was. For these reasons, the single stage economized tests were reduced to a single ambient temperature in an attempt to reduce possible damage to the compressor.

When operated in two stage economized mode, the injection was used to control the amount of super-heat at the inlet of the HP compressor.

5.1.4 Intermediate Pressure

During the modelling study, the intermediate pressure was fixed by setting the saturation temperature of the intermediate states directly. The ideal intermediate pressure was then determined through trial and error. In the real two stage system, the intermediate pressure could not be controlled directly. However, it could be controlled indirectly by varying the speed of the LP or HP compressor relative to the other. This was illustrated with a study in EES which considered the effect that changing the LP compressor speed had on an isentropic two stage compression process.

Figure 5.2 shows the two stage compression system that was considered for this study.

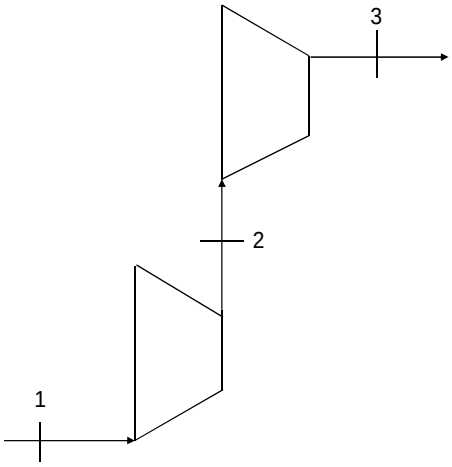

Figure 5.2: Two Stage Compression Process

The compression process was assumed to be supporting a heat pump whose evaporator and condenser saturation temperatures were -20°C and 40°C respectively. The HP compressor's volumetric displacement was set to 33 cm^3/rev and its rotational speed was fixed at 1800 rpm. The LP compressor's volumetric displacement was set to 18 cm^3/rev and its rotational speed was increased from 1000 rpm to 6400 rpm in 200 rpm increments. These volumetric displacements and speeds are representative of the equipment that was used during testing. The resulting intermediate pressures were plotted against the LP compressor speed, shown in Figure 5.3.

This shows that there is an almost linear relation between the LP compressor speed and the intermediate pressure for a given HP compressor speed. This result, combined with the effect that intermediate pressure has on COP, as outlined in Section 2.7.1, indicates that there is an ideal LP compressor speed that will produce the maximum COP for the system at each ambient temperature.

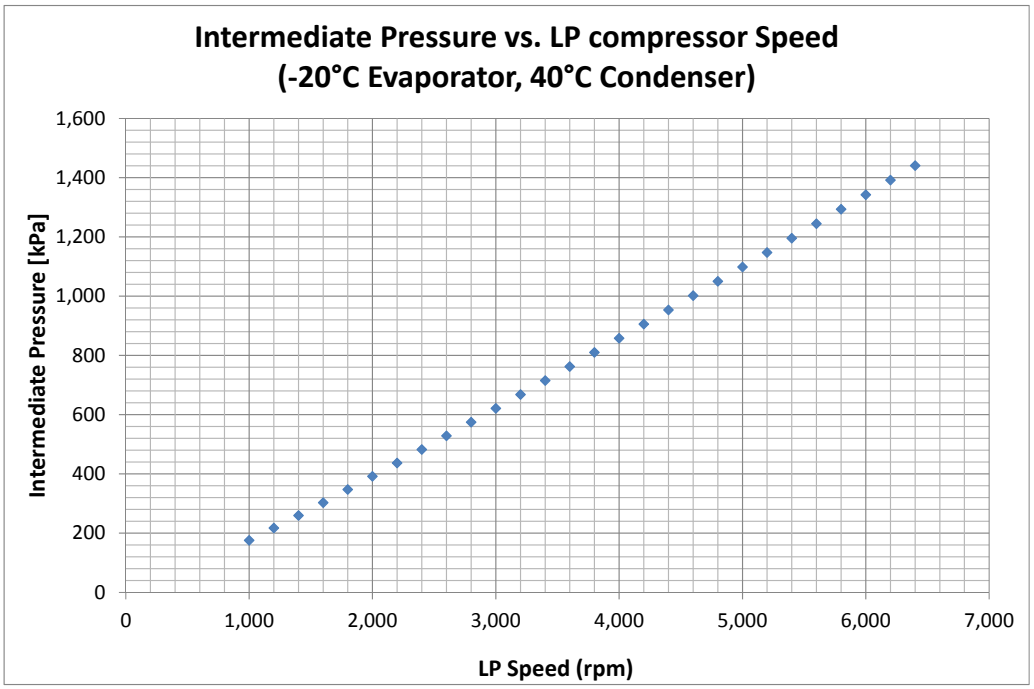

Figure 5.3: Intermediate Pressure vs. LP Compressor Speed

5.1.5 LP Compressor

The LP compressor speed was varied at each operating point to locate the ideal intermediate pressure and to characterize its effect on the system performance.

5.1.6 Steady State Operation

Once the system was operating using the super-heat control algorithm, it was allowed to run until the HP compressor discharge temperature, measured at state point 4 on Figure 5.1d, stabilized. This parameter was the slowest to stabilize in the system and for deviations of 5°C to 10°C, no measurable change in performance was observed. For these reasons, the HP discharge temperature was used as an indicator of system stability and the system was considered to be operating at steady state when the deviation in this parameter was less than 1°C/min. Once stabilized, the system was operated for a minimum of twenty minutes. The final five minutes of data collected were used to create a data point for analysis.

After data for a test point were collected, the temperature of the cold chamber was reduced to the next test point and the system was allowed to stabilize again. This approach proved to have the shortest wait time between system stability when compared to changing the system configuration while keeping the cold chamber at a constant temperature.

5.1.7 Defrost Cycle

During commissioning of the heat pump, the evaporator required defrosting only once. This was accomplished by operating the heat pump in single stage mode with the reversing valve in the cooling position. The evaporator fans were shut off and the system was run until the evaporator was visibly free of frost. Defrost is a challenging problem for heat pump manufactures as it requires additional energy that is not used to provide heating within the home. This reduces the long term performance of a heat pump and requires an intelligent strategy to ensure minimal energy is used during the defrost cycle. As testing here was limited to characterizing the steady state performance of the heat pump, the impact of the defrost cycle was not considered. During testing, no frost accumulation was observed on the evaporator.

5.2 Closing Remarks

A series of experiments were conducted for the operating conditions that are outlined in Table 5.2. The following chapter will discuss the results of this work.

Chapter 6

Results and Discussion

This chapter outlines the results of the experimental study and discusses the observed benefits of operating a two stage economized heat pump.

The single stage data were split into two sets labelled [SJ] and [WJ] which correspond to the VFD model used to run the HP compressor during data collection. The data show a negligible change in COP and a slight reduction in the heating capacity between the VFD models. The reduction in heating capacity was attributed to reducing the HP compressor speed from 90 Hz to 80 Hz which slightly reduced the work performed by the HP stage.

With the two stage economized cycle, there was a negligible effect on the system COP when switching VFDs, so the data were combined and plotted as a single data set. The two stage economized heating capacity varied with the LP compressor speed which was operated at speeds from 200 Hz to 320 Hz for all but one of the operating points. This was done to characterize the effect on system performance and also to isolate the highest performing conditions at each ambient temperature. The lowest performance point observed during two stage economized operation in terms of both COP and heating capacity was recorded with the LP compressor operating at 110 Hz. As discussed in Chapter 5, the HP compressor was only operated at low speeds to match its capacity to the smaller LP stage.

6.1 Heating Capacity

The data in Figure 6.1 show the increase in heating capacity of the heat pump due to the addition of the LP compressor. They also show the variability in the heating capacity that resulted from changing the speed of the LP compressor. Specifically, increasing the LP compressor speed from 200 Hz to 320 Hz increased the heating capacity from 4.4 kW to 5.6 kW at an ambient temperature of -14°C, 4.0 kW to 5.2 kW at an ambient temperature of -23°C, and 3.8 kW to 4.4 kW at an ambient temperature of -31°C.

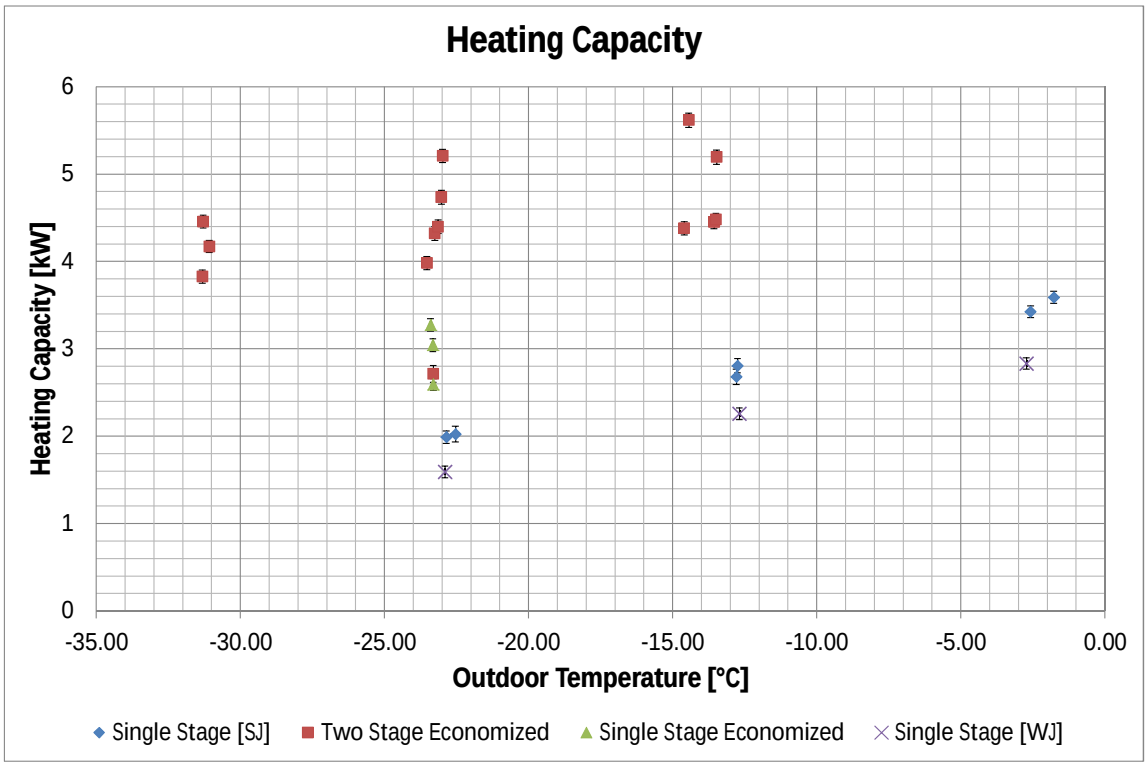

Figure 6.1: Measured Heating Capacity During Experimental Investigation

6.2 COP

The data in Figure 6.2 show a reduction in COP with decreasing ambient temperature for both the single stage and two stage economized operating modes. At each temperature tested, the two stage economized cycle outperformed the single stage cycle.

The single stage economized results show a similar COP to what was observed during two stage economized testing. However, it should be noted that the injection rates used during single stage economized operation were assumed to be higher than what would occur during normal operation. If these levels of injection were used regularly, there would be potential for liquid refrigerant to be injected which would damage the compressor.

The two stage economized data show a strong grouping in the COP when the LP compressor speed was operated in the range of 200 Hz to 320 Hz. At an ambient temperature of -23°C, the COP was reduced from 1.6 to 1.3 when the LP compressor speed was reduced to 110 Hz. This suggests that the COP has low sensitivity for a range of LP compressor speeds at each ambient temperature. This agrees with the correlations of COP to intermediate pressure and intermediate pressure to LP compressor speed that were outlined in Sections 2.7.1 and 5.1.4 respectively. The low sensitivity of the COP to the LP compressor speed also suggests that the system was operated near its maximum COP during testing.

6.3 Comparison With Modelling Results

The data agree relatively well with the modelling results that were outlined in Section 2.7. However, the modelling results overestimated the performance observed during the experimental investigation. For comparison, the experimental and modelling results are shown in Figure 6.3.

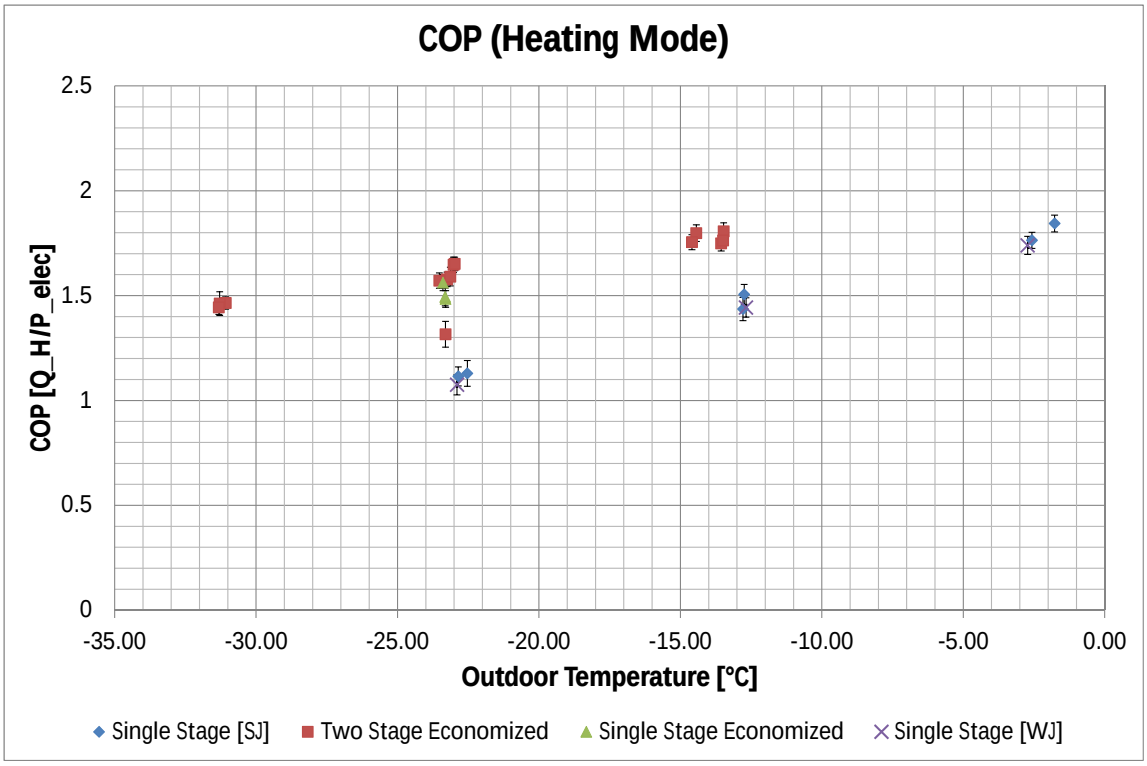

Figure 6.2: Measured COP During Experimental Investigation

The single stage results were similar at lower ambient temperatures, but the model predicted higher COPs at ambient temperatures above -10°C. The two stage economized model showed higher COPs across the entire operating range with an overestimation of 0.5 at -30°C that increased to 0.9 at -15°C.

The simplicity of the cycle model outlined in Section 2.6 could be the source of the overestimation of the COP. However, it is assumed that the main source of error was the compressor data used to fit the compressor isentropic efficiency model outlined in Equation 2.6. The data used was representative of a modern high performance scroll compressor. If the HP compressor had a lower isentropic efficiency than the compressor data used to fit the model, the model would have over-predicted the performance of the system in the operating region where data was not representative of the HP compressor.

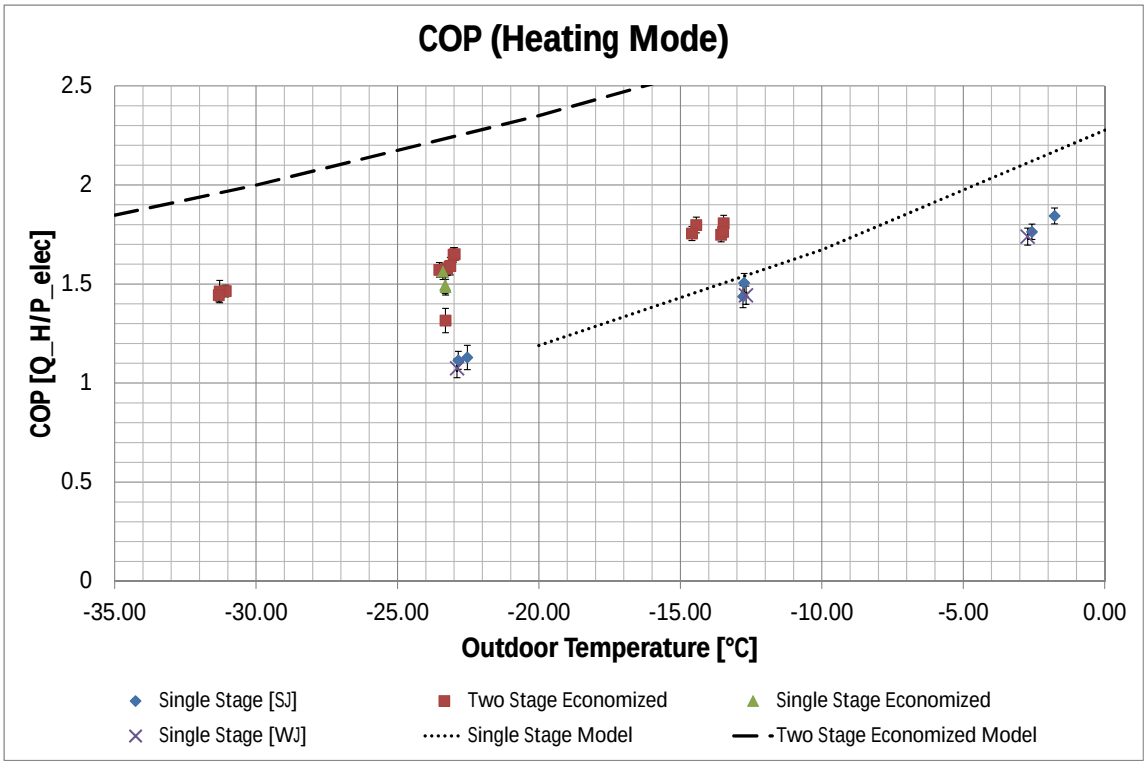

Figure 6.3: Comparison Between Measured and Modelled COP

This overestimation would also affect the predicted COP of the two stage economized results, because during two stage operation, the HP and LP compressors split the total pressure ratio of the cycle. This allows both compressors to operate with relatively low pressure ratios. Since the compressor isentropic efficiency model predicts the highest isentropic efficiencies at lower pressure ratios, the resulting performance of each compression process would be overestimated. Also, the LP compressor was expected to have a lower isentropic efficiency than a modern residential scroll compressor. This was assumed because the LP compressor was constructed without an axial seal which is normally used in residential compressors. The absence of the axial seal increases the internal leakage in the compressor, lowering its efficiency.

Lastly, the power receiver in the cycle was not present in the model as the model was developed before the details of the cycle were known. The power receiver added a substantial amount of additional super-heat to the refrigerant at the HP compressor

inlet during single stage operation and at the LP compressor inlet during two stage economized operation. Under some testing conditions, the power receiver added an additional 30°C of super-heat to the inlet vapour when compared to the modelling results. This is a significant difference in operating conditions between the experimental apparatus and the modelling assumptions.

These differences could be accounted for if the modelling study was repeated. However, the initial modelling results are still considered to be representative of what would be achievable if the experimental system was designed as a whole. The cycle could be constructed without the power receiver and the compressors could be selected with isentropic efficiencies that are closer to those used during modelling. This is also in agreement with the work of Bertsch et al. [8] whose experimental investigation showed results that are comparable to the modelled results of the two stage economized heat pump.

6.4 Real-World Implications

The increased COP of the two stage economized cycle reduces the energy required to operate a heating system when compared to a single stage cycle or a backup resistive element. This also extends the range of operation of the heat pump to ambient temperatures below -30°C. The system tested maintained a COP of 1.5 at this temperature which represents a 50% increase in performance compared to a resistive heating element. As well, the addition of the second stage compressor more than doubled the heating capacity of the cycle across the operating range. This could eliminate the need for a backup system whose capital cost could be used to partially offset the cost of the second compressor. Therefore, the two stage economized cycle offers more benefits than a single stage cycle in cold climate operation.

Although not exploited during this work because the HP compressor was much larger than the LP compressor, both compressors were capable of variable speed operation. This capability adds two major benefits to the cycle. First, the proportion of work contributed by each compressor can be controlled at every ambient temperature by varying their relative speeds. Second, the heating capacity can be controlled by varying the speeds of both compressors together.

6.4.1 Optimized COP

The ability to control the intermediate pressure by varying the speed of the LP compressor relative to the speed of HP compressor, allows the COP of the system to be optimized at each ambient temperature. This is evident from the relationship between the COP and the intermediate pressure outlined in Section 2.7.1 and from the relationship between the intermediate pressure and the LP compressor speed outlined in Section 5.1.4. This is an important factor for a real-world system as it allows the system to operate with high performance under variable operating conditions. If fixed speed compressors are used, the intermediate pressure would be optimized for a single operating condition. When the system is operated under conditions other than the design specifications, the system's performance could be negatively effected.

6.4.2 Variable Heating Capacity

The ability to vary the speeds of both compressors together would allow the heating capacity of the system to be varied which could increase the comfort of the user. By matching the heating capacity to the loading on the house, the temperature fluctuations within the heated space could be minimized.

6.5 Closing Remarks

The results of the experimental study show an increase in the COP of the heat pump when using a two stage economized cycle versus a single stage cycle. They also show an increase in the heating capacity of the system and an extension of the operating range to an ambient temperature of -31°C. The average data that are shown in this chapter are shown in detail in Appendix H. The following chapter will summarize the findings of this work and discuss areas where future work could be done.

Chapter 7

Conclusions and Recommendations

7.1 Conclusions and Contributions

As discussed in Chapter 1, the purpose of this work was to increase the performance and extend the operating range of an air source heat pump to enable its use in Canadian climates without requiring a backup heating system.

Three EES models of two stage heat pump cycles with various modifications were compared to the performance of a traditional single stage cycle. The results indicated that a COP of greater than 1.5 could be expected at an ambient temperature of -40°C and a supply temperature of 50°C. They also indicated that the two stage economized cycle was the best candidate for experimental work.

An experimental apparatus was constructed by modifying a Mitsubishi Zuba heat pump to operate as a two stage economized heat pump. The system was tested in a refrigerated container to simulate the ambient temperatures that are present in cold climates. A COP of 1.5 was measured at an ambient temperature of -31°C with a supply temperature of 40 °C.

This research has shown the benefits of using a two stage heat pump cycle for heating in Canadian climates. This was accomplished through the successful integration of an automotive air conditioning compressor into a residential heat pump. The addition of the second compressor extended the operating range of the heat pump to an ambient temperature of -31°C, thus demonstrating suitability for Canadian climates without a backup heating system. This work is also evidence that existing technologies can achieve these results if the components are integrated properly.

7.2 Recommendations for Future Work

This work could be continued or improved in many ways. The compressor model used during the EES modelling investigation discussed in Chapter 2 should be updated to a model that is a function of both inlet density and pressure ratio, rather than pressure ratio alone. This could be accomplished using a developed model for scroll compressors from literature or by developing a detailed relation using compressor performance data. This would improve the accuracy of the modelled results.

A model should be developed for the experimental prototype. This would provide an improved comparison between the modelling and experimental results as there were differences between the physical construction of the prototype and the modelling assumptions that were used. Any discrepancies that arise between the results of the new model and the experimental results should be investigated. This would help to identify areas of weakness in the modelling approach.

The isentropic efficiencies of the compressors could be calculated using the data that were collected during the experimental work. These efficiencies could be used in a model of the experimental prototype which would provide a better understanding of the performance of the cycle.

Multiple refrigerants should be considered to determine if there is potential for increased performance using a refrigerant other than R-410a. This is also important because R-410a, along with other HFCs, may be phased out in the future.

An appropriately scaled model of the two stage economized cycle should be created to simulate residential use of the system in Canadian climates. The model should include compressor isentropic efficiencies from appropriate compressor data, and realistic heat transfer models for the heat exchangers. This would provide a better representation of the system performance and also allow simulation studies to determine the long term performance of the system.

A two stage economized heat pump should be built from highest quality hardware and software for experimental purposes. Results from testing this system would give a better indication of the performance that can be achieved using existing compressors and heat exchangers.

An intelligent approach to defrosting the evaporator should be developed and studied using the experimental heat pump. This would determine the impact the defrost cycle has on the long term performance of the heat pump.

The temperature of the heating fluid should also be varied to characterize the affect this parameter has on the performance of the system. This would determine the performance of the heat pump if it were used to provide heating using a method other than forced air. For example, the COP of the heat pump could be increased by reducing the supply temperature for use with radiant flooring.

The potential for providing domestic hot water using the heat pump should also be studied. This could be accomplished by either increasing the supply temperature when there is a demand for hot water, or by adding an additional heat exchanger to provide domestic water heating using the high temperature refrigerant as it exits the compressors. If possible, this could offset the cost of the system by removing the need for a separate domestic hot water heating system.

Lastly, improvements at the component level should be made. Centrifugal compressors and micro-channel heat exchangers could be combined to investigate the performance of a system which uses emerging technologies.

References

[1] CAN/CSA-F280-M80. Determining the Required Capacity of Residential Space Heating and Cooling Appliances. 2012.

[2] Environment Canada Historical Climate Data. http://climate.weather.gc.ca. Accessed: 2013-10-10.

[3] UNEP. Report Of The Task Force on HCFC Issues And Emissions Reduction Benefits Arising From Earlier HCFC Phase-Out and Other Practical Measures, journal = Montreal Protocol on Substances That Deplete The Ozone Layer, Technology and Economic Assessment Panel. 2007.

[4] EIA. HFCs, the Montreal Protocol and the UNFCCC: Eliminating 1 of the 6 Kyoto gases. *Bangkok climate change conference*, 2012.

[5] A. D. Parekh and P. R. Tailor. Thermodynamic Analysis of R507A-R23 Cascade Refrigeration System. *International Journal of Aerospace and Mechanical Engineering*, 2012.

[6] Souvik Bhattacharyya, Anirban Garai, and Jahar Sarkar. Thermodynamic analysis and optimization of a novel $N_2O - CO_2$ cascade system for refrigeration and heating. *International Journal of Refrigeration*, 32:1077–1084, 2009.

[7] Stefan S. Bertsch and Eckhard A. Groll. Air Source Heat Pump for Northern Climates Part I: Simulation of Different Heat Pump Cycles. *International Refrigeration and Air Conditioning Conference*, Paper:783, 2006.

[8] Stefan S. Bertsch and Eckhard A. Groll. Air Source Heat Pump for Northern Climates Part II: Measurement and Verification. *International Refrigeration and Air Conditioning Conference*, Paper:784, 2006.

[9] Stephen Caskey, Shuai Deng, Derek Kultgen, Tobias Menzi, Eckhard Groll, William Hutzel, and Stefan Bertsch. Field Test Simulation of an Air-Source Heat Pump with Two-Stage Compression and Economizing For Cold Climates. *International Refrigeration and Air Conditioning Conference*, Paper:2381, 2012.

[10] Tobias Menzi, Stephen Caskey, Derek Kultgen, Eckhard Groll, William Hutzel, and Stefan Bertsch. Analysis of heating and cooling options for military barracks in the midwest u.s. Technical report, Interstate University of Applied Sciences of Technology NTB.

[11] Xudon Wang, Yunho Hwang, and Reinhard Radermacher. Two-stage heat pump system with vapor-injected scroll compressor using R410A as a refrigerant. *International Journal of Refrigeration*, 32:1442–1451, 2009.

[12] Kai Du, Shaoqian Zhang, Weirong Xu, and Xiaofeng Niu. A study on the cycle characteristics of an auto-cascade refrigeration system. *Experimental Thermal and Fluid Science*, 33:240–245, 2009.

[13] Brian T Austin and K Sumathy. Transcritical carbon dioxide heat pump systems: A review. *Renewable and Sustainable Energy Reviews*, 15:4013–4029, 2011.

[14] Detlef Westphalen. Converting a Military Environmental Control Unit to Propylene Refrigerant. *International Refrigeration and Air Conditioning Conference*, Paper:840, 2006.

[15] Emerson Climate Technologies Online Product Information and Technical Data. http://www.emersonclimate.com/en-ca/resources/online_product_information/pages/online_product_information.aspx. Accessed: 2014-06-10.

[16] J Schiffmann and D Favrat. Design, experimental investigation and multi-objective optimization of a small-scale radial compressor for heat pump applications. *Energy*, 35:436–450, 2009.

[17] J Schiffmann and D Favrat. Experimental investigation of a direct driven radial compressor for domestic heat pumps. *International Journal of Refrigeration*, 32:1918–1928, 2009.

[18] E. W. Lemmon. Psuedo-Pure Fluid Equations of State for the Refrigerant Blends R-410A, R-404A, R-507A, and R-407C. *International Journal of Thermophysics*, 24(4):991 – 1006.

[19] Robert J Moffat. Describing the Uncertainties in Experimental Results. *Experimental Thermal and Fluid Science*, 1988.

[20] Dow. A guide to glycols. http://www.dow.com/webapps/lit/litorder.asp?filepath=propyleneglyc 01682.pdf, 2003. Accessed: 2014-06-10.

[21] LabVIEW, PID and Fuzzy Logic Toolkit User Manual. www.ni.com/pdf/manuals/372192d.pdf, 2009. Accessed: 2014-09-20.

Appendix A

EES Models

This appendix contains copies of the EES models that were used during the modelling study that was outlined in Chapter 2.

```
"Model #1, single compression stage (valid for single component refrigerants or azeotropic mixtures with critical temperatures >60 C)"
"Design Conditions"

T_supply=50
T_high=T_supply+3+T_subcool
T_ambient=0
T_low=T_ambient - T_superheat - 3
T_superheat=11.1 [C]                    "Degree of superheat at compressor inlet (Controlled by expansion valve)"
T_subcool=8.3 [C]                       "Degree of subcooling at condensor outlet (Controlled by refrigerant charge)"
R$='R410a'                              "Refrigerant Variable"
eta_lowCompressor=(a+b*Pr+C*Pr^2)/100   "Compressor Isentropic Efficiency"
a=93.7884
b=-8.13742
c=0.156422
P_drop=1.0                              "Pressure Drop Through Heat Exchangers (1.0 = Neglected)"

"Q_vap=enthalpy_vaporization(R$,T=T[2])"
Q_superheat=H[2]-enthalpy(R$,p=p[2],x=1)

"State Point 1 - Compressor Inlet"
    "Set Variables"
T[1]=T_low+T_superheat                  "Compressor inlet temperaturer controlled by expansion valve"
P[1]=Pressure(R$,T=T_low,X=1)
    "Calculated Variables"
H[1]=enthalpy(R$,T=T[1],P=P[1])
S[1]=entropy(R$,T=T[1],P=P[1])
V[1]=volume(R$,T=T[1],P=P[1])

"State Point 2 - Compressor outlet"
    "Set Variables"
P[2]=pressure(R$,T=T_high,X=0)/P_drop   "P_drop applied to HX inlet as P_sat should remain the same."
    "Isentropic Conditions"
S_e2=S[1]
H_e2=enthalpy(R$,S=S_e2,P=P[2])
    "Calculated Variables"
H[2]=H[1]+(H_e2-H[1])/eta_lowCompressor  "From isentropic efficiency of compressor"
S[2]=entropy(R$,H=H[2],P=P[2])
T[2]=temperature(R$,H=H[2],P=P[2])
V[2]=volume(R$,H=h[2],p=p[2])

"State Point 3 - Condenser Outlet"
    "Set Variables"
P[3]=P[2]
T[3]=T_high-T_subcool                   "Subcooling is a function of refrigerant charge (designed subcooling for system)"
    "Calculated Variables"
H[3]=enthalpy(R$,T=T[3],P=P[3])
S[3]=entropy(R$,T=T[3],P=P[3])

"State Point 4 - Expansion Valve Outlet"
    "Set Variables"
H[4]=H[3]                               "Isenthalpic expansion is most commonly used approach"
P[4]=P[1]*P_drop                        "Pressure is determined by compressor inlet with a factor for pressure drop"
    "Calculated Variables"
T[4]=temperature(R$,H=H[4],P=P[4])
S[4]=entropy(R$,H=H[4],P=P[4])

"State Point 5 - repeat of State 1 for closure of cycle"
T[5]=T[1]
```

Figure A.1: Single Stage Cycle EES Model Page. 1

```
P[5]=P[1]
H[5]=H[1]
S[5]=S[1]

"Energy Balance"
Q_input=m[1]*(H[5]-H[4])
Q_output=m[1]*(H[3]-H[2])
W_input=m[1]*(H[2]-H[1])
W_input=1
COP_heating=abs((Q_output/W_input))
COP_cooling=abs((Q_input/W_input))

"Design Requirements"
Pr=P[2]/P[1]                                    "Pressure Ratio Required for operation"
Vr=V[1]/V[2]
```

Figure A.2: Single Stage Cycle EES Model Page. 2

```
"Model #2, Two Stage Cascade Cycle (valid for single component refrigerants or azeotropic mixtures with critical temperatures >60 C)"
"Design Conditions"

T_supply=50
T_high=T_supply + 3 + T_subcool                    "Condensor saturation temperature"
T_intermediate=-18 [C]                             "Intermediate Temperature, (upper cycle evaporator Temp)"
T_ambient = -40
T_low=T_ambient - T_superheat - 3 [C]              "Evaporator saturation temperature"
T_superheat=11.1 [C]                               "Degree of superheat at compressor inlet (Controlled by expansion valve)"
T_subcool=8.3 [C]                                  "Degree of subcooling at condensor outlet (Controlled by refrigerant charge)"
RH$='r410a'                                        "Refrigerant Variable"
RL$='r410a'
eta_highCompressor=0.7"(a+b*Pr_High+c*Pr_high^2)/100"
a=93.7884
B=-8.13742
c=0.156422
eta_lowCompressor=(a+b*Pr_Low+c*Pr_Low^2)/100      "Compressor Isentropic Efficiency"
P_drop=1                                           "Pressure Drop Through Heat Exchangers (1.0 = Neglected)"


"Upper Cycle"
    "State Point 1 - Compressor Inlet"
    "Set Variables"
    T[1]=T_intermediate+T_superheat                "Compressor inlet temperaturer controlled by expansion valve"
    P[1]=Pressure(RH$,T=T_intermediate,x=1)
    "Calculated Variables"
    H[1]=enthalpy(RH$,T=T[1],P=P[1])
    S[1]=entropy(RH$,T=T[1],P=P[1])

    "State Point 2 - Compressor outlet"
    "Set Variables"
    P[2]=Pressure(RH$,T=T_high,x=1)/P_drop         "P_drop applied to HX inlet as P_sat should remain the same."
    "Isentropic Conditions"
    S_e2=S[1]
    H_e2=enthalpy(RH$,S=S_e2,P=P[2])
    "Calculated Variables"
    H[2]=H[1]+(H_e2-H[1])/eta_HighCompressor       "From isentropic efficiency of compressor"
    S[2]=entropy(RH$,H=H[2],P=P[2])
    T[2]=temperature(RH$,H=H[2],P=P[2])

    "State Point 3 - Condenser Outlet"
    "Set Variables"
    P[3]=P[2]
    T[3]=T_high -T_subcool                         "Subcooling is a function of refrigerant charge (designed subcooling for system)"
    "Calculated Variables"
    H[3]=enthalpy(RH$,T=T[3],P=P[3])
    S[3]=entropy(RH$,T=T[3],P=P[3])

    "State Point 4 - Expansion Valve Outlet"
    "Set Variables"
    H[4]=H[3]                                      "Isenthalpic expansion is most commonly used approach"
    P[4]=P[1]/P_drop                               "Pressure is determined by compressor inlet with a factor for pressure drop"
    "Calculated Variables"
    T[4]=temperature(RH$,H=H[4],P=P[4])
    S[4]=entropy(RH$,H=H[4],P=P[4])

    "State Point 5 - repeat of State 1 for closure of cycle"
    T[5]=T[1]
```

Figure A.3: Two Stage Cascade Cycle EES Model Page. 1

```
    P[5]=P[1]
    H[5]=H[1]
    S[5]=S[1]

    "Energy Balance"
    "Q_intermediate=m[1]*(H[5]-H[4])"
    Q_output=m[1]*(H[3]-H[2])
    W_high=m[1]*(H[2]-H[1])
    COP_High=abs((Q_output/W_high))
    Q_HighInput=m[1]*(H[5]-H[4])

    "Design Requirements"
    Pr_high=P[2]/P[1]                                   "Pressure Ratio Required for operation"

"Lower Cycle"
    "State Point 6 - Compressor Inlet"
    "Set Variables"
    T[6]=T_low+T_superheat                              "Compressor inlet temperaturer controlled by expansion valve"
    P[6]=Pressure(RL$,T=T_low,x=1)
    "Calculated Variables"
    H[6]=enthalpy(RL$,T=T[6],P=P[6])
    S[6]=entropy(RL$,T=T[6],P=P[6])
    "m[6]=m[1]*(H[5]-H[4])/(H[10]-H[9])"

    "State Point 7 - Compressor outlet"
    "Set Variables"
    P[7]=Pressure(RL$,T=T_intermediate+3+T_subcool,x=1)/P_drop                                  "P_drop
applied to HX inlet as P_sat should remain the same."
    "Isentropic Conditions"
    S_e7=S[6]
    H_e7=enthalpy(RL$,S=S_e7,P=P[7])
    "Calculated Variables"
    H[7]=H[6]+(H_e7-H[6])/eta_lowCompressor             "From isentropic efficiency of compressor"
    S[7]=entropy(RL$,H=H[7],P=P[7])
    T[7]=temperature(RL$,H=H[7],P=P[7])

    "State Point 8 - Condenser Outlet"
    "Set Variables"
    P[8]=P[7]
    T[8]=T_intermediate+3                               "Subcooling is a function of refrigerant charge (designed subcooling
for system)"

    "Calculated Variables"
    H[8]=enthalpy(RL$,t=t[8],p=p[8])
    S[8]=entropy(RL$,T=T[8],P=P[8])

    "State Point 9 - Expansion Valve Outlet"
    "Set Variables"
    H[9]=H[8]                                           "Isenthalpic expansion is most commonly used approach"
    P[9]=P[6]/P_drop                                    "Pressure is determined by compressor inlet with a factor for
pressure drop"
    "Calculated Variables"
    T[9]=temperature(RL$,H=H[9],P=P[9])
    S[9]=entropy(RL$,H=H[9],P=P[9])

    "State Point 10 - repeat of State 6 for closure of cycle"
    T[10]=T[6]
    P[10]=P[6]
    H[10]=H[6]
    S[10]=S[6]

    "Energy Balance"
    Q_input=m[6]*(H[10]-H[9])
```

Figure A.4: Two Stage Cascade Cycle EES Model Page. 2


```
    "Q_intermediate=m[6]*(H[7]-H[8])"
    m[6]=m[1]*(H[4]-H[5])/(H[8]-H[7])
    W_lowOutput=m[6]*(H[10]-H[9])
    W_Low=m[6]*(H[7]-H[6])
    W=W_low+W_high
W=1
    COP_Low=abs((Q_output/W_Low))
    COP_Heating=abs((Q_output/(W_low+W_high)))

    "Design Requirements"
    Pr_low=P[7]/P[6]                                    "Pressure Ratio Required for operation"
```

Figure A.5: Two Stage Cascade Cycle EES Model Page. 3

```
"Model #1, single compression stage (valid for all refrigerants and azeotropic mixtures with critical temperatures >60 C)"
"Design Conditions"

T_supply=50
T_high=T_supply+3+T_subcool                    "Condensor saturation temperature"
T_ambient=-40
T_low=T_ambient-T_superheat-3                  "Evaporator saturation temperature"
"T_inj=0"                                      "Flash tank temperature (Controlled directly)"
W_input=1
m[2]=m[1]-m_inj
T_superheat=11.1 [C]                           "Degree of superheat at compressor inlet (Controlled by expansion
valve)"
T_subcool=8.3 [C]                              "Degree of subcooling at condensor outlet (Controlled by refrigerant
charge)"
R$='r410a'                                     "Refrigerant Variable"
"eta_LPComp=(a +b*Pr_LP+c*Pr_LP^2)/100
"eta_LPComp=0.7
a=93.7884
b=-8.13742
c=0.156422
"eta_HPComp=(a+b*Pr_HP+c*Pr_HP^2)/100
"eta_HPComp=0.7
P_drop=1.0                                     "Pressure Drop Through Heat Exchangers"


"State Point 1 - LP Compressor Inlet"
    "Controlled"
    T[1]=T_low+T_superheat                     "Controlled by expansion device and evap temp"

    "Dependent"
    P[1]=pressure(R$,T=T_low,x=1)
    H[1]=enthalpy(R$,t=t[1],p=p[1])
    S[1]=entropy(R$,t=t[1],p=p[1])
    V[1]=volume(R$,t=t[1],p=p[1])
    C[1]=soundspeed(R$,T=T[1],P=P[1])

"State Point 2 LP compressor outlet"
    "Controlled"
    P[2]=Pressure(R$,T=T_inj,x=1)              "Controlled by intermediate pressure"
    "Isentropic Compression"
    S_s2=S[1]
    H_s2=enthalpy(R$,P=P[2],S=s_s2)

    "Dependent"
    H[2]=(H_s2-H[1])/eta_LPComp+H[1]
    T[2]=temperature(R$,p=p[2],h=h[2])
    S[2]=entropy(R$,p=p[2],h=h[2])

"State Point 3 HP compressor inlet"
    "Controlled"
    P[3]=P[2]                                  "Same as 2"
    "T[3]=Temperature(R$,P=P[3],x=1)+T_superheat"
    "Dependent"
    "H[3]=enthalpy(R$,P=P[3],T=T[3])"
    H[3]=(m[2]*H[2]+m_inj*H[11])/m[1]          "Ideal Mixing Process"
    T[3]=temperature(R$,p=p[3],h=h[3])
    S[3]=entropy(R$,p=p[3],h=h[3])
    V[3]=volume(R$,p=p[3],h=h[3])

"State Point 4 HP compressor outlet"
    "Controlled"
    P[4]=pressure(R$,T=T_high,x=0)             "Controlled by Condenser temp"
```

Figure A.6: Two Stage Flash Separation Cycle EES Model Page. 1

```
    "Isentropic Compression"
    S_s4=S[3]
    H_s4=enthalpy(R$,P=P[4],S=S_s4)

    "Dependent"
    H[4]=(H_s4-H[3])/eta_HPComp+H[3]
    T[4]=temperature(R$,p=p[4],h=h[4])
    S[4]=entropy(R$,p=p[4],h=h[4])

"State point 5 Condenser Outlet"
    "Controlled"
    T[5]=T_high-t_subcool                    "Controlled by refrigerant charge, condensor temp"

    "Dependent"
    P[5]=P[4]
    H[5]=enthalpy(R$,t=t[5],P=P[5])
    S[5]=entropy(R$,t=t[5],p=p[5])

"State point 6 Flash tank inlet"
    "Controlled"
    H[6]=H[5]                                "Constant enthalpy expansion"
    m_inj=m[1]*(quality(R$,P=P[6],H=h[6]))
    "T[6]=T_inj"
    "Dependent"
    "P[6]=Pressure(R$,H=H[6],T=T[6])"
    P[6]=Pressure(R$,t=T_inj,x=1)
    T[6]=temperature(R$,p=p[6],h=h[6])
    S[6]=entropy(R$,p=p[6],h=h[6])

"State point 7 liquid stream outlet"
    P[7]=P[6]
    X[7]=0

    "dependent"
    H[7]=enthalpy(R$,p=p[7],x=x[7])
    S[7]=entropy(R$,p=p[7],x=x[7])
    T[7]=temperature(R$,p=p[7],x=x[7])

"State Point 8 Evaporator inlet"
    P[8]=P[1]
    H[8]=H[7]                                "Constant Enthalpy expansion"

    "dependent"
    T[8]=temperature(R$,p=p[8],h=h[8])
    S[8]=entropy(R$,p=p[8],h=h[8])

"State Point 9 Repeat of 1"
    P[9]=p[1]
    H[9]=h[1]
    T[9]=t[1]
    S[9]=S[1]

"State point 10 Repeat of 6"
    P[10]=p[6]
    H[10]=h[6]
    T[10]=t[6]
    S[10]=s[6]

"State Point 11 Vapor stream tank outlet"
    P[11]=P[10]
    X[11]=1

    "Dependent"
```

Figure A.7: Two Stage Flash Separation Cycle EES Model Page. 2

```
H[11]=enthalpy(R$,p=p[11],X=x[11])
S[11]=entropy(R$,p=p[11],x=x[11])
T[11]=temperature(R$,p=p[11],x=x[11])

"State Point 12 Repeat of 3"
P[12]=P[3]
H[12]=h[3]
T[12]=t[3]
S[12]=s[3]

"Energy Balance"
Q_evap=m[2]*(H[9]-H[8])
Q_cond=m[1]*(H[5]-H[4])
W_input=W_LP+W_HP
W_LP=m[2]*(H[2]-H[1])
W_HP=m[1]*(H[4]-H[3])
COP_heating=abs((Q_cond/W_input))
COP_cooling=abs((Q_evap/W_input))
Q_residual=W_input+Q_evap+Q_cond

"Design Requirements"
Pr_LP=P[2]/P[1]                    "Pressure Ratio Required for operation"
Pr_HP=P[4]/P[3]
Pr_total=P[4]/P[1]
```

Figure A.8: Two Stage Flash Separation Cycle EES Model Page. 3

```
"Model #1, single compression stage (valid for all refrigerants with critical temperatures >60 C)"
"Design Conditions"
ErrorCheck=T[7]-T[11]

T_supply=50
T_high=T_supply + 3 + T_subcool                    "Condensor saturation temperature"
T_ambient=0
T_low=T_ambient-T_superheat-3                      "Evaporator saturation temperature"
T_inj=21                                           "Flash tank temperature (Controlled directly)"
m[1]=0.01688 [kg/s]                                "Mass flow rate"
m_inj=m[1]*X_inj
X_inj=0.321
m[2]=m[1]-m_inj

T_superheat=11.1 [C]                               "Degree of superheat at compressor inlet (Controlled by expansion
valve)"
T_subcool=8.3 [C]                                  "Degree of subcooling at condensor outlet (Controlled by refrigerant
charge)"
R$='r410a'                                         "Refrigerant Variable"
"eta_LPComp=(a +b*Pr_LP+c*Pr_LP^2)/100"            "Compressor Isentropic Efficiency"
eta_LPComp=0.7
a=93.7884
b=-8.13742
c=0.156422
"eta_HPComp=(a+b*Pr_HP+c*Pr_HP^2)/100"
eta_HPComp=0.7
P_drop=1.0                                         "Pressure Drop Through Heat Exchangers"


"State Point 1 - LP Compressor Inlet"
    "Controlled"
    T[1]=T_low+T_superheat                         "Controlled by expansion device and evap temp"

    "Dependent"
    P[1]=(0.5)*(pressure(R$,T=t_low,X=1)+pressure(R$,T=T_low,x=0))
    H[1]=enthalpy(R$,t=t[1],p=p[1])
    S[1]=entropy(R$,t=t[1],p=p[1])
    V[1]=volume(R$,t=t[1],p=p[1])
    C[1]=soundspeed(R$,T=T[1],P=P[1])

"State Point 2 LP compressor outlet"
    "Controlled"
    P[2]=Pressure(R$,T=T_inj,x=1)                  "Controlled by intermediate pressure"
    "Isentropic Compression"
    S_s2=S[1]
    H_s2=enthalpy(R$,P=P[2],S=s_s2)

    "Dependent"
    H[2]=(H_s2-H[1])/eta_LPComp+H[1]
    T[2]=temperature(R$,p=p[2],h=h[2])
    S[2]=entropy(R$,p=p[2],h=h[2])

"State Point 3 HP compressor inlet"
    "Controlled"
    P[3]=P[2]                                      "Same as 2"

    "Dependent"
    H[3]=(m[2]*H[2]+m_inj*H[12])/m[1]              "Ideal Mixing Process"
    "T[3]=temperature(R$,p=p[3],h=h[3])"
    H[3]=enthalpy(R$,P=P[3],T=T[3])
```

Figure A.9: Two Stage Economized Cycle EES Model Page. 1

```
    T[3]=temperature(R$,P=P[3],X=1)+T_superheat
    S[3]=entropy(R$,p=p[3],h=h[3])
    V[3]=volume(R$,p=p[3],h=h[3])

"State Point 4 HP compressor outlet"
    "Controlled"
    P[4]=(0.5)*(pressure(R$,T=t_high,X=1)+pressure(R$,T=T_high,x=0))          "Controlled by
Condenser temp"

    "Isentropic Compression"
    S_s4=S[3]
    H_s4=enthalpy(R$,P=P[4],S=S_s4)

    "Dependent"
    H[4]=(H_s4-H[3])/eta_HPComp+H[3]
    T[4]=temperature(R$,p=p[4],h=h[4])
    S[4]=entropy(R$,p=p[4],h=h[4])

"State point 5 Condenser Outlet"
    "Controlled"
    T[5]=T_high-t_subcool                    "Controlled by refrigerant charge, condensor temp"

    "Dependent"
    P[5]=P[4]
    H[5]=enthalpy(R$,t=t[5],P=P[5])
    S[5]=entropy(R$,t=t[5],p=p[5])

"State point 6 Receiver outlet"
    P[6]=P[5]
    H[6]=H[5]
    "dependent"

    S[6]=entropy(R$,p=p[6],h=H[6])
    T[6]=temperature(R$,p=p[6],h=H[6])

"State point 7 Main Econo Out"
    "Controlled"
    H[7]=(m_inj*(H[11]-H[12])/m[2])+H[6]

    "Dependent"
    P[7]=P[4]
    T[7]=temperature(R$,p=p[7],h=h[7])
    S[7]=entropy(R$,p=p[7],h=h[7])


"State Point 8 Evaporator inlet"
    P[8]=P[1]
    H[8]=H[7]                                "Constant Enthalpy expansion"

    "dependent"
    T[8]=temperature(R$,p=p[8],h=h[8])
    S[8]=entropy(R$,p=p[8],h=h[8])

"State Point 9 Repeat of 1"
    P[9]=p[1]
    H[9]=h[1]
    T[9]=t[1]
    S[9]=S[1]

"State point 10 Repeat of 6"
    P[10]=p[6]
    H[10]=h[6]
```

Figure A.10: Two Stage Economized Cycle EES Model Page. 2

```
    T[10]=t[6]
    S[10]=s[6]

"State Point 11 Econo Inlet"
    P[11]=P[3]
    H[11]=H[6]

    "Dependent"
    S[11]=entropy(R$,p=p[11],H=H[11])
    T[11]=temperature(R$,p=p[11],H=H[11])

"State Point 12 Repeat of 3"
    P[12]=P[3]
    "H[12]=h[3]"
    T[12]=temperature(R$,P=P[12],H=H[12])
    S[12]=entropy(R$,P=P[12],H=H[12])

"State Point 13 Repeat of 3"
    P[13]=P[3]
    H[13]=h[3]
    T[13]=t[3]
    S[13]=s[3]

"Energy Balance"
Q_evap=m[2]*(H[9]-H[8])
Q_cond=m[1]*(H[5]-H[4])
W_input=W_LP+W_HP
W_LP=m[2]*(H[2]-H[1])
W_HP=m[1]*(H[4]-H[3])
COP_heating=abs((Q_cond/W_input))
COP_cooling=abs((Q_evap/W_input))
Q_residual=W_input+Q_evap+Q_cond

"Design Requirements"
Pr_LP=P[2]/P[1]                    "Pressure Ratio Required for operation"
Pr_HP=P[4]/P[3]
Pr_total=P[4]/P[1]
```

Figure A.11: Two Stage Economized Cycle EES Model Page. 3

Appendix B

FPGA

This appendix outlines the basic function of a field programmable gate array that was used during the experimental work.

B.1 FPGA Function

A FPGA is a reconfigurable piece of hardware that allows for rapid prototyping of integrated circuits. It is constructed using an array of logic gates that are interconnected by a variety of switching elements. The switching elements are programed to link the logic gates in a configuration which provides the required function. Figure B.1 shows the basic building block that is used to construct a FPGA chip.

These building blocks are connected to provide millions of gates within a single FPGA chip. The NI cRIO-9074 controller that was used contained a Xilinx Spartan 3 FPGA which was constructed with 2 million gates.

The FPGA is configured using a machine code that is specific to the chip which is used. LabVIEW simplifies this process by allowing the user to program the FPGA using the same block diagram interface that is used in to program regular LabVIEW applications, with a reduced set of tools. The program is then compiled to machine code using a compiler.

The main benefit of using the FPGA in a LabVIEW controller is how it functions. Normally, a software function is placed into a real-time application that is deployed to the controller. This application runs in the operating system and is subjected to the processor's speed and the processor and memory queues. The FPGA functions much

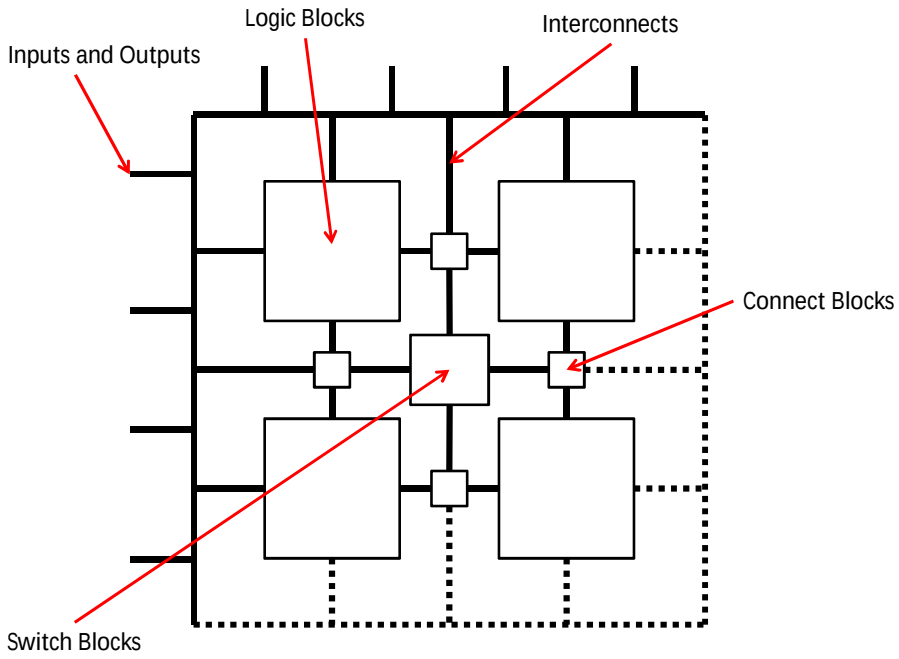

Figure B.1: Architecture of FPGA Building Block

differently. Once the unit has been configured, the entire operation of the FPGA is computed on each clock cycle of the machine. This allows it to operated at extremely fast speeds. This allows an input channel to be read, a function to be performed with the signal, and an output channel to be updated on every clock cycle. For the NI cRIO-9074, this occurs at a speed of 40 MHz. This also reduces the load on the processor which can speed up other applications.

Appendix C

Expansion Valve Control

This appendix outlines the operation of the expansion valves.

C.1 Expansion Valves

The expansion valves operated using stepper motors to control their positions. The motors were constructed with a base set of four electrical coils and could have contained any multiple of the base set of coils in their physical construction. The rotor position was controlled by systematically energizing the coils to produce the desired motion. Table C.1 outlines the energizing sequence that was specified for the expansion valves.

Table C.1: Expansion Valve Stepping Sequence

	Step #							
Phase	1	2	3	4	5	6	7	8
1	ON	ON	OFF	OFF	OFF	OFF	OFF	ON
2	OFF	ON	ON	ON	OFF	OFF	OFF	OFF
3	OFF	OFF	OFF	ON	ON	ON	OFF	OFF
4	OFF	OFF	OFF	OFF	OFF	ON	ON	ON

This shows that eight positions were achievable for each set of four coils within the motor. This includes the in-between positions when two coils were energized together. This stepping sequence shows how to either open or close the valve. This was done by cycling through the above sequence in either direction. To open the valve, the sequence was performed in the decreasing 8-to-1 direction and to close the valve the

sequence was performed in the increasing 1-to-8 direction. A total of five hundred steps were required to move the valve from fully closed to fully opened.

To control the position, a FPGA code was written in LabVIEW which accepted a numeric position from a higher level real-time software outlined in Appendix G. The numeric position was intended to indicate the desired position of the valve and could have had a value of 0 - 500. The FPGA monitored this parameter and output the sequence that was required to move the valve to the desired position. For example, if the position parameter was changed from 100 to 125, the FPGA would make 25 steps in the correct direction. Figure C.1 outlines the operation of the FPGA software.

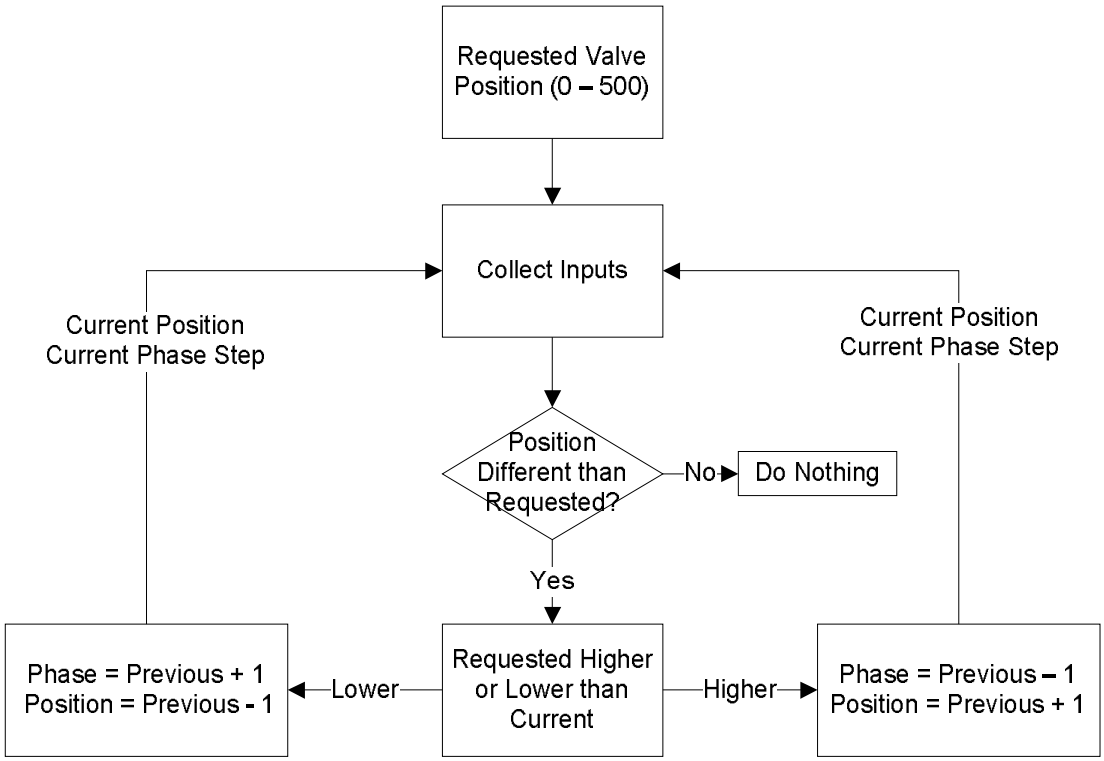

Figure C.1: Expansion Valve FPGA Software Operation

The FPGA was configured to control the NI-9401 digital output modules of the controller. With this approach, each digital output channel directly controlled a phase of the stepper motor.

The digital output module was only capable of supplying a maximum of 1 mA of current and the stepper motor windings required 350 mA. To operate the stepper motor, a current driving circuit was designed using the ULN2003AN integrated circuit (IC) to increase the current supplied to the coils. This IC incorporates seven Darlington circuits into a single chip. A Darlington circuit is constructed by placing two transistors together so that the emitter of the first is connected to the base of the second, assuming NPN transistors are used. Since the current delivered to the emitter of a transistor is a function of the current supplied to its base, the small current delivered by the NI module is increased in the first transistor. Then the increased current is multiplied again in the second transistor. Typical emitter currents can be 20 to 200 times greater than the base current. The Darlington circuit takes advantage of this twice which allows the small 1 mA output to control up to 500 mA. Figure C.2 shows the current driving circuit that was used.

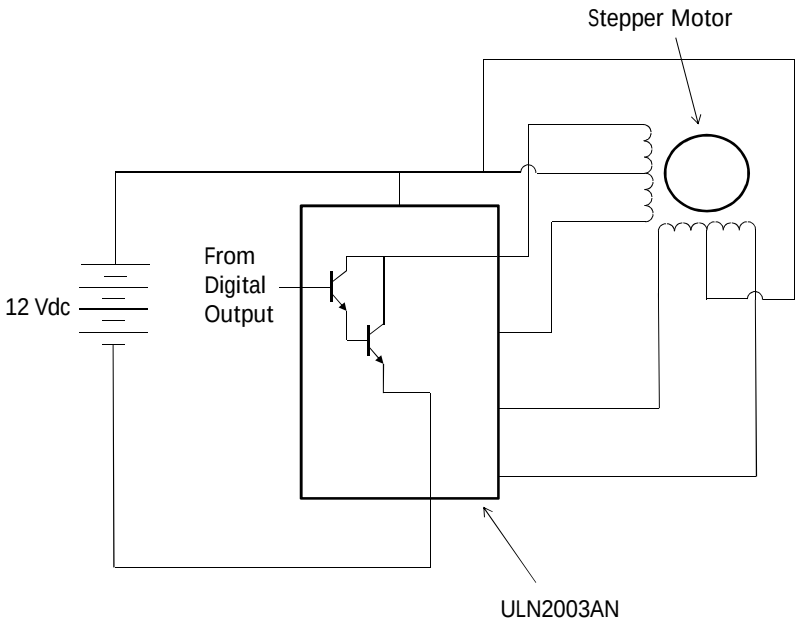

Figure C.2: Expansion Valve Current Driving Circuit (Showing One Internal Darlington)

Using this approach, the high level PID algorithm, outlined in Appendix G, was used to control the desired position of the valve, and the FPGA code would control the operation of the coils in the stepper motor. When the software was initialized, the valve position was calibrated by supplying 700 steps in the closed direction and setting the position parameter to zero. This forced the motor to lock when the valve closed and set the position reference to match the closed position. It is possible that over time the position reference could drift from the real position of the valve. In practice, the valve position would be calibrated at some frequency to minimize this effect. For this work, the valves were calibrated daily as part of the startup procedure and no effects of drift were observed during operation.

Appendix D

Fans

This appendix will describe the operation of the fans which were located in the outdoor unit.

D.1 Fans

The fans in the outdoor unit were originally controlled by the heat pump control board. There are two separate fans which are each variable speed and were controlled individually. To simplify the modifications, both fans were wired in parallel.

The fans were originally wired to the heat pump control board using a seven pin connector. The function of the pins of this connector were determined by monitoring the electrical signals present when the heat pump control board was powered. The results of this are shown in Table D.1.

Table D.1: Outdoor Unit Fan Pinout

Pin	Description
1	280 Vdc, Main power supply for fans
2	No connection
3	No connection
4	Common
5	15 Vdc, Logic level power supply
6	0 - 6.5 Vdc, Variable speed control
7	0 - 15 Vdc Pulse, Tachometer Signal

This shows that 3 separate direct current power signals were measured. It was assumed that the 280 Vdc signal was the main power supply for the motors and the 15 Vdc signal was the power supply for the internal electronics within the motor. The 0 - 6.5 Vdc signal was assumed to be the input which controlled the speed of the motor.

For the 280 Vdc power supply, a rectifier circuit was constructed which operated from a 208 Vac line to line power supply. The rectifier circuit used a GBJ2508-BP 25 A bridge rectifier with a 470 μF capacitor that was used to filter the voltage ripple on the output. Due to the size of the capacitor, a 100 kΩ resistor was placed across the output terminals to ensure that the capacitor would discharge within five minutes of the input power being disconnected. This was done to reduce the danger of working on the electrical system after it was installed. Figure D.1 shows the schematic of the rectifier circuit.

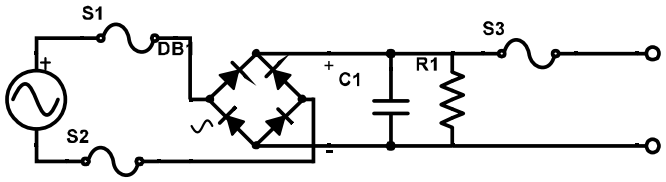

Figure D.1: DC Rectifier Circuit

The 15 Vdc and 0 to 6.5 Vdc were powered via a Sorenson dual channel dc power supply. As this equipment was available, it was the simplest approach to finish the circuit for the fans. The tachometer signal was ignored for simplicity.

Appendix E

Software

This appendix will outline the architecture and general operation of the control software.

E.1 Architecture

The software was distributed across three pieces of hardware in four applications. This included a desktop computer, two embedded real-time controllers, and a FPGA layer within one of the controllers. Figure E.1 outlines this distribution.

E.1.1 Desktop PC

The desktop computer operated the main user interface and provided the location where data were stored. The graphical user interface (GUI) is shown in Figure E.2

The GUI was used to configure and provide feedback from the system during operation. A detailed diagram of the refrigeration cycle was included which displayed real-time data from the instrumentation. The compressor speeds, super-heat setting, pump speed, and valve positions were controlled using inputs on this diagram. The data logging location and interval were also configured using this interface.

E.1.2 Main Controller

The main controller was configured to read the measured values from the instrumentation and to convert their readings to the desired units using the calibrated scales.

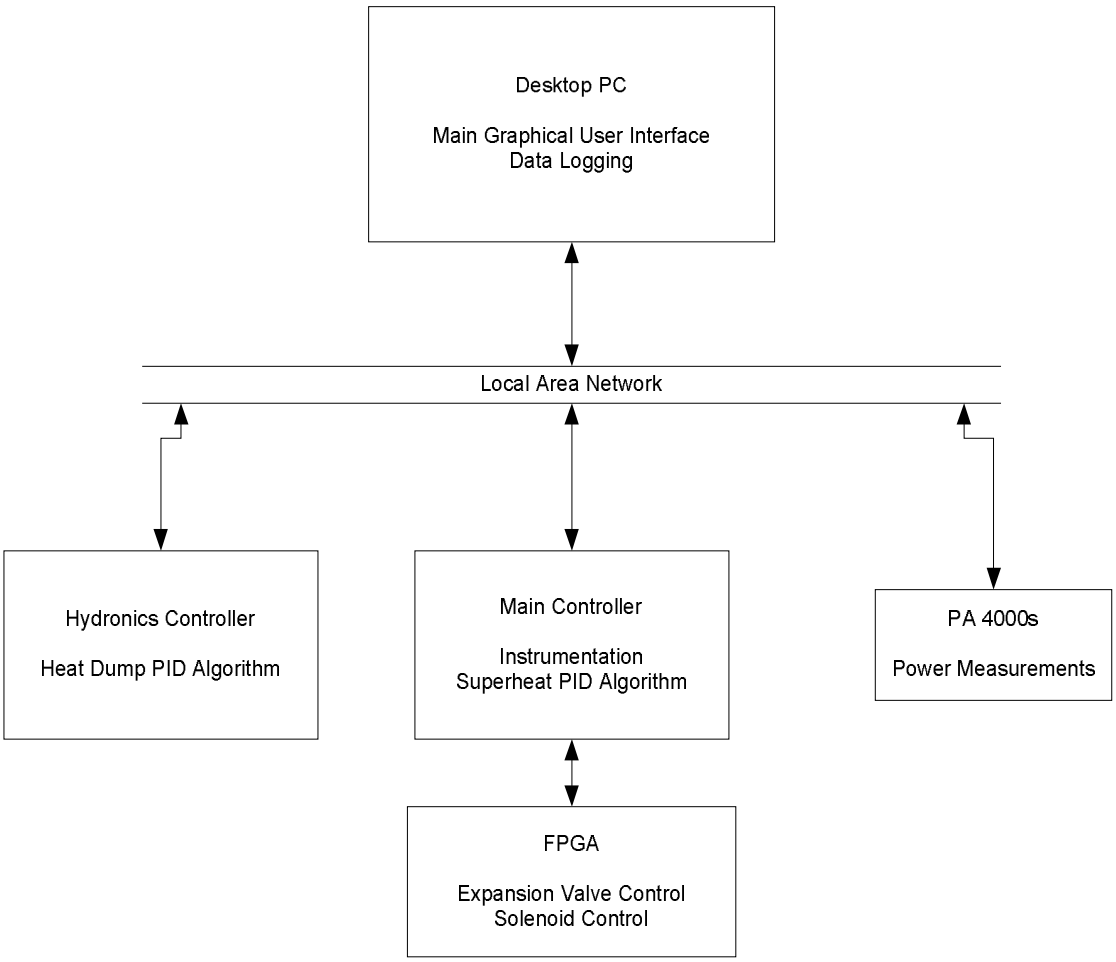

Figure E.1: System Software Architecture

The data were then published to the network to be recorded in the desktop PC. The main controller also operated the super-heat control algorithm as outlined in Appendix G. The output of this algorithm was then sent to the FPGA.

E.1.2.1 FPGA

The FPGA was used to control the position of the expansion valves. The operation of this is described in Appendices B and C.

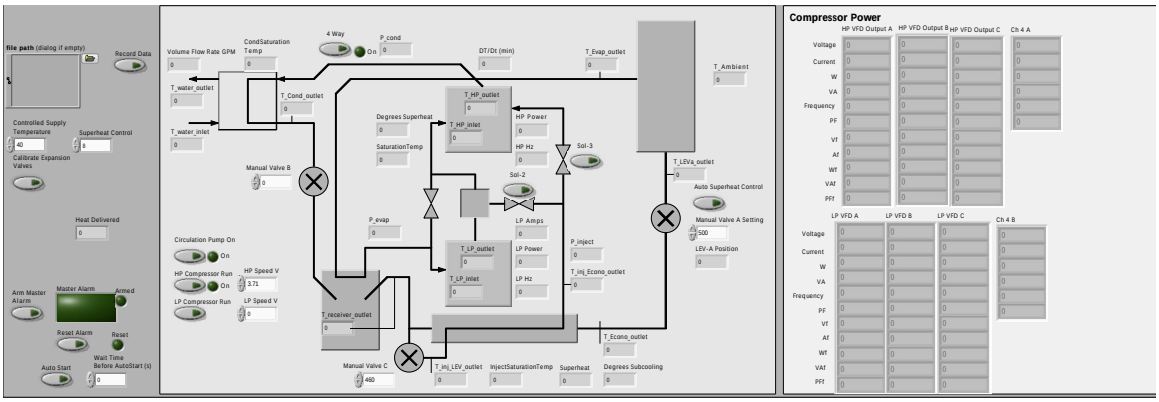

Figure E.2: System Graphical User Interface

E.1.3 Hydronics Controller

The hydronics controller was used to control the heat dump outlined in Section 3.3.7. It operated a PID control algorithm which controlled the supply temperature to the condenser by varying the fan speed of the heat dump. The flow rate measurement was also performed by this controller as it was located closer to the flow meter than the main controller.

E.1.4 PA-4000

The power analyzers were connected to the network which allowed their measurements to be recorded directly on the Desktop PC.

Appendix F

Uncertainty

This appendix contains the uncertainties that were calculated for each of the test points using the procedure outlined in Chapter 4.

F.1 PA-4000 Additional Terms

The PA-4000 power analyzers were configured to the 200 V, 50 A, and 45 Hz to 850 Hz ranges during testing. According to the manual, the corresponding terms from Equation 4.7 are shown in Table F.1.

Table F.1: PA-4000 Bias Error Terms

$V_{rms_{acc}}$	$\pm 0.04\%$ of reading $\pm 0.04\%$ of range ± 0.02 V
$A_{rms_{acc}}$	$\pm 0.04\%$ of reading $\pm 0.04\%$ of range $\pm(20\ \mu V/Z_{ext})$
Z_{ext}	9.375 mΩ
$Vh1_{pherr}$	$\pm 0.025\ \pm[0.005 * (V_{rms}/V_{range})] \pm (0.05/V_{range}) \pm (0.001F)$
$Ah1_{pherr}$	$\pm 0.025\ \pm[0.005 * (A_{rms}/A_{range})] \pm (0.0001/A_{range} * Z_{ext}) \pm (0.001F)$

where Z_{ext} is the impedance of the current shunt, V_{range} is the voltage range of the analyzer, A_{range} is the current range of the analyzer, and F is the measured frequency of the first voltage harmonic.

F.2 Uncertainty

The uncertainties given in the plots from Chapter 6 were calculated as outlined in Chapter 4. The values used to compute the uncertainty of the derived quantities for each data point are given in Figures F.1 and F.2.

Data Pt#	T_water_outlet/Inlet				T_delta	Sparling				Cp	Density	P_in kW	Q_output
	B_SPRT	B_Readout	B_RTD	B_j	B_j	B_meter	B_NI_Gain	B_BI_Offset	B_j	B_j	B_j	B_j	Theta_V
1	0.011	0.009	0.021	0.025	0.036	0.003	0.000	0.000	0.003	0.006	0.003	0.004	10.180
2	0.011	0.009	0.021	0.025	0.036	0.003	0.000	0.000	0.003	0.006	0.003	0.004	7.962
3	0.011	0.009	0.021	0.025	0.036	0.003	0.000	0.000	0.003	0.006	0.003	0.004	5.646
4	0.011	0.009	0.021	0.025	0.036	0.003	0.000	0.000	0.003	0.006	0.003	0.004	8.609
5	0.011	0.009	0.021	0.025	0.036	0.003	0.000	0.000	0.003	0.006	0.003	0.004	9.262
6	0.011	0.009	0.021	0.025	0.036	0.003	0.000	0.000	0.003	0.006	0.003	0.002	12.573
7	0.011	0.009	0.021	0.025	0.036	0.003	0.000	0.000	0.003	0.006	0.003	0.002	12.324
8	0.011	0.009	0.021	0.025	0.036	0.003	0.000	0.000	0.003	0.006	0.003	0.003	11.877
9	0.011	0.009	0.021	0.025	0.036	0.003	0.000	0.000	0.003	0.006	0.003	0.002	14.732
10	0.011	0.009	0.021	0.025	0.036	0.003	0.000	0.000	0.003	0.006	0.003	0.002	12.712
11	0.011	0.009	0.021	0.025	0.036	0.003	0.000	0.000	0.003	0.006	0.003	0.003	15.928
12	0.011	0.009	0.021	0.025	0.036	0.003	0.000	0.000	0.003	0.006	0.003	0.002	13.430
13	0.011	0.009	0.021	0.025	0.036	0.003	0.000	0.000	0.003	0.006	0.003	0.003	14.773
14	0.011	0.009	0.021	0.025	0.036	0.003	0.000	0.000	0.003	0.006	0.003	0.002	11.305
15	0.011	0.009	0.021	0.025	0.036	0.003	0.000	0.000	0.003	0.006	0.003	0.002	7.707
16	0.011	0.009	0.021	0.025	0.036	0.003	0.000	0.000	0.003	0.006	0.003	0.003	12.629
17	0.011	0.009	0.021	0.025	0.036	0.003	0.000	0.000	0.003	0.006	0.003	0.002	9.713
18	0.011	0.009	0.021	0.025	0.036	0.003	0.000	0.000	0.003	0.006	0.003	0.002	7.604
19	0.011	0.009	0.021	0.025	0.036	0.003	0.000	0.000	0.003	0.006	0.003	0.002	5.746
20	0.011	0.009	0.021	0.025	0.036	0.003	0.000	0.000	0.003	0.006	0.003	0.001	8.071
21	0.011	0.009	0.021	0.025	0.036	0.003	0.000	0.000	0.003	0.006	0.003	0.001	6.432
22	0.011	0.009	0.021	0.025	0.036	0.003	0.000	0.000	0.003	0.006	0.003	0.001	4.540
23	0.011	0.009	0.021	0.025	0.036	0.003	0.000	0.000	0.003	0.006	0.003	0.002	7.377
24	0.011	0.009	0.021	0.025	0.036	0.003	0.000	0.000	0.003	0.006	0.003	0.002	12.460
25	0.011	0.009	0.021	0.025	0.036	0.003	0.000	0.000	0.003	0.006	0.003	0.002	12.505
26	0.011	0.009	0.021	0.025	0.036	0.003	0.000	0.000	0.003	0.006	0.003	0.002	10.888

Figure F.1: Details of Uncertainty Analysis - 1

Q_output cont..									COP						
Theta_T_Delta	Theta_Cp	Theta_Density	B_T	S_hat	t	U_hat	+/- Error %		Theta_Pin	Theta_Q	B_T	S_hat	t	U_hat	+/- Error %
1.434	0.889	3.565	0.059	0.001	1.960	0.070	1.955		0.947	0.514	0.031	0.000	1.960	0.040	2.177
1.434	0.695	2.787	0.056	0.002	1.960	0.082	2.906		0.808	0.537	0.030	0.001	1.960	0.047	3.140
1.432	0.492	1.975	0.054	0.001	1.960	0.072	3.640		0.625	0.561	0.030	0.001	1.960	0.045	4.052
1.437	0.753	3.021	0.057	0.001	1.960	0.074	2.442		0.733	0.491	0.028	0.000	1.960	0.042	2.822
1.437	0.811	3.251	0.058	0.001	1.960	0.071	2.175		0.745	0.477	0.028	0.000	1.960	0.039	2.468
1.439	1.102	4.418	0.063	0.001	1.960	0.073	1.645		0.687	0.393	0.025	0.000	1.960	0.036	2.044
1.426	1.070	4.290	0.062	0.001	1.960	0.078	1.815		0.576	0.365	0.023	0.000	1.960	0.034	2.184
1.428	1.033	4.142	0.062	0.001	1.960	0.070	1.671		0.514	0.351	0.022	0.000	1.960	0.029	2.010
1.434	1.286	5.157	0.067	0.001	1.960	0.082	1.577		0.628	0.348	0.023	0.001	1.960	0.041	2.252
1.433	1.109	4.447	0.063	0.001	1.960	0.072	1.611		0.694	0.394	0.025	0.000	1.960	0.035	1.985
1.434	1.391	5.578	0.069	0.001	1.960	0.082	1.461		0.575	0.320	0.022	0.001	1.960	0.040	2.221
1.434	1.172	4.702	0.065	0.001	1.960	0.079	1.679		0.573	0.348	0.023	0.000	1.960	0.036	2.215
1.434	1.290	5.172	0.067	0.001	1.960	0.076	1.462		0.523	0.317	0.021	0.000	1.960	0.032	1.956
1.432	0.986	3.954	0.061	0.001	1.960	0.075	1.875		0.620	0.395	0.024	0.000	1.960	0.037	2.354
1.431	0.672	2.694	0.056	0.003	1.960	0.095	3.501		0.638	0.485	0.027	0.002	1.960	0.062	4.684
1.435	1.103	4.424	0.063	0.001	1.960	0.073	1.629		0.479	0.328	0.021	0.001	1.960	0.057	3.866
1.434	0.848	3.402	0.059	0.001	1.960	0.068	1.976		0.908	0.515	0.030	0.000	1.960	0.039	2.192
1.434	0.664	2.662	0.056	0.002	1.960	0.087	3.260		0.769	0.536	0.030	0.001	1.960	0.055	3.862
1.432	0.501	2.009	0.054	0.003	1.960	0.090	4.469		0.630	0.558	0.030	0.001	1.960	0.062	5.452
1.427	0.701	2.812	0.056	0.001	1.960	0.065	2.306		1.069	0.614	0.035	0.000	1.960	0.043	2.479
1.427	0.559	2.241	0.054	0.001	1.960	0.068	3.015		0.923	0.640	0.035	0.000	1.960	0.046	3.198
1.426	0.394	1.581	0.053	0.001	1.960	0.065	4.115		0.726	0.675	0.036	0.001	1.960	0.048	4.447
1.428	0.642	2.573	0.056	0.001	1.960	0.066	2.532		0.850	0.573	0.032	0.000	1.960	0.040	2.684
1.429	1.084	4.347	0.063	0.001	1.960	0.077	1.748		0.703	0.401	0.025	0.000	1.960	0.036	2.037
1.430	1.089	4.366	0.063	0.001	1.960	0.077	1.761		0.575	0.362	0.023	0.001	1.960	0.044	2.790
1.430	0.948	3.801	0.060	0.001	1.960	0.075	1.948		0.545	0.377	0.023	0.000	1.960	0.033	2.307

Figure F.2: Details of Uncertainty Analysis - 2

Appendix G

Super-heat Algorithm

This appendix outlines the operation of the algorithm that was used to control the amount of super-heat that was present in the refrigerant at the evaporator outlet, shown as state point (9) in Figure 5.1d, by controlling the position of the heating expansion valve.

G.1 Super-heat Defined

The super-heat at state point (9) is defined in Equation 5.1 which is shown below for convenience.

$$T_{super-heat} = T_{evap_{outlet}} - T_{evap_{saturation}}$$

where, $T_{super-heat}$ is the amount of super-heat that is present in the refrigerant at the outlet of the evaporator, $T_{evap_{outlet}}$ is the refrigerant temperature at state point (9), as shown in Figure 5.1d, and $T_{evap_{saturation}}$ is the refrigerant saturation temperature that corresponds to the evaporator pressure.

This is the main controlled parameter in all heat pumps and air conditioners. This parameter is used to prevent liquid from entering the compressor by ensuring that the state of the refrigerant at the compressor inlet is a super-heated gas.

G.2 PID Algorithm

The super-heat algorithm functioned using a standard proportional-integral-derivative (PID) feedback system that was included in LabVIEW. The PID equation is outlined in Equation G.1.

$$U(t) = K_c \left\{ e + \frac{1}{T_i} \int_0^t e dt + T_d \frac{de}{dt} \right\} \tag{G.1}$$

where K_c is the proportional gain, T_i is the integral time constant, T_d is the derivative time constant, and e is the error calculated using Equation G.2.

$$e = SP - PV \tag{G.2}$$

where, SP is the super-heat set-point of 8°C and PV is the process variable $T_{super-heat}$ from Equation 5.1.

The output of Equation G.1 was limited to a range of 0 to 500 which directly corresponded to the position of the heating expansion valve.

The constants required in Equation G.1 were determined by performing an open loop tuning procedure which was described in the reference manual for the LabVIEW PID Toolkit [21]. This was accomplished by recording the parameter $T_{super-heat}$ with the system operating under steady condition, and manually changing the heating expansion valve position to observe the system response. The resulting dataset was analyzed to obtain the parameters that are outlined in Figure G.1.

where Δn is the change in the controlled parameter, t_d is the system lag time, and T is the time required for the process variable to reach 63.2% of its final value. For this process all of the time parameters are measured with units of minutes. Lastly, the system gain is calculated using Equation G.3.

$$K = \frac{\Delta T_{super-heat}}{\Delta n} \tag{G.3}$$

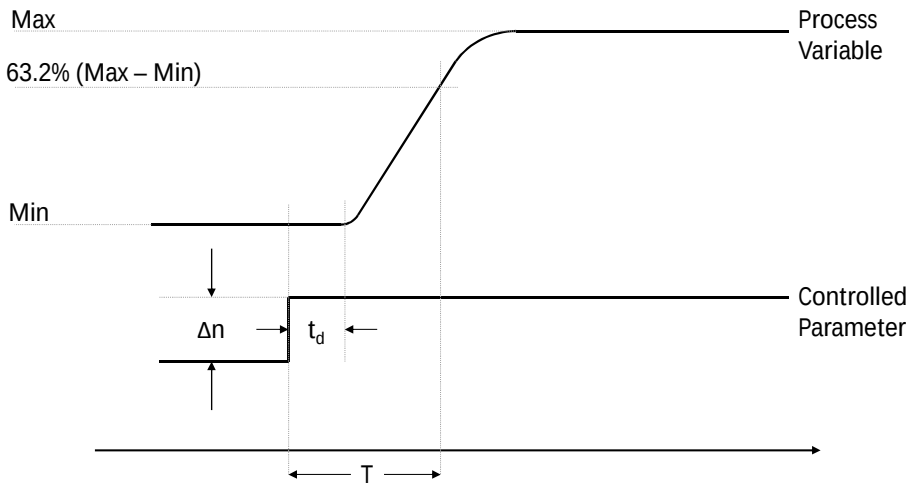

Figure G.1: Super-heat Open Loop Step Response

where $\Delta T_{super-heat}$ is the change in the process variable from Min to 63.2%(Max-Min) as shown in Figure G.1. Table G.1 shows the corresponding values that were measured.

Table G.1: Measured Open Loop Response Parameters

Δn	6
$\Delta T_{super-heat}$	8.3°C
K	1.383
t_d	0.167 [min]
T	0.583 [min]

The tuning parameters in Equation G.1 were calculated using Equations G.4, G.5 and G.6. Which were taken from the closed-loop-quarter-decay response table from the LabVIEW manual [21].

$$K_c = 100\frac{Kt_d}{T} = 39.6 \tag{G.4}$$

$$T_i = 2.00t_d = 0.334 \tag{G.5}$$

$$T_d = 0.50 t_d = 0.084 \tag{G.6}$$

Appendix H

Data

The data collected were used to produce a total of twenty six data points. This appendix includes the averaged data that were used for analysis.

H.1 Data Points

Figure H.1 shows the legend for the data points that were collected.

The average values that were used to determine the performance of the system for each of these data points are shown in Figure H.2. The highlighted fan power values were not measured during testing and were added based on the later measured values.

Data Point #	Date Tested	System Configuration	Ambient Temperature [C]
1	December 15, 2014	Single Stage	-1.77
2	December 15, 2014	Single Stage	-12.75
3	December 15, 2014	Single Stage	-22.85
4	December 15, 2014	Single Stage Economized	-23.31
5	December 15, 2014	Single Stage Economized	-23.39
6	December 16, 2014	Two Stage Economized	-13.56
7	December 16, 2014	Two Stage Economized	-23.25
8	December 16, 2014	Two Stage Economized	-31.07
9	December 17, 2014	Two Stage Economized	-13.47
10	December 17, 2014	Two Stage Economized	-13.49
11	December 17, 2014	Two Stage Economized	-14.44
12	December 18, 2014	Two Stage Economized	-23.02
13	December 18, 2014	Two Stage Economized	-22.98
14	December 18, 2014	Two Stage Economized	-23.52
15	December 18, 2014	Two Stage Economized	-23.30
16	December 18, 2014	Two Stage Economized	-31.29
17	December 30, 2014	Single Stage	-2.57
18	December 30, 2014	Single Stage	-12.79
19	December 30, 2014	Single Stage	-22.53
20	January 20, 2015	Single Stage [WJ]	-2.72
21	January 20, 2015	Single Stage [WJ]	-12.68
22	January 20, 2015	Single Stage [WJ]	-22.90
23	January 20, 2015	Single Stage Economized [WJ]	-23.30
24	January 22, 2015	Two Stage Economized [WJ]	-14.59
25	January 22, 2015	Two Stage Economized [WJ]	-23.13
26	January 22, 2015	Two Stage Economized [WJ]	-31.32

Figure H.1: Data Point Legend

Data pt #	Delta T Water	Volume Flow m^3/s	Mass Flow kg/s	Q Delivered kJ/s	Mitsu Power kW	Denso Power kW	Fan Power kW	COP
1	2.50	0.35	0.36	3.59	1.66	0.00	0.29	1.84
2	1.96	0.35	0.35	2.81	1.57	0.00	0.29	1.51
3	1.39	0.35	0.35	1.99	1.49	0.00	0.29	1.11
4	2.12	0.35	0.36	3.04	1.75	0.00	0.29	1.49
5	2.28	0.35	0.36	3.27	1.81	0.00	0.29	1.56
6	3.09	0.35	0.36	4.45	1.61	0.64	0.29	1.75
7	3.03	0.35	0.35	4.32	1.61	0.84	0.29	1.58
8	2.92	0.35	0.35	4.17	1.61	0.95	0.29	1.46
9	3.62	0.35	0.35	5.19	1.63	0.95	0.29	1.81
10	3.13	0.35	0.35	4.48	1.61	0.64	0.29	1.76
11	3.92	0.35	0.36	5.62	1.65	1.18	0.29	1.80
12	3.30	0.35	0.36	4.74	1.62	0.97	0.28	1.65
13	3.63	0.35	0.36	5.21	1.64	1.23	0.28	1.65
14	2.78	0.35	0.35	3.98	1.59	0.66	0.28	1.57
15	1.90	0.35	0.35	2.71	1.51	0.27	0.28	1.32
16	3.11	0.35	0.36	4.45	1.62	1.16	0.28	1.46
17	2.39	0.35	0.36	3.43	1.65	0.00	0.29	1.76
18	1.87	0.35	0.35	2.68	1.57	0.00	0.29	1.44
19	1.41	0.35	0.35	2.02	1.51	0.00	0.28	1.13
20	1.98	0.35	0.35	2.83	1.33	0.00	0.29	1.74
21	1.58	0.35	0.35	2.26	1.27	0.00	0.29	1.44
22	1.12	0.35	0.35	1.59	1.20	0.00	0.29	1.07
23	1.81	0.35	0.35	2.59	1.46	0.00	0.29	1.48
24	3.06	0.35	0.35	4.38	1.14	1.07	0.29	1.75
25	3.07	0.35	0.35	4.40	1.28	1.19	0.29	1.59
26	2.68	0.35	0.35	3.83	1.30	1.06	0.28	1.44

Figure H.2: Averaged Data From Analysis